ABSTRACT

WU, BINGYAN. Factors Controlling Alkylbenzene Sorption and Desorption in Municipal Solid Waste (Under the direction of Dr. Detlef R. Knappe and Dr. Morton A. Barlaz).

The sorption and desorption of toluene and *o*-xylene from individual municipal solid waste (MSW) constituents [office paper, newsprint, model food and yard waste, high density polyethylene (HDPE), and poly(vinyl chloride) (PVC)] were evaluated. Effects of sorbent decomposition and solvent composition on alkylbenzene sorption and desorption were studied by evaluating biodegradable sorbents in both fresh and anaerobically decomposed form and by conducting single-solute sorption isotherm tests and batch desorption tests in acidogenic and methanogenic leachate. To determine the effects of aging on alkylbenzene desorption rates, desorption tests were performed for samples that were contacted with toluene for 30 and 250 days. Selected samples containing *o*-xylene were analyzed after an aging time of 250 days.

Alkylbenzene sorption to plastics was greater than to biopolymer composites, and differences in sorbate/sorbent solubility parameter compatibility explained this observation. Alkylbenzene sorption to biopolymer composites yielded linear isotherms, and sorption capacities [log (K_{oc}/K_{ow})] decreased linearly with increasing sorbent polarity as expressed by the O-alkyl/alkyl ratio. Leachate composition had little effect on alkylbenzene sorption with one exception, volatile fatty acids in acidogenic leachate appeared to convert PVC from a glassy to a rubbery polymer. The results of

this study showed that sorbent organic matter affinity for hydrophobic organic contaminants (HOCs) increased with increasing extent of MSW decomposition because of the recalcitrance of plastics and the preferential degradation of polar biopolymers. Furthermore, the plasticizing effect of volatile fatty acids in acidogenic leachate may enhance the bioavailability of HOCs sorbed to glassy organic matter in MSW or in soils contaminated with acidogenic leachate.

Desorption tests showed that alkylbenzene desorption rates were slowest for PVC and fastest for fresh rabbit food and newsprint. For the biopolymer composites, desorption rates decreased as aging time increased, suggesting that the bioavailability of HOCs in landfills decreases over time as HOCs are physically sequestered or undergo humification. Consistent with its larger molecular size, *o*-xylene desorption rates were slower than those of toluene. A single-parameter polymer diffusion model successfully described PVC and HDPE desorption data, but it failed to simulate desorption rate data for biopolymer composites such as rabbit food, newsprint, and office paper. Therefore, three-parameter biphasic polymer diffusion model was applied to describe desorption rate data from biopolymer composites. Toluene desorption rates from mixed MSW were predicted for two landfill scenarios. Model results showed that 50% of the initially sorbed toluene desorbed in 5.83 days for an old landfill scenario containing little plastics waste (1960 MSW composition) and in 3.97 years for a new landfill scenario containing more plastics (1997 MSW composition). Consequently, the mineralization rate of toluene is likely controlled by biological processes in old landfills but by desorption in new landfills.

Factors Controlling Alkylbenzene Sorption and Desorption in Municipal Solid Waste

by

BINGYAN WU

A dissertion submitted to the Graduate Faculty of

North Carolina State University

in partial fulfillment of the

requirements for the Degree of

Doctor of Philosophy

DEPARTMENT OF CIVIL ENGINEERING

Raleigh

2002

APPROVED BY:

Dr. Detlef R. Knappe Chair of Advisory Committee	Dr. Morton A. Barlaz Co-Chair of Advisory Committee
Dr. Francis L. III De Los Reyes Advisory Committee	Dr. Dean L. R. Hesterberg Advisory Committee

BIOGRAPHY

Bingyan Wu received her B.S. of Environmental Engineering from Tsinghua University, Beijing, P. R. China, in 1994 and her M.S. of Environmental Engineering from the same university in 1997. In the Fall of 1998, she came to the United States to start her Ph.D. studies in the Department of Civil Engineering at North Carolina State University. Her research interests include water and wastewater treatment, solid waste management and statistical analysis of environmental data.

ACKNOWLEDGMENTS

I wish to express my sincere appreciation to my advisors: Dr. Detlef R. Knappe, for his thoughtful advice, encouragement, kindness and guidance throughout my Ph.D. study; and Dr. Morton A. Barlaz, for his kindness, patience and valuable advice. I am also grateful to Dr. Francis L. III De Los Reyes and Dr. Dean L.R. Hesterberg for their teaching, serving as my committee members and thoughtful comments.

I would like to thank Phil Calvert for providing practical advice on my experimental design, and David Black for countless help in last four years. Lots of thanks also go to my friends in the office for sharing their research information, all the conversations and laughs. Specially, I would like to thank Brenda Ress, for her kindness and assistance from my first day in this lab.

Love and thanks to my parents, Shuzhen Gao, and Jin Wu, for always trusting me and encouraging me. I am deeply indebted to them for their enduring love and support. Also, thanks to my little brother, Yufeng Wu, for the enjoyable communications we had through telephone and e-mail, that relieved my homsickness a lot. Finally, I would like to thank my beloved boyfriend, Yi Liao, for his unconditional love and endless support. The last three years with him is the happiest time in my life. I can never imagine how I could finish this work without his company.

Contents

List of Figures viii

List of Tables xi

1 Introduction and Objectives 1

2 Literature Review 4

2.1 Properties of Municipal Solid Waste Components 4

2.1.1 Classification of Polymer States 4

2.1.2 Cellulose and Hemicellulose 6

2.1.3 Lignin 8

2.1.4 Lipids and Proteins 10

2.1.5 High-Density Polyethylene (HDPE) and Poly(vinyl chloride) (PVC) 10

2.2 Factors Controlling Bioavailability 11

2.2.1 Physical Factors 12

2.2.2 Chemical Factors 15

2.3 Factors Affecting Sorption 17

2.3.1 Sorbent Effects 17

2.3.2 Sorbate Effects 20

2.3.3 Solvent Effects 21

2.4 Desorption 23

2.4.1 Desorption Hysteresis 23

2.4.2 Desorption Models 25

3 Experimental Design and Methods **36**

3.1 Model Municipal Solid Waste Components and Characterization . . . 36

3.1.1 MSW Components 36

3.1.2 MSW Component Characterization 37

3.2 Sorbates 39

3.3 Leachates 39

3.4 Isotherms 41

3.5 Desorption Tests 42

3.6 Mass Balances 43

4 Results and Discussion - Sorption **46**

4.1 Solids Characterization 46

4.1.1 Elemental Analysis and Chemolytic Characterization 46

4.1.2 ^{13}C Nuclear Magnetic Resonance Spectra (NMR) 51

4.2 Sorbate Properties and Leachate Characterization 51

4.3 Single-Solute Sorption Isotherms 55

4.3.1 Sorption Capacity of MSW Components 55

4.3.2 Isotherm Linearity 61

4.3.3 Relationship between K_{oc} and K_{ow} 62

4.3.4 Correlation between Normalized Sorption Parameter and Sorbent Polarity 63

4.3.5 Effect of Sorbent Polarity on Toluene Sorption before and after Removal of Lipophilic Extractives 67

4.4 Leachate Effects on Sorption Isotherms 68

5 Results and Discussion - Desorption **74**

5.1 Model Development 74

5.1.1 One-Compartment Polymer Diffusion Model 74

5.1.2 Biphasic Polymer Diffusion Model 76

5.2 Model Verification and Interpretation 78
5.2.1 Model Verification 78
5.2.2 Model Interpretation 79
5.3 Effects of Sorbent Type on Desorption Rate 85
5.4 Aging Effects 91
5.5 Solute Effects 93
5.6 Leachate Effects 95
5.7 Mass Balances 99
5.8 Model Prediction for Desorption Kinetics from Mixture of MSW Components 100

6 Conclusions and Future Research **107**
6.1 Conclusions 107
6.2 Future Research 109

Bibliography **111**

Appendices **131**
A. Mathematical model 131
A.1 Crank-Nicholson Implicit Finite Difference Scheme 131
A.2 Derivation of the Intraparticle Solute Mass Remaining M_j 131
A.3 One-compartment polymer diffusion model 132
A.4 Biphasic polymer diffusion model for searching Φ_s, D_s, D_r. 139
A.5 Biphasic polymer diffusion model for searching Φ_s only 146
A.6 C++ program for predicting desorpiton of alkylbenzene in mix of MSW 152
A.7 SAS Program for Analytical Solution of one-compartment model (HDPE as an example) 159
A.8 SAS Program for Analytical Solution of two-compartment model (fresh rabbit food as an example) 161
B. Desorption Experimental Data 162

C. Isotherms 173

List of Figures

2-1 Cellulose microfibrils structure (from Bristow et al. 1986) 7

2-2 The molecular structure of cellulose 8

2-3 Representative lignin structure 9

2-4 Schematic representation of intraparticle diffusion in natural particles 27

2-5 Schematic representation of intraorganic diffusion 30

3-1 Desorption apparatus 44

4-1 Single-solute o-xylene isotherms for model MSW components. Solid lines through all other data sets indicate best fits of the linear partition model, and partition coefficients are shown in Table 4.8. 58

4-2 Dependence of log K_{oc} on log K_{ow} for individual MSW components and mixed MSW. PVC data represent Freundlich K-values divided by f_{oc} and provide a valid comparison only at an equilibrium liquid-phase concentration of 1 $\mu g/L$. Data for mixed MSW are from ref. 121. . . 64

4-3 Dependence of normalized sorption parameter on sorbent polarity as expressed by the polarity index [(O+N)/C] 66

4-4 Dependence of normalized sorption parameter on sorbent polarity as expressed by % polar organic carbon (= O-alkyl + carbonyl from Table 4.3) 67

4-5 Effect of sorbent polarity on toluene sorption to MSW components before and after lipophilic extraction 69

4-6 Dependence of normalized sorption parameter on sorbent polarity as expressed by O-alkyl/alkyl ratio (from Table 4.3). 70

4-7 Effect of aqueous phase composition on toluene sorption to PVC . . . 71

5-1 Comparison of analytical and numerical solutions for one and two-compartment models 80
5-2 Experimental toluene desorption data and one-compartment polymer diffusion model simulations for MSW components in acidogenic leachate after 250 days aging 82
5-3 Experimental toluene desorption data for degraded rabbit food in acidogenic leachate and biphasic polymer diffusion model simulations . 84
5-4 Experimentally determined toluene desorption rates from MSW components after aging of 30 days in acidogenic leachate 86
5-5 The relationship between log (Φ_r/Φ_s) and O-alkyl/alkyl ratio of sorbent organic matter 90
5-6 Toluene desorption from HDPE and degraded office paper in methanogenic leachate at two aging times 92
5-7 Toluene and *o*-xylene desorption from HDPE, fresh rabbit food and fresh newsprint in acidogenic leachate after 250 days aging 94
5-8 Toluene desorption from HDPE and biopolymer composites in two leachate phases after 30 days of aging 97
5-9 pH effects on toluene desorption rates for fresh office paper 98
5-10 Model prediction for toluene desorption from mixed MSW components as a function of solid size 105

C-1 Toluene isotherm with degraded newsprint in acidogenic leachate . . 174
C-2 Toluene isotherm with fresh newsprint in acidogenic leachate 174
C-3 Toluene isotherm with degraded office paper in acidogenic leachate . . 175
C-4 Toluene isotherm with fresh office paper in acidogenic leachate 175
C-5 Toluene isotherm with fresh rabbit food in acidogenic leachate 176
C-6 Toluene isotherm with degraded rabbit food in acidogenic leachate . . 176
C-7 Toluene isotherm with HDPE in acidogenic leachate 177
C-8 Toluene isotherm with PVC in acidogenic leachate 177

C-9 Toluene isotherm with degraded newprint in methanogenic leachate . 178
C-10 Toluene isotherm with fresh newprint in methanogenic leachate . . . 178
C-11 Toluene isotherm with degraded office paper in methanogenic leachate 179
C-12 Toluene isotherm with degraded rabbit food in methanogenic leachate 179
C-13 Toluene isotherm with fresh rabbit food in methanogenic leachate . . 180
C-14 Toluene isotherm with HDPE in methanogenic leachate 180
C-15 Toluene isotherm with PVC in methanogenic leachate 181
C-16 o-xylene isotherm with degraded newsprint in acidogenic leachate . . 181
C-17 o-xylene isotherm with fresh newsprint in acidogenic leachate 182
C-18 o-xylene isotherm with fresh rabbit food in acidogenic leachate 182

List of Tables

2.1 Composition of municipal refuse 5
2.2 Classification of pore size 15

4.1 Characteristics of solid materials 49
4.2 Elemental composition of acid-washed solid materials 50
4.3 Distribution of functional groups in biopolymer-containing materials based on ^{13}C CP-MAS NMR data 51
4.4 Sorbate properties 52
4.5 Leachate characteristics 53
4.6 Volatile fatty acid (VFA) analysis for acidogenic leachate 54
4.7 Isotherm parameters describing toluene sorption to MSW components 56
4.8 Isotherm parameters describing o-xylene sorption to MSW components 57
4.9 Isotherm parameters describing toluene sorption to lipophilic extracted MSW components 66
4.10 Partition coefficients describing tolune sorption to MSW components in acidogenic leachate and methanogenic leachate A 72
4.11 Freundlich isotherm parameters and partition coefficients describing toluene sorption to MSW components in methanogenic leachates B . 73
4.12 Partition coefficients describing o-xylene sorption to MSW components in acidogenic leachate and methanogenic leachate A 73

5.1 Properties of model MSW components 79
5.2 Diffusion coefficient estimates for the one-component polymer diffusion model 81

5.3 Desorption rate parameter estimates for the two-component polymer diffusion model in acidogenic leachate 85
5.4 Dr/a^2 and Ds/a^2 values for toluene desorption from biopolymer composites 89
5.5 VFA analysis for acidogenic leachate with/without PVC 99
5.6 Mass balence analysis 100
5.7 Composition of sorbent organic matter in municipal solid waste (1997) 102
5.8 Properties of plastics 103
5.9 Composition of sorbent organic matter in munipal solid waste (1960) 104
5.10 Thickness of MSW components used in model prediction 104

B.1 Toluene desorption data from fresh rabbit food after 1 month aging . 162
B.2 Toluene desorption data from fresh rabbit food after 8 month aging . 163
B.3 Toluene desorption data from degraded rabbit food after 1 month aging 163
B.4 Toluene desorption data from degraded rabbit food after 8 month aging 164
B.5 Toluene desorption data from fresh newsprint after 1 month aging . . 164
B.6 Toluene desorption data from fresh newsprint after 8 month aging . . 165
B.7 Toluene desorption data from degraded newsprint after 1 month aging 165
B.8 Toluene desorption data from degraded newsprint after 8 month aging 166
B.9 Toluene desorption data from fresh office paper after 1 month aging . 166
B.10 Toluene desorption data from office paper after 8 month aging 167
B.11 Toluene desorption data from degraded office paper after 1 month aging 167
B.12 Toluene desorption data from degraded office paper after 8 month aging 168
B.13 Toluene desorption data from HDPE after 1 month aging 168
B.14 Toluene desorption data from PVC after 1 month aging 169
B.15 Toluene desorption data from PVC after 8 month aging 169
B.16 o-xylene desorption data from fresh and degraded rabbit food in acidogenic leachate after 8 month aging 170
B.17 o-xylene desorption data from fresh and degraded newsprint in acidogenic leachate after 8 month aging 171

B.18 o-xylene desorption data from fresh and degraded office paper in acidogenic leachate after 8 month aging 172
B.19 o-xylene desorption data from PVC and HDPE in acidogenic leachate after 8 month aging 173

Chapter 1

Introduction and Objectives

Landfilling is the principal disposal method for municipal solid waste, and this practice is not likely to change in the near future. Approximately 25% of the sites on the National Priority List (NPL) of Superfund are municipal landfills that accepted hazardous waste (Carra and Cossu 1990). Unlined landfills usually result in groundwater contamination, and priority pollutants such as alkylbenzenes are typically present. Ultimately, strategies are needed to manage these landfills, as well as thousands of sites not on the NPL, in a manner that is both cost-effective and protective of the environment. To select cost-effective risk management alternatives, better information on factors controlling the fate of contaminants in landfills is required.

Sorption/desorption processes are major factors that limit both the biodegradation and transport of hydrophobic organic contaminants (HOCs) in landfills (Sanin et al. 2000, Reinhart et al. 1991). Results from prior studies also suggest that sorbed contaminants are less bioavailable than dissolved contaminants (Ogram et al. 1985). Factors that reduce bioavailability include partitioning into glassy/hard organic matter (Pignatello and Xing 1996, Weber. et al. 1995), adsorption in micropores (Nam and Alexander 1998) and strong hydrophobic interactions such as encapsulation in paraffinic organic matter (Lerch et al. 1997, Guthrie et al. 1999). These sorption mechanisms reduce the bioavailability of HOCs by greatly decreasing their desorption rate into the bulk liquid phase, where HOCs would be more bioavailable.

Few studies have investigated the sorption/desorption of organic contaminants

to municipal solid waste MSW components. In contrast, numerous studies investigated sorption and desorption processes in environments involving soils and sediments, where the involved geosorbents exhibited lower organic carbon contents than MSW, and the aqueous phases contained lower organic carbon concentrations than landfill leachate. Therefore, a fundamental understanding of sorption and desorption mechanisms specific to MSW components is critical for predicting the fate of HOCs in landfills.

Many factors can influence the extent and rate of sorption and desorption such as sorbent and sorbate properties, dissolved organic compounds in the aqueous phase, pH, and temperature. Furthermore, sorbent biodegradation affects HOC sorption and desorption in landfills because (1) the organic fraction of MSW components decreases (Reinhart et al. 1990, Pichler and Kögel-knabener 2000) and (2) the polarity of the remaining organic fraction decreases as a result of the preferential degradation of more polar constituents such as cellulose and hemicellulose over less polar components such as lignin and lipids (Pichler and Kögel-knabener 2000, Eleazer et al. 1997). As previously shown for sediments, biologically mediated increases in sorbent hydrophobicity can lead to enhanced HOC sequestration (Guthrie et al. 1999), and similar effects may be expected in landfills. Furthermore, contaminant aging can reduce the bioavailability of HOCs in landfills, where HOCs are exposed to sorbents for long periods of time. As the residence time of the HOCs in landfills increases, sequestration involving slow partitioning of HOCs into glassy organic matter (Hatzinger et al. 1995) or slow diffusion into micropores (Pignatello et al. 1993) could take place, which would reduce the desorption rate and bioavailability of HOCs. Finally, dissolved organic matter in landfill leachate can affect HOC sorption to and desorption from MSW components. Leachate generated from MSW contains high concentrations of dissolved organic matter (Chian and Dewalle 1977, Harmsen 1983, Schultz and Kjeldsen 1986, Barlaz et al. 1990), and some dissolved organic compounds in landfill leachate can bind HOCs (Larsen et al. 1992, Bauer and Herrman 1998).

To develop a more fundamental understanding of sorption/desorption processes in landfills, the research described in this thesis is designed to meet the following

objectives:

1. Evaluate the distribution of sorbed contaminants in MSW by measuring the sorptive capacity of individual components,

2. Evaluate the effects of sorbent decomposition on sorbent hydrophobicity, HOC sorption equilibria and desorption rates,

3. Determine the effects of leachate composition on HOC sorption and desorption rates,

4. Investigate the effects of HOC aging time on HOC desorption rates, and

5. Simulate HOC desorption rates from polymers and biopolymer composites with suitable diffusion models.

Chapter 2

Literature Review

2.1 Properties of Municipal Solid Waste Components

The composition of municipal refuse is summarized in Table 2.1 (EPA 1999). Table 2.1 shows that the principal components of MSW consist of paper, food and yard waste, and plastics; i.e., organic solids that are expected to sorb HOCs. Apart from plastics, which are synthetic polymers, organic MSW components are comprised of biopolymers such as cellulose, hemicellulose, lignin, protein and lipids. To enhance the understanding of HOC sorption to polymeric sorbents, the properties of cellulose, hemicellulose, lignin, protein, lipids, high density polyethylene, and poly(vinyl chloride) are summarized in this section. Furthermore, the degradation of biopolymers under methanogenic conditions is described.

2.1.1 Classification of Polymer States

Organic polymers can exist either in a crystalline state or in an amorphous state. Polymers in an amorphous state have a loose structure, in which polymer molecules are arranged randomly. Consequently, the structure of amorphous polymers is in many ways similar to the structure of liquids. In contrast, the cystalline state is characterized by molecules or segments of molecules that are regularly arranged in a crystal lattice. Crystalline regions in polymers contain a large number of very small

crystals existing in close proximity to the remainder of the material, which is in the disordered or amorphous state (Tobolsky and Mark 1980). Polymers typically contain cystalline and amorphous components. While it is possible to prepare completely amorphous polymers, it is not possible to prepare polymers that are completely crystalline because not all segments of polymer molecules can be packed into the crystal lattice.

Table 2.1 Composition of municipal refuse

Component	Percent by wet weight
Paper	38.6
Yard waste	12.8
Food waste	12.1
Plastics	9.9
Metals	7.7
Glass	5.5
Wood	5.3
Miscellaneous [a]	6.8

[a] Includes rubber, leather and textiles

Amorphous polymers can be classified as rubbery or glassy polymers. Both glassy and rubbery polymers are structurally similar in that the polymer molecules exhibit a disordered type of arrangement. The important difference between glassy and rubbery polymers lies in the magnitude of intermolecular forces. In a rubbery polymer, the forces among molecules are weak and cannot prevent one molecule or segment of a molecule from moving away from a neighboring molecule. Therefore, rubbery polymers are soft and deformable. In contrast, forces between neighboring molecules or segments are much stronger in a glassy polymer and the molecules are bound together as a rigid mass. Consequently, glassy polymers are hard and nonresilient. Crystalline polymer characteristics lie between those of rubbery and glassy polymers due to their peculiar structure, that is, cystalline polymers are moderately hard, yet flexible and strong (Treloar 1974).

A particular polymer can change from the rubbery to the glassy state when it is cooled below a certain temperature, which is called the glass-transition temperature (T_g). The glass transition temperature is an important property of a polymer, because it determines whether a polymer is to be classified as a rubber or a glass at a given environmental temperature. For a polymer to be rubbery at room temperature, its T_g should be low (e.g. polyethylene has a T_g of -68 ^oC). In contrast, T_g should be high for a polymer to be glassy at room temperature (e.g. poly(vinyl chloride) has a T_g of 80 ^oC) (Brandup et al. 1989).

2.1.2 Cellulose and Hemicellulose

Cellulose is the most abundant natural organic compound and is the primary and secondary structural component of the cell walls of plants. It is a partly crystalline and partly amorphous polymeric compound. Figure 2.1 presents a model cellulose structure with both crystalline and amorphous regions (Bristow et al. 1986). The degree of crystallinity is determined by the source of cellulose. Cotton and various algal celluloses are highly crystalline ($\sim$70%), whereas wood cellulose is less crystalline ($\sim$40%) (Treloar 1974). The chemical structure of celluose is represented in Fig 2.2 (Roberts 1996). Cellulose is an unbranched polymer containing several thousand D-glucose units joined via $\beta - 1{,}4-$ glycosidic linkages. Celluose is insoluble in water, but because of its hydrophilic nature, it can be wetted by water. In the presence of water, water is absorbed only by the non-cystalline component in cellulose, while the crystalline structure remains unchanged (Treloar 1976).

Celluose has two major crystalline forms: cellulose I and cellulose II. Cellulose I is found in native cellulose, where cellulose II can be obtained by dissolution and regeneration, or by simply treating cellulose I with sodium hydroxide (Bristow and Kolseth 1986). Studies have shown that the crystallinity of celluose can be reduced either by fine grinding or ball-milling (Caulfield and Moore 1974, Bertran et al. 1985). It is also known that the degree of crystallinity of dry-ground cellulose increases during acid hydrolysis or moisture wetting. The form of crystalline cellulose recovered on wetting

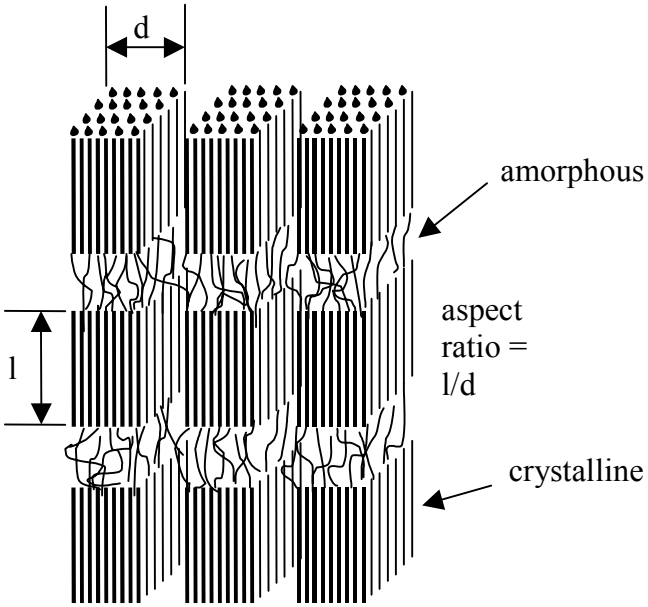

Figure 2-1: Cellulose microfibrils structure (from Bristow et al. 1986)

or acid hydrolysis is related to the extent of initial decrystallization. Partially decrystallized native cellulose due to fine grinding or ball milling tends to regain cellulose I crystallinity, even at low levels of humidity, whereas completely decrystallized or totally amorphous cellulose recovers cellulose II crystallinity only if exposed to high moisture levels (Caulfield and Steffes 1969, Caulfield and Moore 1974, Bertran et al. 1985).

Amorphous regions of dry cellulose behave like a glassy polymer and the glass transition temperature ranges from 220-230^oC. However, water-wet amorphous cellulose is in the rubbery state with a T_g of -45^oC (Akim 1978, Leboeuf et al. 2000). Furthermore, the amorphous regions of cellulose are preferentially attacked by enzymes, and the digestibility of cellulose increases greatly as the crystallinity decreases during dry grinding processes. The digestibility of the crystalline component in cellulose increases as the crystallite size decreases (Caulfield and Moore 1974, Bertran et al. 1985). Under simulated landfill conditions, cellulose was readily biodegraded (Eleazer et al. 1997).

Hemicelluloses are a group of non-structural, low molecular weight polysaccharides

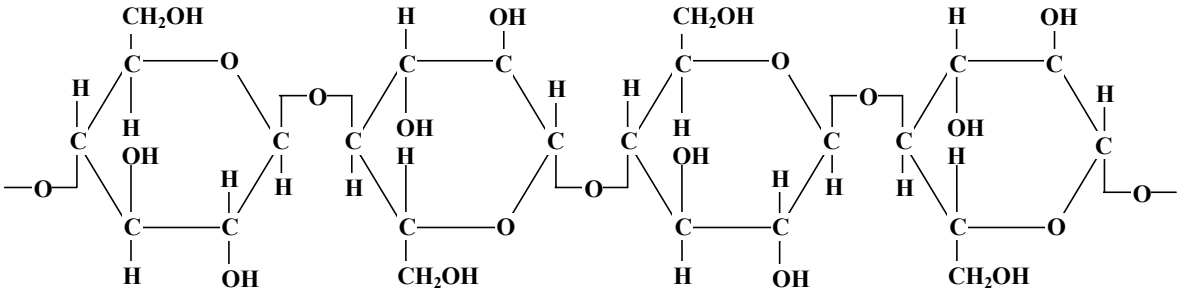

Figure 2-2: The molecular structure of cellulose

associated with cellulose and lignin in the cell walls of plants. They are heteropolysaccharides composed of D-xylose, D-mannose, D-galactose, D-glucose, L-arabinose as well as uronic acids. The major hemicelluloses present in soft woods are galactoglucomannan and arabino-(4-O-methylglucurono) xylans. The major group of hemicellulose found in hard woods are glucuronoxylans.

The tensile strength of paper is mainly attributed to its hemicellulose content. Hemicellulose is non-crystalline and more easily hydrolyzed by acids than cellulose. Also, hemicellulose is soluble in alkali and can therefore be separated from cellulose by base extraction. Glass transition temperatures of hemicellulose vary from 150-220^oC, and the variation may be due to differences in chemical composition and configuration. For native hemicelluloses, the most probable T_g is around 180^oC, and 30% moisture can lower the glass transition temperature to room temperature (Back and Salmen 1982). Furthermore, hemicellulose can be linked to lignin via covalent bonding (Gerasimowicz et al. 1984, Salmėn and Olsson 1998, Helm 2000). Similar to cellulose, hemicellulose can be substantially biodegraded under anaerobic conditions (Eleazer et. al. 1997, Pichler and Kögel-knabener 2000).

2.1.3 Lignin

Lignin is the second most abundant naturally occurring polymer, and it is located primarily in the cell walls of vascular plants (Crawford 1981). Lignin is an aromatic polymer composed of phenylpropane subunits randomly linked by a variety

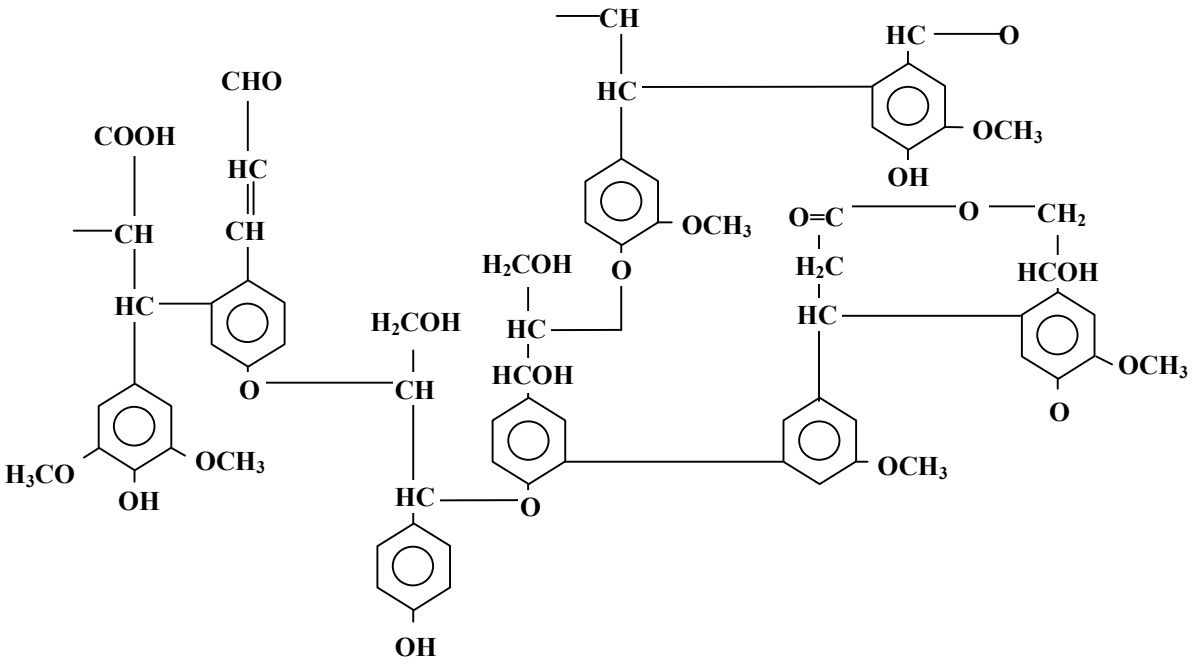

Figure 2-3: Representative lignin structure

of carbon-carbon and ether bonds. The structure of lignin is given in Figure 2.3 (Young et al. 1987). Native lignin is classified as a glassy polymer with T_g of 250^oC (Back and Salmen 1982). Water is not capable of softening native lignin efficiently. Lignin reaches an equilibrium state at a low moisture content after which additional water content shows little effect on the T_g. For native lignin, this saturation state corresponds to a T_g of 115^oC (Sakata et al. 1975, Back and Salmen 1982).

The existence of lignin in paper makes paper brittle and also gives rise to yellowing and discoloration. Newsprint contains large amounts of lignin, but lignin is usually removed for high quality paper such as printing paper. Lignin is resistant to biodegradation in anaerobic environments because microorganisms cannot use lignin as a sole energy or carbon source (Odier et al. 1983, Young 1987, Pichler and Kögelknabener 2000). Lignin is also intimately associated with cellulose and hemicellulose in wood, and the resistance of lignin to biodegradation is thought to retard complete biodegradation of the associated hemicellulose and cellulose polysaccharides (Young et al. 1987).

2.1.4 Lipids and Proteins

In landfills, food wastes contain large amounts of lipids and proteins. Lipids can be $\beta-$oxidized to acetate by H_2-producing syntrophic bacteria under fermentative conditions. Apart from the degradation of lipids, bacteria synthesize various long-chain fatty acids from carbohydrate or amino acid carbon in the form of cell walls and lipid bilayers of cell membranes (Demeyer et al. 1998). Such microbial long-chain, high-molecular lipids are not easily attacked by microorganisms (Dinel et al. 1996).

Proteins exist in a wide variety of plant and animal products. Proteins are polymers of amino acids with chain repeating units of the general form -NH-CH-R-CO-, in which R varies in each successive unit along the chain, and the different proteins are characterized by different R groups. Dry protein is a glassy polymer. Some studies have shown that the glass transition temperature of protein decreases as the amount of protein-bound water increases. It has been suggested that water molecules replace the interchain protein-protein bonds by water-protein bonds, which increases the segmental mobility of protein molecules (Green et al. 1994, Sochava 1997). The anaerobic degradation of proteins is important for the cycling of N, S and C. Under anaerobic conditions, proteins are hydrolyzed to peptides and amino acids; then the amino acids are fermented to pyruvate, which is converted to acetyl-CoA.

2.1.5 High-Density Polyethylene (HDPE) and Poly(vinyl chloride) (PVC)

Polyethylene is the most widely used synthetic polymer on earth, and it consists of repeating ethylene (CH_2=CH_2) monomers. High-density and low-density polyethylene are the most commonly used forms of polyethylene. High-density polyethylene has no branches or side-chains to interfere with crystallization, consequently, the crystallinity of HDPE typically ranges from 80% to 95%. Low density polyethylene has a lower degree of crystallinity (55%-75%), which renders it softer and more flexible than high-density polyethylene. The glass transition temperature of polyethylene is -68^oC (Brandup et al. 1989).

PVC consists of repeating vinyl chloride (-CH_2-CH-Cl) monomers. The glass transition temperature of PVC is 80^oC, making it a glassy polymer at room temperature. PVC is only slightly crystalline with a typical crystallinity range from 5% to 10% (Tobolsky et al. 1980). Polyvinyl chloride can be converted to a rubbery polymer by the incorporation of a non-volatile liquid or "plasticizer" such as phthalate ester (Treloar 1974). The presence of plasticizer reduces the number of contacts between polymer molecules, therefore reducing the strength of the forces between neighboring molecules and increasing the mobility of the polymer chains.

2.2 Factors Controlling Bioavailability

Bioremediation is a naturally occurring process by which microorganisms transform toxic, hazardous or other unwanted organic compounds to innocuous end products. Bioremediation can be an effective and inexpensive cleanup technology; however, bioremediation technologies frequently do not yield complete decontamination (Alexander 1991). It is believed that poor bioavailability of sorbed organic pollutants is the major limitation for the completeness of bioremediation. Therefore, the determination of factors that govern the bioavailability of pollutants can help explain and overcome the constraints limiting the the effectiveness of bioremediation technologies.

Bioavailability, defined by Bosma et al. (1999), is the rate of mass transfer of a chemical to the cell relative to the rate of uptake and metabolism. For sorbed pollutants, the rate of pollutant metabolism may be controlled by the mass transfer rate of the compound from an unavailable to an available form. In landfills, bioavailability can therefore be defined as the accessibility of organic pollutants to landfill micro-organisms. Organic chemicals can be sorbed to organic municipal solid waste (MSW) components such as plastics and biopolymer composites (paper, food and yard waste, wood). If microorganisms are not able to consume sorbed organic pollutants, then mineralization of the pollutants would be dependent on their desorption rate; i.e., desorption becomes the rate-limiting step if the desorption rate is slower than the biodegradation rate (Hatzinger and Alexander 1995, Scow and Alexander

1992, Chiou et al. 1996, Shaw et al. 2000). Therefore, sorption is one factor that limits both the biodegradation (Sanin et al. 2000) and transport (Reinhart et al.1991, Öman et al. 1999 2001) of hydrophobic organic contaminants (HOCs) in landfills. On the other hand, if microorganisms are able to use sorbed pollutants, the desorption rate would not be a limiting factor for bioavailability. However, many studies showed that chemicals in the aqueous phase are more readily bioavailable than in the sorbed phase (Sanin et al. 2000, Chiou et al. 1996, Shaw et al. 2000). Thus, the rate of mass transfer from the solid to the aqueous phase can limit biodegradation if desorption rate is slower than biodegradation rate However, contradictory results were found by Laor et al. (1996). They found that the mineralization of phenanthrene was not affected by sorption because organisms were able to consume sorbed phenanthrene directly at the same rate as from the free phase.

In landfills, sorption may reduce the bioavailability of HOCs because of the slow desorption of HOCs sorbed to glassy/hard organic matter (Pignatello and Xing 1996, Weber et al. 1995), adsorbed in micropores (Nam and Alexander 1998) and/or encapsulated in paraffinic organic matter (Lerch et al. 1997, Guthrie et al. 1999). Furthermore, the exposure of HOCs to landfill sorbents for long periods of time can enhance HOC sequestration. In the following sections, the factors controlling bioavailability will be discussed.

2.2.1 Physical Factors

Physical factors that reduce the bioavailability of organic contaminants include partitioning into glassy/hard organic matter and adsorption in micropores or on the surfaces of nanovoids in glassy organic matter.

Partitioning into Glassy/Hard Sorbent Organic Matter

"Partitioning" describes the uptake of aqueous compounds into a network or matrix of solids by forces such as van der Waals forces, dipole-dipole interactions, and hydrogen bonding (Xing et al. 1994). Sorbent organic matter can be envisioned as a mixture of

glassy and rubbery polymers. The polymer segments of the glassy phase have higher cohesive forces and are more rigid while those of the rubbery phases exhibit greater mobility and flexibility and can be considered as a dynamic and viscous liquid. The rubbery state of organic matter behaves as a partitioning medium. Consequently, rubbery organic matter exhibits rapid diffuision and linear isotherms. The glassy polymer, due to its rigidity, possesses long-lived, closed internal nanoscale pores that can serve as adsorption sites. "Adsorption" refers to the surface accumulation of a sorbate by physical or chemical bonds at either solid-solid, liquid-solid, gaseous-liquid, or gaseous-solid interfaces. The presence of amorphous polymer segments and internal nanovoids in glassy polymer gives rise to HOC sorption by linear dissolution (partitioning) and nonlinear hole-filling (adsorption) mechanisms. As a result, the total sorption capacity of glassy polymer is the sum of HOC solid-phase concentrations in the partitioning and adsorption domains. Therefore, the dual-mode model has been proposed to describe HOC sorption isotherms for glassy polymers (Weber et al. 1992, Pignatello et al. 1998). Because the relaxation speeds of glassy organic matter are slow, diffusion of solute molecules into and out of condensed and highly cross-linked organic matter could be very slow (Brusseau et al. 1991, Huang and Weber 1996, 1998, Pignatello and Xing 1996, Luthy et al. 1997). According to Xing et al. (1996), for homogeneous glassy polymers such as PVC, the adsorption sites are uniformly distributed, and partitioning into bulk polymer takes place concurrently with adsorption in nanovoids. The sorption rate is limited by diffusion through the bulk polymer because adsorption are ordinarily inactivated or only slightly activated, so adsorption takes place fast. Desorption of HOCs adsorbed on nanovoid surfaces is generally activated, however. As a result, these adsorption sites fill faster than they empty, and HOC desorption from nanovoid surfaces can limit desorption rates (Pignatello and Xing 1995). For SOM, the authors further suggest that adsorption sites are less abundant in external regions and more abundant in internal regions for the soils in their study. In addition, desorption from glassy polymer is hampered not only by slow diffusion of sorbed molecules out of highly cross-linked matrices and nanovoids, but also by continued diffusion into them, i.e. true sorption equilibrium

for glassy polymers may never have been achieved in many experiments.

Sorption/desorption rates of HOCs can be quantified by calculating HOC diffusivities in the sorbent organic matter, and diffusivity values depend on polymer structure as well as penetrant size and shape. Diffusivities of organic compounds in glassy polymer are more sensitive to the size and shape of sorbates than in rubbery polymers. Diffusivities in rubbery polymers are generally several orders of magnitude larger than in glassy polymers. It was reported that the diffusivity of CCl_4 at 25-30°C is $10^{-7} cm^2/s$ in rubbery polyethylene, but only $10^{-17} cm^2/s$ in glassy poly(vinyl chloride) (Pignatello and Xing, 1996).

The holes in glassy polymer are flexible and may be deformed by the penetrant, that is, the glassy region could be softened by the penetrant, which can lead to the destruction of holes due to the relaxation of the glassy matrix (Xia and Pignatello 2001). After the glassy region is converted to the rubbery sate, mass transfer rates of organic compounds from the solid phase to the aqueous phase would be enhanced.

The structure of natural organic matter varies with geological age. Overtime, diagenetic processes transform relatively young, expanded, lightly cross-linked "rubbery" organic matter into more condensed, highly cross-linked, more aromatic "glassy" organic matter (Weber et al. 1995). Consequently, more highly diagenetically altered organic fractions yield nonlinear isotherms and lower HOC diffusivities.

Adsorption in Micropores

A second mechanism that has been proposed to explain the reduced bioavailability of organic pollutants is the adsorption of organic contaminants in micropores (Ball and Roberts 1991). The classification of pores is inconsistent between the International Union of Pure and Applied Chemistry (IUPAC) and Soil Science Society of American (SSSA), and Table 2.2 sumarizes the classifications used by IUPAC (1972) and SSSA (1997). In this study, the IUPAC convention was adopted. Organic pollutants can slowly diffuse into extremely small pores ($<1\ \mu m$), in which microorganisms are absent because of size exclusion effects. It was observed that bacteria mainly live in pores with sizes of 0.8-3 μm (Bosma et al. 1997). Nam and Alexander (1998) found

that little phenanthrene was biodegraded when sorbed to hydrophobic polystyrene beads that contained micropores. This result suggests that the bioavailability of hydrophobic compounds can be greatly reduced by particles containing micropores with hydrophobic surfaces. They further found that the bioavailability of sorbed HOCs was not reduced when sorbents contained micropores with polar surfaces or no micropores. The small diffusivity of HOCs in micropores can be explained by the multipoint interaction between micropore walls and sorbates in pores with dimensions that are roughly similar to the sorbate diameter. As a result, the sorbate interacts with both pore walls, which can increase the interaction potential up to 5-fold, compared to that for adsorption on a planar surface (Pignatello and Xing 1996).

Table 2.2 Classification of pore size

	Macropores	Mesopores	Micropores
IUPAC (1972)	>50 nm	2-50 nm	<2 nm
SSSAC (1997)	>75 μm	30-75 μm	5-30 μm

2.2.2 Chemical Factors

Hydrophobic Interactions

Hydrophobic interaction describes the sorption of organic contaminants to organic matter via bonding mechanisms that involve the hydrophobic sites of both the sorbate and the sorbent (Lerch et al. 1997). Hydrophobic interaction has been considered as the primary mechanism by which herbicides are sorbed to soils (Chiou et al. 1979, Karickhoff 1981). Lerch et al. (1997) studied the sorption of hydroxylated atrazine degradation products (HADPs) to soils, and found that cation exchange and hydrophobic interaction mechanisms controlled HADP sorption to soil. Their study also showed that hydrophobic interaction and cation exchange mechanisms rather than irreversible covalent bonding assumed in previous studies could explain why some fraction of atrazine residues was not bioavailable. Guthrie et al (1999) also suggested that pyrene was non-covalently associated with hydrophobic sites of humin.

The noncovalent interaction between pyrene and humin probably involved van der Waals forces and hydrogen bonding, which were strong enough to prevent removal of pyrene by solvent extraction methods.

Humification

Humus is a complex and rather resistant mixture of brown or dark-brown amorphous, colloidal substances synthesized from the tissues of decomposing plants, animals and microorganisms (Brady 1974). Humic materials are usually divided into three fractions: humic acid, fulvic acid and humin. Humification refers to irreversible chemical reactions that incorporate organic compounds into humic polymers. Both biological and nonbiological mechanisms are involved in humification (Michel et al. 1995), and binding of xenobiotics to humic substances can take place under both aerobic and anaerobic conditions (Bollag and Loll 1983). The latter study showed that xenobiotic phenols had to be oxidized by enzymes to aryloxy free radicals in order to undergo binding to humic substances (Bollag et al. 1983, Sarker 1988). A study by Kazano et al. (1972) indicated that oxidative polymerization or oxidative coupling is an important mechanism by which phenols are incorporated into humic substances. Wolf and Martin (1976) found that 12% of the radioactivity from ^{14}C-labelled 2,4-dichlorophenoxyacetic (2,4-D) was incorporated into humic-like polymers produced by fungi. The results suggested that phenolic derivatives of the pesticide polymerized with the humic substances by oxidative coupling. Dec et al. (1997) investigated the binding mechanisms for soil-bound residues of the fungicide cyprodinil and demonstrated that a considerable portion of the fungicide underwent cleavage between the aromatic rings followed by covalent binding of the separated phenyl and pyrimidyl moieties to humic acid. At same time, a fraction of the unaltered fungicide was sequestered in humic matter by physical forces. It has been widely accepted that bound xenobiotic residues persist in soil and become immobilized. Microbial release studies for humified chlorophenols and catechol showed that less than 5% of the xenobiotics appeared extractable in the methylene chloride after 13 weeks (Dec and Bollag 1988). Nonetheless, Dec et al. (1990) showed that humification of ^{14}C-labeled,

2,4-dichlorophenol did not preclude $^{14}CO_2$ production.

2.3 Factors Affecting Sorption

Many factors can affect the extent and rate of HOC sorption. Among them are sorbent and sorbate properties, dissolved organic compounds in the aqueous phase, pH and temperature.

2.3.1 Sorbent Effects

Regarding sorbent properties, the organic fraction of soils and sediments primarily contributes to the sorption of hydrophobic organic compounds (Karickhoff et al. 1979, Means et al. 1982, Chiou et al. 1979). Consequently, partition coefficients (K_p) normalized to the organic carbon content (f_{oc}); i.e., $K_{oc} = K_p/f_{oc}$, have been used to compare HOC sorption capacities of soils and sediments. Lambert et al. (1965) pointed out that not all organic matter in soils and sediments was active in the sorption process and suggested that various soils be indexed according to their active fraction. A technique for calculating percent "active" organic matter was provided in their study. Isaacson et al. (1984) studied the sorption of three phenols by two sediment fractions, and found that sorption mechanisms involved hydrogen-bonding interactions between sorbate phenolic hydroxyl groups and hydrogen-bonding sites on the sediment organic matter in addition to hydrophobic interactions. The penetrability and accessibility of organic matter associated with sediment had a major impact on the sorption behavior related to hydrogen-bonding interactions; i.e., the sediment fraction with the more condensed and rigid structure was less easily penetrated by solute and exhibited lower sorption capacity than the fraction with relatively loose structure.

There is growing awareness that the affinity of SOM for HOCs depends on its origins and histories. Grathwohl (1990) demonstrated that the composition and structure of organic matter varies due to its origin and geological history and strongly influences the sorption affinity for HOCs. Organic matter in unweathered shales and

high-grade coals showed one order of magnitude greater sorption capacity than organic matter in recent soils or geologically young material, or low-grade coal. Weber et al. (1992) made similar inferences with respect to the shale fraction of soils. Young and Weber (1995) measured the sorption of phenanthrene on two "young" soils of relatively high organic carbon content and one ancient shale material containing a lower organic carbon content. They showed that organic matter from shale sorbed phenanthrene much stronger than that from "young" surface soils.

Numerious studies have shown that the sorption of HOCs to soils and sediments is dependent not only on organic carbon contents but also on the hydrophobicity of the organic matter, which is controlled by its hydrogen, oxygen and nitrogen contents (Garbarini and Lion 1986, Carter et al. 1982, Schwarzenbach et al. 1981, Isaacson et al. 1984, Kile et al. 1995, Grathwohl 1990). High C/O or H/O ratios in the organic sorbent indicate relatively low amounts of oxygen-containing functional groups and thus the presence of hydrophobic sorbent organic matter with a large sorption capacity for HOCs. Garbarini and Lion (1986) reported that lignin with a C/O ratio of 2.6 has a higher HOC sorption capacity than humic acids with a C/O ratio of 0.93. The ratio $(O + N)/C$, defined as the polarity index of a sorbent by Rutherford et al. (1992), describes the ratio of polar to nonpolar groups in sorbent organic matter. They observed that K_{oc} decreased as the polarity index increased. Similarly, Xing et al. (1994) observed that K_{oc} values describing the sorption of benzene, toluene and *o*-xylene to organic sorbents decreased with increasing polarity index. However, Öman and Camilla (1999) observed no correlation between partition coefficient (K_p) of organic compounds and H/C,O/C or H/O atomic ratios of municipal solid waste samples.

Stuer-Lauridsen and Pedersen (1997) used the normalized sorption parameter ($\log K_{oc} - \log K_{ow}$) to compare K_{oc} values from several studies involving sorbates with different $\log K_{ow}$ values. They grouped sorbents into several categories, including sorbents of geological origin, peat and muck soils, extracts of soils, commercially available humic acids, extracts of dissolved organic matter, and non-processed biological materials. Non-processed biological materials referred to materials that were not

altered by biological or chemical procesess and included sorbents such as cellulose, zein, lignin, tannic acid. They found that sorption was most strongly correlated with the sorbent polarity index for materials of geological origin such as coal, shale, lignite, anthracite as well as for non-processed biological materials. However, sorption was independent of the polarity index for organic materials that had undergone biological or chemical processing such as peat and muck soils, as well as soil extracts (humic acid, fulvic acid, extracted peat).

Biopolymer composites in municipal solid waste decompose as a result of biological activity in landfills. The preferential degradation of polar biopolymers increases the hydrophobicity of sorbent organic matter. As previously shown for sediments, biologically mediated increases in sorbent hydrophobicity can lead to enhanced HOC sequestration (Guthrie et al. 1999). Guthrie et al. (1999) demonstrated that alcohols, carbohydrates and proteins in the humin fraction of sediments were biodegraded after 60 days of incubation, whereas aromatic and paraffinic functional groups were preserved. Degraded sediments were less polar and the amount of sequestered hydrophobic pollutants increased. Similar effects may be expected in landfills. It has been observed that the organic carbon content of MSW components decreases in landfills (Reinhart et al. 1990, Pichler and Kögel_knabener 2000) as a result of the preferential degradation of polar biopolymers such as cellulose and hemicellulose (Eleazer et al. 1997, Pichler and Kögel_knabener 2000). Reinhart et al. (1990) found that the sorption capacity of stable refuse decreased as compared to fresh refuse due to the loss of sorbent organic matter during stabilization. Pichler et al. (2000) measured the loss of organic matter in municipal solid waste in an anaerobic fermentation system. They observed that losses of cellulose and non-cellulosic carbohydrates (i.e. hemicellulose) were greatest during the initial 2.5 weeks of fermentation treatment. Lipid and protein losses were much lower due to microbial resynthesis and recalcitrance and no lignin was degraded. Their study clearly showed a shift of organic mater in MSW toward recalcitrant components.

2.3.2 Sorbate Effects

The structure of the sorbate (nature, size and reactivity of functional groups) also affects sorption (Brusseau and Rao 1989, 1991). Numerous studies showed that increasing sorbate hydrophobicity enhanced sorption to organic matter (Karickhoff et al. 1985, Wu et al. 1986). Moreover, a linear correlation between $\log K_{oc}$ and $\log K_{ow}$, the sorbate octanol/water partition coefficient, has been observed for soils and sediments (Karickhoff et al. 1979, Schwarzenbach and Westall 1981). These correlations illustrate that the HOC sorption capacity increases with increasing K_{ow}; i.e., with increasing sorbate hydrophobicity. Reinhart et al. (1990) studied the sorptive behavior of selected organic pollutants on MSW and suggested that $\log K_p$ was linearly correlated with $\log K_{ow}$, a result consistent with previous studies investigating HOC sorption to soils and sediments. Öman and Spännar (1999) also examined the sorption of organic compounds to six landfill samples. A linear correlation between $\log K_p$ and $\log K_{ow}$ was demonstrated in agreement with the results of Reinhart et al. (1990).

Using literature data, Brusseau and Rao (1989) investigated the effect of sorbate structure on the rate and magnitude of chlorinated alkene, chlorobenzene, alkylbenzene and polyaromatic hydrocarbon sorption to soils. They reported that relatively complex sorbates such as pesticides exhibited significantly higher non-equilibrium sorption than simpler sorbates such as alkylbenzenes and chlorobenzenes. Brusseau and Rao (1991) confirmed that sorbate with complex branched structures such as pesticides diffused more slowly than unbranched sorbates such as benzene and chlorobenzene for a given sorbent and solvent. They hypothesized that the addition of functional groups to a molecule led to an increased potential for entanglement with the sorbent organic matter matrix. As a result, diffusion was constrained. Furthermore, they found that the diffusion coefficient decreased exponentially with increasing molecular weight or the size of sorbate. Piatt et al. (1998) studied the sorption of homologous series of polycyclic aromatic hydrocarbons, alkylated benzenes, chlorinated benzenes and chlorinated alkenes to two soils and indicated that the diffusion coefficients for

the most soluble HOCs (benzene, toluene and DCB) were almost two orders of magnitude higher than phenanthrene and pyrene. Their results also confirmed that the diffusion within SOM matrix was highly dependent on sorbate shape/structure.

2.3.3 Solvent Effects

The nature of the solvent (e.g., solvent polarity, presence of dissolved organic matter) affects HOCs sorption (Rao et al. 1990, Brusseau et al. 1991, Nkedi-kizza et al. 1989). At waste-disposal sites, mixtures of multiple solvents may exist, and organic cosolvents may affect the solubility of HOCs. Rao et al. (1990) suggested that the presence of organic cosolvent could enhance HOC solubility, which was reflected by decreased sorption to soils and increased mobility of HOCs.

Another possible solvent effect on sorption is the binding of organic pollutants to dissolved humic substances. Humic substances are the most significant component of dissolved organic matter in aquatic systems. HOCs associate with hydrophobic sites in humic materials to form solute-humate complexes as a result of hydrophobic interaction (Rebhun et al. 1992). Binding of organic pollutants by humic substances could reduce or enhance the sorption of organic solutes (Hasset and Anderson 1979, Carter and Suffet 1982).

In landfills, solid wastes are leached by rainwater, which result in the solubilization or suspension of high concentrations of organic matter in the liquid phase; i.e., the leachate (Imai et al. 1995). As described by Farquhar et al. (1973), there are two types of leachate that are related to the fermentation stage of refuse. Leachate produced in the acidification stage is called acidogenic leachate while leachate produced in the methane fermentation stage is called methanogenic leachate. In the acidification stage, complex organic compounds are fermented anaerobically, and soluble organic acids (e.g., volatile fatty acids), amino acids and other low molecular weight compounds and gases like H_2 and CO_2 are produced. Free volatile acids are fermented to CH_4 and CO_2 as gaseous end-products in the methane stage.

The characteristics of leachate are highly variable depending on the composition of the solid waste, rate of water application, refuse moisture content, landfill design,

operation and age. The composition of organic compounds in leachate has been analyzed by some researchers (Chian and De Walle 1977, Harmsen 1983, Schultz et al. 1986). Harmsen (1983) identified that free volatile fatty acids in acidogenic leachate contributed to 95% of the TOC, while volatile amines and ethanol were present at 0.8 and 0.7% of the TOC, respectively. About 32% of the organic carbon in methanogenic leachate consisted of compounds with a molecular weight >1000 Da. Volatile fatty acids, volatile amines and ethanol could not be detected. Schultz et al. (1986) also detected that low concentration of aromatic hydrocarbons, including benzene, various xylenes, and toluene in leachate.

Dissolved organic compounds in landfill leachate may bind organic contaminants and thus affect HOC sorption to MSW (Larsen et al. 1992, Bauer and Herrmann 1998). Reinhart et al. (1990) studied the sorptive uptake of 1,4-dichlorobenzene (DCB) by refuse from distilled water and from acidogenic leachate and suggested that acidogenic leachate with a high volatile fatty acid concentration did not affect sorption. Larsen et al. (1992) evaluated the effects of different methanogenic leachates on the sorption of organic compounds on aquifer materials. A methanogenic leachate with a high DOC concentration (about 600 mg/L) reduced the partition coefficient by approximately 50%, but a different leachate increased contaminant sorption relative to groundwater. They suggested that landfill leachate may increase the distribution coefficients and mobility of HOCs. Bauer and Herrmann (1998) demonstrated that dissolved organic matter in landfill leachate appeared to contribute to the high aqueous solubility of phthalate esters. Their results suggested that the fraction of phthalate esters (PAEs) transported by suspended solids in landfill was less important than that resulting from the solubilization of the hydrophobic PAEs by dissolved organic matter.

2.4 Desorption

Desorption rates are critical in determining bioavailability of sorbed HOCs in the environment. As biodegradation proceeds, HOC concentrations in solution are depleted and a concentration gradient develops. Consequently, sorbed contaminants diffuse back into solution. Thus, the rate of HOC mass transfer from the solid phase to the aqueous phase can limit the overall remediation rate of sorbed compounds (Chiou et al 1998, Shaw et al. 2000).

2.4.1 Desorption Hysteresis

It is often observed that the desorption isotherm is not same as the sorption isotherm, and this difference is known as sorption/desorption hysteresis (Brusseau and Rao 1991, Kan et al. 1994). Differences in sorption and desorption isotherms can increase with sorbent-solute contact time because HOCs become increasingly desorption-resistant. This phenomenon is commonly termed "aging" (Hatzinger et al. 1995, Huang et al. 1997, Pignatello 1993). Hysteresis behavior between sorption and desorption can be attributed to experimental artifacts and non-artifactual mechanisms.

Experimental artifacts involved in sorption and desorption hysteresis may result from: (1) equilibrium being attained in the sorption step but not in the desorption step, (2) equilibrium being reached only in desorption step but not in the sorption step, or (3) equilibrium not being reached in either step. These artifacts are commonly due to short contact time such as several hours to several days (DiToro et al. 1982, Kan et al. 1994, Huang et al. 1998). Another common type of experimental artifact is the loss of sorbate to dissolved organic matter and colloidal particles in the aqueous phase when the aqueous phase is intermittently replaced by clean water for studying desorption. Thus, an apparent change in the equilibrium distribution of solute may be caused by removal of dissolved organic matter and/or colloidal particles (Karickhoff and Brown 1978, Gschwend and Wu 1985). Furthermore, sorbate losses to reactor system components can occur; e.g., teflon stoppers used in many batch reacors are permeable to volatile organics and can absorb low molecular weight

organic compounds (Zief et al. 1976). In experiments with radiochemicals, radiochemical impurities may be mistaken for the studied compound and thus introduce errors in distribution calculations (McCarthy et al. 1986). It has been confirmed that the flame-sealed ampule technique described by several researchers may be best way to avoid slow solute losses to reactor systems for volatile chemicals (Ball and Roberts 1991, Harmon and Roberts 1992, Huang et al. 1998).

Non-artifactual factors that cause desorption hysteresis include (1) entrapment of sorbed molecules within the sorbent organic matter matrix, (2) irreversible chemical bonding of solute to certain components of soil organic matter, and/or (3) adsorption within sorbent micropores.

As discussed in section 2.1, the desorption-resistant fraction of organic compounds may result from the slow diffusion of organic compounds within condensed organic matter, where HOCs become entrapped (Brusseau and Rao 1991, Carroll et al. 1994). Carrol et al. (1994) examined the desorption of PCBs from Hudson river sediment and observed both a rapidly desorbing labile fraction and a slowly desorbing resistant fraction. They proposed that condensed phases of the sediment organic matter contribute to the slow release of PCBs. Diffusion coefficients for PCBs in swollen and condensed phases of sediment organic matter were calculated to be $2.6 \times 10^{-18} cm^2/s$ and $7.3 \times 10^{-21} cm^2/s$, respectively. Burgos et al. (1996) studied the sorption of naphthalene to two soils and observed that about 2-8% of naphthalene that was not extracted after a 2-d sorption period was entrapped within micropores of soils but not covalently bound. However, it is also possible that the formation of strong bonds between organic compounds and solid organic matter may account for the desorption-resistance of organic compounds (Isaacson and Frink 1984, Bhandari et al. 1996, McGroddy et al. 1996). McGroddy et al. (1996) studied the desorption of PAHs from Boston harbor sediments and suggested the desorption-resistant PAH fraction could be result of strong PAH sorption to highly aromatic soot particles in sediment.

It also has been hypothesized that the rate-limiting desorption of HOCs from soils and sediments may be caused by rearrangement of the flexible humic polymer

chains of the SOM after solute sorption. Rearrangement of SOM could potentially block diffusion pathways causing diffusional resistance during desorption. Kan et al. (1997) examined the sorption/desorption of naphthalene and tetrachlorobiphenyl to Lula and surrogate sediments. They observed that desorption-resistant fraction was not time dependent over a period of 6 months, and the surrogate sediment, which is nonporous and homogeneous in organic composition, exhibited similar desorption characteristics as natural sediment. Therefore, the desorption process for their sediments cannot be explained by diffusion-limited transport through heterogeneous organic phases or micropores. They hypothesized that irreversibility may be due to the occlusion of chemicals by cooperative conformational changes of SOM during the sorption process or due to physical rearrangement of SOM. The conformational or physical rearrangement of SOM in the presence of sorbed chemicals could cause the chemical environment of the sorbate to change and hence a portion of sorbed HOC becomes unavailable for desorption. Several other findings support the hypothesis that conformational changes in the amorphous and glassy regions of the SOM may influence the rate of solute mass transfer in the SOM. Brusseau et al. (1991) suggested that the rate of organic pollutant desorption was increased by the ability of organic cosolvents to swell SOM and reduce diffusive resistance. Furthermore, Sahooet al. (1997, 1998) found that nonionic surfactant Triton X-100 was able to increase the mass-transfer coefficient of TCE. It was proposed that surfactants can swell SOM, thus increasing diffusion rates.

2.4.2 Desorption Models

HOC desorption is generally characterized by a two-stage desorption process, in which an initial fast stage (completed within hours) is followed by a long, slow phase (Wu and Gschwend 1986, Pavlostathis and Jaglal 1991, Pignatello and Huang 1991, Pavlostathis and Matharan 1992, Harmson 1994). The slow fraction has also been called desorption-resistant fraction (Pignatello et al. 1993, Harmon and Roberts 1994, Carroll et al. 1994). Fast and slow fractions have been interpreted using models based on chemical kinetics or mass transfer concepts (Pignatello et al. 1993).

Chemical Kinetics

Chemisorption is one of the causes for the slow release of chemicals from sediments and soil (Burgos et al. 1996). Chemisorption occurs when covalent bonds or charge transfer complexes are formed between the contaminant and the sorbent. An example of chemisorption is the binding of phenolic compounds to SOM. However, chemisorption is limited to specific changes of pollutants and usually is not a major consideration for most neutral HOCs (Brusseau et al. 1991, Kan et al. 1998).

Mass Transfer Limitations

The resistances encountered during mass transport include film diffusion (external mass transfer), intraparticle diffusion and intraorganic matter diffusion. Physical mass transfer limitations, such as slow intraparticle diffusion or intraorganic matter diffusion can produce apparent irreversible sorption. Mass transfer limited transport processes are distinct from chemisorption because no covalent linkage are formed between sorbents and sorbates. Mass transfer limited transport has been used to explain the common two stage desorption process observed in many studies (Weber and Miller 1988, Ball and Roberts 1991, Harmon et al. 1994).

Film Diffusion. Sorbing or desorbing HOCs encounter external mass transfer resistance during transport across a fluid boundary layer external to the particle. The film diffusion process is described by the following equation:

$$N = k_f \left(C - C_p \left(r = a \right) \right) \tag{2.1}$$

where, N is the flux of solute per unit area of external surface, $[M_x/L^2T]$, C is the concentration of the well-mixed bulk solution, $[M_x/L^3]$, $C_p\left(r=a\right)$ is the solute concentration at the particle surface (radius=a), $[M_x/L^3]$ and k_f is the film mass transfer coefficient $[L/T]$.

Many researchers have shown that film diffusion is generally not rate-limiting in comparison to other mechanism (Brusseau et al. 1981).

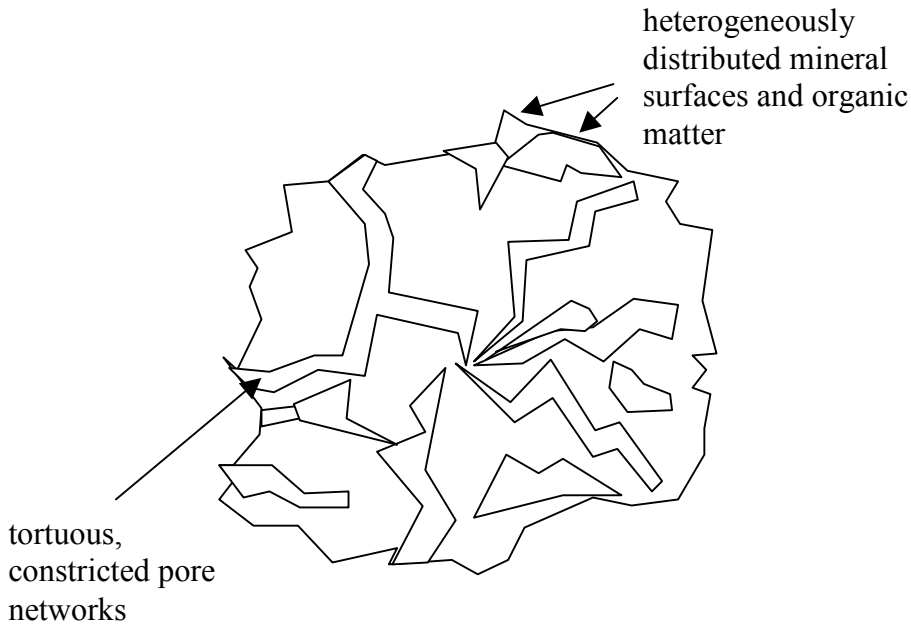

Figure 2-4: Schematic representation of intraparticle diffusion in natural particles

Intraparticle Diffusion. For sediments and aquifer materials, intraparticle diffusion refers to the aqueous-phase diffusion of solute within the pores of microporous particles. The radial pore diffusion model has been employed to characterize mass transfer in porous soils or sediments. Three assumptions are used to simplify modeling: (1) each particle is a porous sphere, (2) pore diffusion is the sole transport mechanism within the particle, and (3) the sorption sites are homogeneously distributed over the pore walls.

For transient conditions of uptake into a sorbent, a mass balance over a volume element of the spherical sorbent particle yields Fick's Second Law:

$$\rho_a \frac{\partial q}{\partial t} + \varepsilon_i \frac{\partial C_r}{\partial t} = \frac{\varepsilon_i D_p}{r^2} \frac{\partial}{\partial r} \left(r^2 \frac{\partial C_r}{\partial r} \right) \tag{2.2}$$

where,

ρ_a = apparent density of the sorbent particle $[M_s/L^3]$;

ε_i = intraparticle porosity [-];

C_r = intraparticle aqueous phase concentration $[M_s/L^3]$;

D_p = effective pore diffusion coefficient $[L^2/T]$;

r = radial coordinate $[L]$;

t = time $[T]$.

For the case of linear partitioning, $q = K_d C_r$, where, q is the equilibrium solid-phase concentration $[M_x/M_s]$, C_r is the equilibrium aqueous concentration $[M_x/L^3]$,and K_d is the partition coefficient $[L^3/M_s]$. By substituting the isotherm equation into equation (2.2), the following expression results:

$$\frac{\partial C_r}{\partial t} = \frac{D_p}{r^2 R_g} \frac{\partial}{\partial r} \left(r^2 \frac{\partial C_r}{\partial r} \right) \tag{2.3}$$

where R_g is the internal or grain retardation factor, which for linear isotherm model is defined by

$$R_g = 1 + \frac{\rho_a K_d}{\varepsilon_i} \tag{2.4}$$

The apparent diffusion coefficient is defined as

$$D_a = \frac{D_p}{R_g} \tag{2.5}$$

For nonlinear isotherms, the Freudlich isotherm expression ($q = K_f C_r^{1/n}$) is typically used, where K_f is the Freundlich capacity coefficient $[(M_x/M_s)/(M_x/L^3)^{1/n}]$ and $1/n$ is the Freundlich exponent.

The resulting diffusion model is similar to equation (2.3), but the grain retardation coefficient is dependent on the aqueous concentration; i.e.,

$$R_g = 1 + \frac{1/n}{\varepsilon_i} \rho_a K_f C_r^{1/n-1} \tag{2.6}$$

Many researchers have suggested that intraparticle diffusion models appropriately describe the uptake of HOCs by sediments and soils. Miller and Pedit (1992) concluded that an intraparticle diffusion model with parameters determined from uptake experiments was able to explain the majority of sorption hysteresis observed for lindane. Wu and Gschwend (1986) applied the spherical intraparticle diffusion model

to quantify the sorption kinetics of four HOCs to three sediments and soils. They demonstrated that the sorption rate was controlled by intraparticle diffusion for natural aggregated sediments and soils. Apparent diffusion coefficients (D_a) ranged from $8 * 10^{-16}$ to $1 * 10^{-13}$ m^2/s. An empirical choice for average soil porosity ($\varepsilon_i = 0.13$) fit the results reasonably well. However, due to soil heterogeneity and the complex structure of natural particles, the use of radial diffusion models with a single diffusion coefficient has been questioned because they frequently failed to account for the complexity of the natural particles (Connaughton et al. 1993, Pedit and Miller 1994, Harmon et al. 1994). Harmon et al. (1994) used a radial diffusion model to describe desorption data of Borden soil and found that the model tended to underestimate the observed desorption rate at early times and to overestimate the observed desorption rate at later times. Consequently, single-parameter, one-compartment desorption models were extended to include two or multiple kinetic compartments, as will be discussed in later sections.

Intraorganic Matter Diffusion. Intraorganic matter diffusion involves the diffusive mass transfer of sorbate within the sorbent organic matter matrix. The primary assumption for the intraorganic matter diffusion model is that sorbent organic matter is a polymeric substance within which the sorbate diffuses. The evidence supporting intraorganic matter diffusion includes (1) inverse correlations between the diffusion coefficient and sorbent organic matter content and (2) organic cosolvents increase the diffusion rate as they "swell" sorbent organic matter. However, these results are also in agreement with pore-diffusion models if the pore walls are coated by organic matter. According to Brusseau et al. (1991), there are two major physical differences between intraorganic matter diffusion and intraparticle diffusion. First, the "pores" associated with organic matter have sizes similar to those of the sorbate molecules, whereas the pores in porous particles are typically larger. Second, the pore networks for porous particles are fixed and rigid, but the "pore network" associated with organic matter is dynamic.

Fick's second law of diffusion can be used to express HOC diffusion into spherical

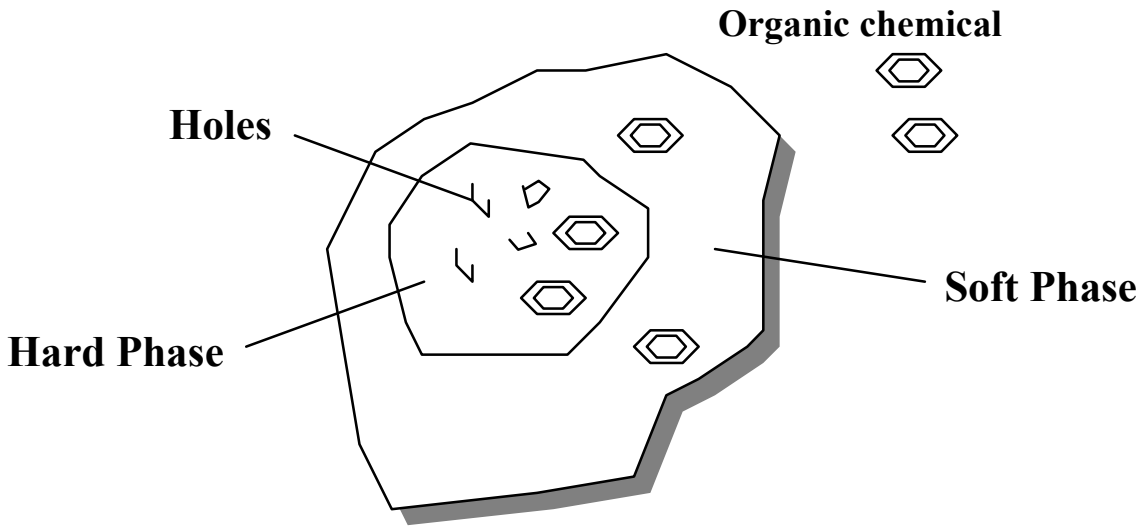

Figure 2-5: Schematic representation of intraorganic diffusion

polymer particles:

$$\frac{\partial q_r}{\partial t} = \frac{D}{r^2}\frac{\partial}{\partial r}\left(r^2\frac{\partial q_r}{\partial r}\right) \tag{2.7}$$

Where D is the intraorganic matter diffusion coefficient [L^2/T], q_r is the intraparticle solid-phase concentration [M_x/M_s], r is the radial position [L], and t is time [T].

Carroll et al. (1994) suggested modeling humic matter in sediment as two types of polymer phases; i.e., as glassy and rubbery phases, and assume that intraorganic matter diffusion is the rate-limiting mechanism. However, it is usually difficult to model SOM as a polymer because SOM properties are highly variable and the structure of SOM can be affected by soil minerals. For a given polymer, the diffusion coefficient is dependent upon the nature and extent of polymer cross-linking as well as the nature of the diffusing molecule, the HOC concentration, and solvent properties (Ball and Roberts 1991, Brusseau et al. 1991). Since little is known about the nature of solute diffusion in natural organic matter, *a priori* estimation of intraorganic matter diffusivity is quite difficult. Therefore, future work is needed to find appropriate polymer models for determining organic matter diffusivities in natural particles.

Two-Compartment Model

Two-compartment models can be divided into two types with respect to the way the rate-limited stage is incorporated: (1) first-order mass transfer models, that are based on a linear driving force approximation (Karickhoff et al. 1980 and 1985, Cornelissen et al. 1997, Johnson et al. 2001), and (2) diffusion models, that are based on Fickian diffusion (Berens and Huvard 1981, Brusseau and Rao 1991, Caroll et al. 1994).

The conceptual model for two compartments is described as follows:

$C \rightleftharpoons S_1 \rightleftharpoons S_2$,

where C denotes the solution phase HOC concentration, and S_1 and S_2 denote solid-phase HOC concentration in the labile and nonlabile sorption compartments, respectively.

Three-Parameter Biphasic First Order Mass Transfer Model. The first order mass transfer model describes the desorption of the labile and resistant HOC fractions using first-order rate equations expressions:

$$\frac{q(t)}{q_0} = \phi_s \exp(-k_s t) + \phi_r \exp(-k_r t) \tag{2.8}$$

where, $q(t)$ is the solid-phase sorbate concentration at time t, q_0 is the initial solid-phase sorbate concentration, ϕ_s is the slowly desorbing HOC fraction, $\phi_r (= 1 - \phi_s)$ is the rapidly desorbing HOC fraction, and k_s and k_r are apparent first-order rate constants describing HOC desorption from the slow and rapid compartments, respectively. Such a three-parameter biphasic model has been applied to successfully fit experimental desorption data measured by either batch or gas purge techniques (Karickhoff et al. 1980, 1985, Cornelissen et al. 1997, Johnson et al. 2001). Karickhoff and Morris (1985) studied the sorption and desorption of pyrene, pentachlorobenzene and hexachlorobenzene to eight sediments. A two-compartment model interpreted sorption and desorption data well, and they found that aggregation was responsible for slowing the release of the contaminant from cohesive soils at high sediment concentration.

The advantage of this model is that its parameters are useful for distinguishing the labile and resistant desorption fractions of organic contaminants, and also it is not computationally demanding.

Three-Parameter Biphasic Polymer Diffusion Model. The biphasic first order mass transfer model above is largely an empirical model. Using a more mechanistic approach to describe HOCs desorption from sediments, Carroll et al. (1994) employed a biphasic polymer diffusion model; i.e.,

$$\frac{q(t)}{q_0} = \frac{6}{\pi^2} \sum_{n=1}^{\infty} \frac{1}{n^2} \left[f_r \exp(\frac{-4n^2\pi^2 D_r t}{a_r^2}) + (1 - f_r) \exp(\frac{-4n^2\pi^2 D_s t}{a_s^2}) \right] \tag{2.9}$$

where, f_r is the rapidly desorbing HOC fraction, D_r and D_s are the diffusion coefficients for the rapidly and slowly diffusing HOC fractions, respectively, and a_r and a_s are the corresponding equivalent spherical diameters. Adjustable parameters in this model are f_r, D_r/a_r^2, and D_s/a_s^2.

The model was originally developed by Berens and Huvard (1981) to analyze the desorption kinetics of small organic molecules from poly(vinyl chloride) powders with a range of particle diameters. The model modified by Carroll et al. (1994) assumes that the organic matter in sediment is composed of both swollen and condensed spherical polymer phases, and that HOC diffusion within sediment organic matter controls the rate of HOC desorption. The desorption process for HOCs sorbed in the swollen, rubber-like polymer phase is fast; in contrast, HOCs sorbed in condensed, glass-like polymer phases is desorption resistant. Therefore, two diffusion coefficients, one for the swollen polymer phase, and one for the condensed polymer phase are needed to model the desorption process. The model fit PCB desorption data from river sediments successfully by assuming that humic organic matter in river sediments is comprised of a network of interconnected swollen and condensed spherical polymeric phases bound to the mineral surfaces of the sediments (Carroll et al. 1994). Johnson et al. (2001) also applied this model to describe phenanthrene desorption data from

geosorbents and found that this model was superior to five other desorption models, including the above-described biphasic first-order mass transfer model and the distributed rate model described below.

Distributed-Rate Model

Recent papers have considered a new mathematical model to interpret sorption/desorption kinetics because one- and two-stage diffusional models do not always capture the complexity of HOC diffusion in geosorbent particles (Steinberg et al. 1987, Weber et al. 1992, MsGroddy et al. 1995). Distributed-rate model was therefore proposed to account for soil heterogeneity. This model replaces one- or two-stage mass transfer rate coefficients with a continuous distribution of mass transfer rate coefficient. Both *Gamma* and log-normal distributions have been tested to generate rate coefficient distributions (Culver et al. 1997, Kan et al. 1997, Deitsch et al. 2000). The probability density function of the *Gamma* distribution is given by

$$P(\alpha) = \frac{\beta^{-\eta}\alpha^{\eta-1}}{\int_0^\infty x^{\eta-1}\exp(-x)dx}\exp(-\frac{\alpha}{\beta}) \tag{2.10}$$

where α is the mass transfer rate coefficient, η (the shape parameter) and β (the scale parameter) are positive parameters, and x is a dummy variable of integration.

The probability density function of the log-normal distribution is given by

$$P(\alpha) = \frac{1}{\sqrt{2\pi}\sigma\alpha}\exp\left(-\frac{1}{2\sigma^2}(\ln(\alpha)-\mu)^2\right) \tag{2.11}$$

where μ and σ are distribution parameters.

In this model, the sorbent is discretized into a finite number of compartments to numerically approximate the continuous distribution of mass-transfer rate coefficient. For a CSTR reactor, the distributed-rate model results in the following expression

(Culver et al. 1997, Deitsch et al. 2000):

$$\begin{aligned} \frac{dS_T}{dt} &= \sum_{i=1}^{N} \alpha_i \left(f K_d C - S_i \right) \\ \frac{dC}{dt} &= -\frac{M_s}{V} \sum_{i=1}^{NK} \alpha_i \left(f K_D C - S_i \right) - \frac{k}{V} C \\ S_T &= \sum_{i=1}^{NK} S_i \\ f &= \frac{1}{NK} \end{aligned} \tag{2.12}$$

where, S_T = the total sorbed concentration $[M_x/M_s]$;

α_i = the first order mass-transfer rate coefficient for compartment $[1/T]$;

f = the mass fraction of the solute sorbed in each compartment at equilibrium;

K_d = the distribution coefficient $[L^3/M_s]$;

C = the aqueous solute concentration $[M_x/L^3]$;

S_i = the solute mass sorbed in compartment i $[M_x/M_s]$;

M_s = the mass of sorbent in the reactor $[M_s]$;

V = the liquid volume $[L^3]$;

N = the number of compartments;

k = a rate coefficient $[L^3/T]$ that accounts for solute losses resulting from sorption to the reactor system.

Culver et al. (1997) tested both *Gamma* and log-normal probability distributions for simulating the desorption of TCE from contaminated soils, and the two-site kinetic model was also used as a comparison. The *Gamma* and log-normal probability distribution models provided similar fitting ability for their desorption study. Compared to the two-site kinetic model, the distributed mass-transfer rate model provided a better fit for long-term desorption tests because the two-site kinetic model overestimated the aqueous phase concentration when aging times exceeded 4 weeks. Deitsch et al. (2000) simulated the sorption and desorption rates of 1,2-dichlorobenzene from five natural sorbents with a distributed-rate model that used the *Gamma* distribution

to generate the distribution of first-order rate coefficients. They demonstrated that a significant fraction of the 1,2-dichlorobenzene appeared to be desorption-resistant after a 2-day sorption period. However, the rate of desorption and the fraction of desorption-resistant sites were not a function of contact time for all sorbents but one. A *Gamma* distribution was also used by Connaughton et al. (1993) to model naphthalene desorption from long-term contaminated soils. They found that the *Gamma*-distributed rate model provided a superior fit to the experimental data than the single rate coefficient model. Chen et al. (1995) also demonstrated that the *Gamma*-distributed rate model provided a superior fit to experimental data for pesticide transport in soil columns than those of two-site kinetic model and the single parameter spherical diffusion model.

Chapter 3

Experimental Design and Methods

To achieve the objectives described in Chapter 1, experiments were performed to characterize model MSW components, and to measure toluene and *o*-xylene sorption to and desorption from MSW components in different aqueous phases. Details of the employed materials and experimental methods are described in this chapter.

3.1 Model Municipal Solid Waste Components and Characterization

3.1.1 MSW Components

The major components of MSW that are expected to sorb hydrophobic organic contaminants (HOCs) include paper, plastics, and food and yard waste. Newsprint and office paper were chosen to represent the range of paper types disposed in landfills. Newsprint represents about 5.1% of MSW and office paper 3.2% (U.S. EPA 1999). Newsprint was collected from The News & Observer Recycling Division (News & Observer Publishing Co., Garner, NC). Newsprint is a mechanical pulp that contains nearly all of the lignin present in wood while office paper is a chemical pulp from which most of the lignin has been removed. As a result, cellulose and hemicellulose are the dominant compounds of office paper. Office paper was collected from the NC State University recycling center. Upon receipt, both office paper and newsprint were shredded into 2-cm squares. Rabbit food (Manna Pro Corporation, St. Louis, MO)

was used to represent a combination of food and yard waste. Rabbit food contains both simple and complex carbohydrates as well as proteins in the form of alfalfa, wheat, soy, and oat products, and it has been used to represent food and yard waste previously (Schwab 1994). High-density polyethylene [HDPE] and poly(vinyl chloride) [PVC] (Catalog numbers 42,799-3 and 18,958-8, Sigma-Aldrich Milwaukee, WI) were tested to represent rubbery and glassy plastic components of MSW, respectively. The crystallinity of HDPE is about 80% while PVC is only slightly crystalline with a crystallinity range of 5 to 10%.

Anaerobically degraded forms of office paper, newsprint and rabbit food were prepared in laboratory reactors using leachate recycle and neutralization as described by Eleazer et al. (1997), except that substrates were seeded with anaerobic sewage sludge instead of well-decomposed refuse. Reactors containing shredded office paper and newsprint were operated for about 9 months to obtain materials that, based on their methane yield, were significantly decomposed relative to the starting materials. Reactors containing rabbit food were operated in semi-batch mode to control excessive volatile fatty acid (VFA) production that otherwise resulted from its rapid biodegradation. Over a 9-month period, rabbit food was added to reactors on a daily to weekly basis, depending on the stability of methane production in the system.

3.1.2 MSW Component Characterization

The physical and chemical characteristics, including cellulose, hemicellulose, lignin, lipophilc extractives, protein as well as elemental composition and BET surface area were measured for each MSW component. The analytical methods for cellulose, hemicellulose and lignin have been described (Wang et al. 1997). Lipophilic extractives were measured by Soxhlet extraction according to the method described by Wu et al. (1995). A known mass of dry, ground MSW sample was placed into a cellulose thimble, which was placed into a Soxhlet extractor. Each sample was extracted with a toluene/ethanol mixture (1:2.3 v/v) for 3 hrs, the extract was evaporated at 100°C and the residue after evaporation was dried at 80°C for 2 hours, and cooled down to room temperature in a desiccator before gravimetric determination of the lipophilic

extractives content. Crude protein content was calculated as 6.25 times the N content (Sweeney 1989). Ash contents were determined by combusting 2 g of dry sample at 550°C for 2 hrs. BET surface area was determined from N_2 adsorption isotherm data collected at 77K. Nitrogen adsorption experiments were conducted using an Autosorb-1 Physisorption Surface Analyzer (AS1MP-LP, Quantachrome, Boynton Beach , FL).

To minimize interference from inorganic compounds, elemental analyses were performed on materials that had been washed with 1N HCl until a constant pH was reached and rinsed with organic-free water until the pH returned to neutral. C, H, and N analyses were performed with a CHN analyzer (Perkin-Elmer PE2400 CHN Elemental Analyzer, Perkin Elmer Corp., Norwalk, CT), and oxygen contents were determined according to ASTM D5622 (Huffman Laboratories, Golden, CO).

At the University of Oklahama, ^{13}C nuclear magnetic resonance (NMR) spectra were obtained with a Chemagnetics CMX-II solid-state NMR spectrometer operating at 75.694 MHz and using a Chemagnetics 5-mm double resonance magic-angle spinning probe. A quasi-adiabatic sequence (Zhang et al. 1994) using two-pulse phase modulation (TPPM) decoupling (Bennett et al. 1995) at 75 kHz was employed. The ^{13}C cross polarization (CP) contact pulse of 1 ms length was divided into 11 steps of equal length with ascending radio-frequency field strength, while the ^{1}H contact pulse had constant radio-frequency field strength of 301.00 MHz. At least 720 scans were acquired with a delay of 15.0 s. The sample spinning frequency was 6.0 kHz, maintained to within a range of +/- 5 Hz or less with a Chemagnetics speed controller.

The particle density of MSW components was measured by water displacement analysis as described by Ball et al. (1990). Except for PVC, the mean diameters of solid materials were obtained from image analysis (MetaMorph, Universal Imaging Corp., Downingtown, PA). The mean diameter of PVC (140 μm) was provided by the manufacturer.

3.2 Sorbates

Toluene and *o*-xylene, two alkylbenzenes with different polarities, were selected as organic contaminants because they are frequently detected in landfill leachates (Christensen et al. 1994), sorb to refuse (Sanin et al. 2000), and biodegrade (toluene, Sanin et al. 2000) or have potential to biodegrade (*o*-xylene). Experiments were conducted with ^{14}C-labeled compounds (Sigma-Aldrich). Stock solutions were prepared by dissolving neat ^{14}C-labeled compounds in 6 mL methanol (HPLC-grade, Fisher Scientific, Pittsburgh, PA) and stored at -10°C. Toluene and *o*-xylene concentrations were assayed by liquid scintillation counting. The purity of ^{14}C-labeled compounds was assessed by gas chromatographic analysis that showed peaks corresponding to toluene and *o*-xylene only as well as sparging tests that showed that 99.85 and 99.4% of the ^{14}C was volatile in aqueous toluene and *o*-xylene solutions, respectively. The remaining non-volatile ^{14}C counts were non-sorbable, and all data were corrected for this non-sorbing impurity.

3.3 Leachates

Three leachates were used in the study: laboratory-generated acidogenic leachate, laboratory-generated methanogenic leachates (methanogenic leachate A) and methanogenic leachate collected from the Greensboro, NC, landfill (methanogenic leachate B). Acidogenic leachate was produced by recirculating water through fresh residential refuse. The leachate was not neutralized to maintain the refuse in the acid-phase of decomposition, which was confirmed by a low leachate pH and the absence of gas production. Methanogenic leachate A was generated in the laboratory from decomposed refuse. Methanogenic leachate B was collected from a site that was actively producing methane at the Greensboro landfill. Acidogenic leachate was filtered through 0.45 μm membrane filter catridge prior to storage at 4°C. Methanogenic leachates A and B were stored in a 55-gallon drum at 4°C with minimum headspace.

Leachate characterization included measurement of DOC, pH, chemical oxygen

demand (COD), UV absorbance at 254 nm (UV_{254}), conductivity and molecular size distribution. DOC of the leachates was measured by a Shimadzu 5000A TOC analyzer (Shimadzu Scientific Instruments Inc., Norcross, GA). UV_{254} was determined with a spectrophotometer (Shimadzu spectronic-210 UV) and COD was determined by the colorimetric, closed reflux method (HACH Co., Loveland, Colo). The pH was measured with a ORION-420A pH meter (ATI ORION, Boston, MA). Conductivity was measured with a conductivity meter (Fisher Scientific, Pittsburgh, PA). High-pressure size exclusion chromatography (HPSEC) was used to measure both number- and weight-averaged molecular weights according to the method of Zhou et al. (2000). A Water Protein-Pak 125 modified silica column (Waters Corp., Milford, MA) was used. The system was calibrated with sodium polystyrene sulfonates (PSS) standards with molecular weights of 1.8, 4.6, 8, 18, 35, and 100 kDa (Polysciences Inc., MA) as well as salicylic acid (138 daltons, 99.999% purity, Aldrich). The concentration of standards was 100 mg/L. Acetone was used to determine permeation volume, and blue dextran was used to determine column void volume. Although the HPSEC column was rated from 2000-80000 Da, the calibration curve was log-linear for PSS standards, salicylic acid and acetone, in agreement with the results observed by Chin et al. (1994) and Pelekani et al. (1999). Leachate organic matter was detected with a variable wavelength detector set at 254 nm (Dionex Corp., Sunnyvale, CA). To determine the fulvic acid content of methanogenic leachate A, an XAD-8 column ($k_{0.5} = 5$) was used following the method of Leenheer (1981). The methanogenic leachate A was acidified to pH=1.5 and then passed through a 54 mL glass column packed with 50 mL XAD-8 resin column. Flow rate was 12.5 ml/min. Fulvic acid, which was retained on the resin, was eluted with 400 mL of 0.1N NaOH at 1.5 ml/min by peristaltic pump. Nonsorbed effluent was non-humic substance. Samples were taken to measure TOC.

3.4 Isotherms

Isotherm experiments were conducted with individual MSW components after they had been ground in a Wiley mill to pass a 1-mm screen. PVC was purchased in powdered form with an average particle diameter of 140-μm and was used directly in experiments. Ground office paper, newsprint and rabbit food were dried in oven at 100-105°C for 24 hrs and stored in a desiccator until use. PVC and HDPE were dried and stored in a vacuum desiccator at room temperature .

Flame-sealed 20-mL glass ampules (VWR Scientific Products, Suwanee,GA) were used to collect batch isotherm data in phosphate-buffered (1 mM) organic-free water and in acidogenic and methanogenic leachates. Flame-sealed ampules were used to minimize volatilization losses of toluene and *o*-xylene (Ball and Roberts 1991). Ampules were washed and baked in a muffle furnace at 325°C overnight prior to use. Sodium azide (100 mg/L) was added to prevent aerobic sorbent and sorbate degradation. Isotherm experiments were conducted at initial sorbate concentrations of 30-1000 $\mu g/L$. Liquid:solid mass ratios ranged from 10:1 to 50:1 for fresh and degraded rabbit food, newsprint and office paper, 8:1 to 500:1 for HDPE, and 10:1 to 1000:1 for PVC at each initial sorbate concentration. Using a gas-tight syringe, toluene and *o*-xylene were spiked into the suspension at the ampule-bottom immediately prior to ampule sealing. Methanol contributions from toluene and *o*-xylene stock solutions were kept below 0.1% v/v in isotherm tests to avoid possible cosolvent effects (Brusseau et al. 1991). To reach sorption equilibria, ampules were tumbled end-over-end to assure effective mixing. Once equilibrated, ampules were centrifuged at 2000 rpm for 20 min and then broken. Subsequently, a 1-mL sample was removed and injected into scintillation cocktail (Ultima Gold^{TM}, Packard Instrument Company, Meriden, CT) for analysis by scintillation counting.

For isotherms conducted in leachates, all glassware was autoclaved prior to use to inhibit bacterial growth. Isotherms in acidogenic leachate were performed in a manner similar to the procedures for single-solute isotherms. For isotherms in methanogenic leachates, ampules were filled with methanogenic leachates in an anaerobic hood to

minimize oxygen effects. Upon removal from the anaerobic hood, samples were spiked immediately with ^{14}C-toluene or ^{14}C-*o*-xylene and then flame-sealed.

Initially, tests were conducted to determine the time needed to reach sorption equilibria in buffered organic-free water and in leachates. Multiple replicate glass ampules were set up using one water:solid ratio and one initial sorbate concentration. Replicate ampules were sampled over 20 days for rabbit food, HDPE, newsprint and office paper and up to 250 days for PVC. With the exception of PVC, no measurable changes in liquid-phase concentrations were detected after 5 days of contact. Approximately 8 months were required to reach sorption equilibrium with PVC.

3.5 Desorption Tests

To determine the effects of aging times and leachate composition on release rates of HOCs sorbed to MSWs, batch desorption tests were performed with an intermittent purging system as shown in Figure 3.1 (Harmon and Roberts 1992, 1994). Batch desorption tests were conducted with flame-sealed glass ampules (20 mL) to minimize volatilization losses of toluene and *o*-xylene during aging. Aging times of 1 month and 8 months were studied. Prior to aging, samples were sterilized with 2.2 Mrad of γ-irridation from a ^{60}Co source to prevent microbial growth. An intermittent purging system (Harmon and Roberts 1992, 1994) was employed to perform the desorption tests. The desorption experiment consisted of four steps: (1) break ampule after desired aging time and withdraw 3 ml of liquid to measure the remaining liquid-phase HOC concentration, (2) place a stir bar into ampule, attach swagelok cap to ampule and attach scintillation cocktail trap to the end of exhaust tubing (3) purge samples with water-saturated nitrogen gas at a flow rate of 40 mL/min, and (4) mix samples several times with stir bar during purging. Samples were purged continuously for the first hour after breaking an ampule, and the scintillation cocktail trap was changed every 15 minutes. After each purging step, the radioactivity in the scintillation cocktail trap was quantified, and the trap was replaced with one containing fresh scintillation cocktail. Subsequently, samples were purged every 12

or 24 hours for 15 minutes. The sample in each ampule was mixed with the stir bar several times between purges. All desorption tests were conducted in duplicate. Blank samples containing only liquid and sorbate were prepared to determine the initial alkylbenzene mass spiked into samples containing solids (M_0). The normalized alkylbenzene mass remaining in the solid-phase during desorption tests was calculated from:

$$\frac{q_t}{q_0} = \frac{q_0 m_s - (M(t) - C_{eq} V_1)}{q_0 m_s}$$

where $q_0 (= \frac{M_0 - C_{eq} V}{m_s})$, is the initial solid-phase concentration, m_s is the solid mass in the ampule, $M(t)$ is the cumulative alkylbenzene mass recovered via purges, C_{eq} is the liquid phase concentration at the end of the aging period, V is the total liquid volume, and V_1 is the remaining liquid volume after the removal of 3 mL supernatant prior to the first purge ($=V - 3$ mL).

3.6 Mass Balances

To determine the remaining solid-phase radioactivity at the end of desorption tests, benzyl alcohol and 0.1N NaOH extractions were conducted. Solid samples were transferred from glass ampules to 30-*ml* Teflon bottles to which 15-*ml* benzyl alcohol was added. After a contact time of 5 days in a rotating tumbler, the Teflon bottles were centrifuged at 3000 rpm for 15 minutes. A 0.5-*ml* benzyl alcohol sample was added into 9-*ml* scintillation cocktail to quantify desorbed ^{14}C and the remaining supernatant volume that could be removed was measured and discarded. Benzyl alcohol extractions were repeated until no additional desorption of ^{14}C was detected in the liquid phase. The solid samples were then rinsed with distilled water for complete removal of benzyl alcohol prior to initiation of base extractions. The base extraction procedure was identical to that followed with benzyl alcohol. The ^{14}C in the 0.1N NaOH extract represents alkylbenzene associated with base extractable sorbent organic matter such as humic and fulvic acids. Following benzyl alcohol and NaOH extractions, solid samples were combusted in a tube furnace at 875^{o}C. The emitted $^{14}CO_2$ gas was trapped in a series of three 2N NaOH traps. The ^{14}C recovered by

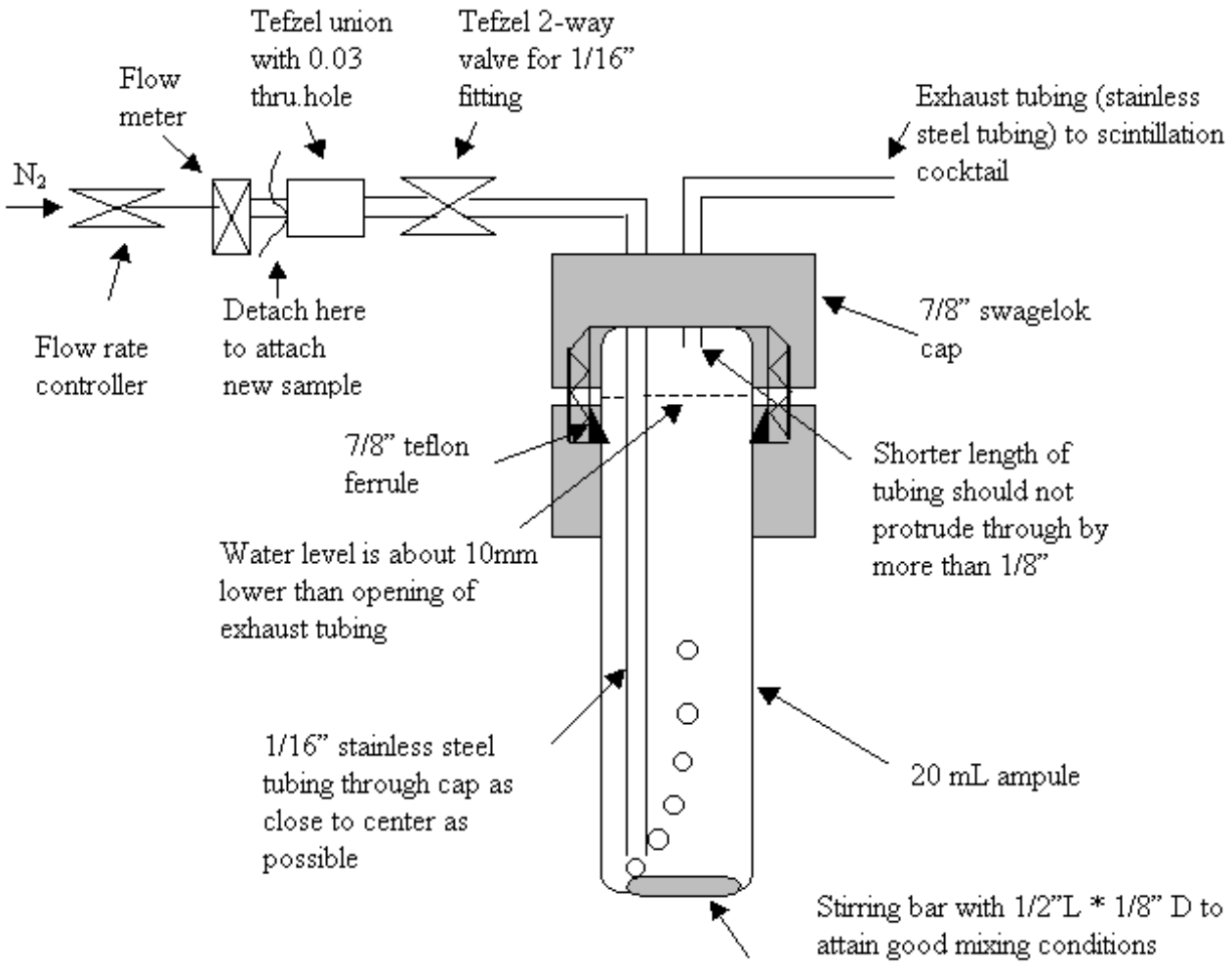

Figure 3-1: Desorption apparatus

combustion represents alkylbenzene that was associated with non-extractable sorbent organic matter such as humins.

Chapter 4

Results and Discussion - Sorption

4.1 Solids Characterization

4.1.1 Elemental Analysis and Chemolytic Characterization

Physical and chemical characteristics of the studied MSW components are summarized in Table 4.1. Table 4.1 shows that cellulose and hemicellulose in biodegradable MSW materials were preferentially removed during anaerobic decomposition. Lignin concentrations increased a result consistent with its known recalcitrance under anaerobic conditions (Eleazer et al. 1997, Picher and Kögel_knabener 2000). The preferential loss of polar cellulose and hemicellulose implies that the polarity of decomposed materials was lower than that of fresh materials. Table 4.1 further shows that protein accumulated during anaerobic degradation, suggesting that microbial cell components constituted a portion of the degraded materials. Relative to cellulose and hemicellulose, losses of lipophilic extractives were smaller, a result that can be explained by microbial resynthesis of lipids (cell walls, lipid bilayers of cell membranes) and the poor biodegradability of such lipids (Dinel et al. 1996). Similar trends were recently observed during the anaerobic degradation of mixed waste (Pichler et al. 2000). Ash contents increased upon biodegradation, a result that can be explained in part by the conversion of organic matter to CO_2 and CH_4, and in part by the addition of sodium carbonate for pH neutralization, especially during the preparation of degraded rabbit food. The organic carbon content (f_{oc}) of each biodegradable material was calculated

from the carbon content of the acid-washed materials (Table 4.2) using following equation:

$$f_{oc} = \frac{C\,(Wt.\%) * (1 - f_{ash,NAW})}{100 * (1 - f_{ash,AW})} \tag{4.1}$$

where, $f_{ash,NAW}$ is the ash content ($Wt.\%/100$) of the non-acid-washed material (Table 4.1), and $f_{ash,AW}$ is the ash content of the acid-washed material (Table 4.2). For PVC and HDPE, materials with known organic carbon content, f_{oc} values in Table 4.1 closely correspond to the theoretical carbon contents of 0.384 and 0.857, respectively. For materials with low ash contents such as fresh and degraded newsprint, the difference between calculated f_{oc} values and directly measured f_{oc} values for non-acid washed materials was less than 1% ($\Delta f_{oc} * 100\%$). Larger discrepancies were observed between calculated and directly measured f_{oc} values for non-acid-washed materials with higher ash contents, such as degraded office paper and degraded rabbit food, because the inorganic matrix contained a substantial amount of carbonates that affected the directly measured carbon content. Anaerobic degradation decreased the organic carbon contents of office paper and rabbit food by about 9.5% ($\Delta f_{oc}^{cal} * 100\%$) while that of newsprint remained approximately constant. Decreases in f_{oc} for office paper and rabbit food were primarily attributed to the accumulation of ash in the degraded materials that was either present in the parent material (office paper) or added during the degradation process (rabbit food). For newsprint, which contained little ash initially and required little sodium carbonate for neutralization during the degradation process, f_{oc} remained approximately constant or increased slightly. Assuming that equimolar amounts of CO_2 and CH_4 were produced during the anaerobic decomposition of cellulose and hemicellulose in newsprint, the organic matter fraction of the sorbent became enriched in carbon because the total mass loss of oxygen and hydrogen exceeded that of carbon. However, because of similar increases in ash and carbon contents during degradation, a negligible overall change in f_{oc} was observed for newsprint.

BET surface area data showed that the plastics as well as fresh and degraded rabbit food exhibited negligible internal porosity (Table 4.1). Nonetheless, glassy

polymers such as PVC contain internal nanovoids that are inaccessible to N_2 at 77K but that provide surfaces for HOC adsorption (Pignatello, 1998). BET surface areas of office paper and newsprint are similar to those of many soils and sediments studied by Weber et al. (1992) and Kile et al. (1995), and they are in agreement with those previously observed for dry pulp fibers (Roberts 1996). While swelling of cellulose in water can increase the BET surface area of wet pulp fibers to 150 m^2/g (Roberts 1996), this surface area is unlikely to contribute significantly to HOC adsorption from aqueous solution because of the strong adsorption of water on polar surfaces.

The elemental composition of the sorbent organic matter is summarized in Table 4.2. The sum of the C, H, N, O, and ash contents in Table 4.2 resulted in recoveries of 97.6 to 102.3%, indicating that the analytical methods effectively characterized the sorbent composition. Elemental data in Table 4.2 were utilized to characterize sorbent polarity by means of the polarity index [(O+N)/C] (Rutherford et al. 1992). Table 4.2 shows that hydrogen and carbon contents changed slightly for biodegradable materials in this study during decomposition. However, the oxygen contents of office paper, newsprint and rabbit food all decreased as a result of anaerobic decomposition. Therefore, the polarity index [(O+N)/C] of degraded materials was smaller than of the correponding fresh materials. Thus, the polarity index values illustrate that the sorbent organic matter became more hydrophobic during anaerobic decomposition, which is in agreement with the preferential degradation of cellulose and hemicellulose over lignin, protein, and lipophilic extractives as shown in Table 4.1 as well as with the ^{13}C CP-MAS NMR data presented in Table 4.3.

Table 4.1 Characteristics of solid materials[a]

Sorbent	Cellulose (%)	Hemicellulose (%)	Lignin (%)	Lipophilic extractives (%)	Crude protein (%)	Ash (Wt %)	$^{c}f_{oc}^{mea}$	$^{d}f_{oc}^{cal}$	BET surface area (m^2/g)
Poly(vinyl chloride)	N/A[b]	N/A	N/A	N/A	N/A	0.00	0.389	0.389	0.8
High density polyethylene	N/A	N/A	N/A	N/A	N/A	0.01	0.876	0.876	0.6
Fresh office paper	64.7	13.0	0.93	0.7	0.31	11.6	0.378	0.373	2.8
Degraded office paper	36.2	6.9	4.8	3.3	4.99	38.4	0.310	0.278	6.0
Fresh newsprint	48.3	18.1	22.1	1.6	0.44	2.0	0.442	0.451	2.6
Degraded newsprint	35.1	16.0	32.3	1.4	3.74	6.4	0.449	0.455	3.4
Fresh rabbit food	30.6	15.4	9.5	4.9	18.1	7.7	0.402	0.423	0.6
Degraded rabbit food	7.1	5.7	25.2	4.5	20.6	34.5	0.383	0.329	0.5

[a] values are averages of replicate analyses
[b] N/A: not analyzed
[c] measured organic carbon fraction of the non-acid-washed materials
[d] calculated organic carbon fraction

Table 4.2 Elemental composition of acid-washed solid materials[a]

Sorbent	C (Wt.%)	H (Wt.%)	N (Wt.%)	O (Wt.%)	Ash (Wt.%)	Total (Wt.%)	(O+N)/C[b]
Poly(vinyl chloride)[c]	38.9	4.7	0.1	1.7	0.0	102.1[d]	-[e]
High density polyethylene[c]	87.6	14.5	0.08	0.1	0.01	102.3	-[e]
Fresh office paper	41.7	5.2	0.04	49.6	1.1	97.6	0.89
Degraded office paper	41.7	5.0	0.8	43.4	7.6	98.5	0.80
Fresh newsprint	45.0	4.9	0.07	47.5	2.3	99.8	0.79
Degraded newsprint	47.6	5.0	0.4	43.7	2.0	98.7	0.70
Fresh rabbit food	45.3	5.4	2.4	45.4	1.1	99.6	0.80
Degraded rabbit food	48.8	5.3	3.2	39.0	2.9	99.2	0.66

[a] Values are averages of replicate analyses
[b] Atomic ratios on a dry, ash-free basis
[c] HDPE and PVC were not acid-washed
[d] Includes theoretical chlorine content of 56.7%
[e] Ratios for PVC and HDPE are not meaningful because of very low oxygen and nitrogen contents

4.1.2 ^{13}C Nuclear Magnetic Resonance Spectra (NMR)

Table 4.3 shows NMR data for fresh and degraded biopolymer composites. NMR signals for biodegradable MSW components in the carbonyl region were attributed to amides and to carboxyl groups in fatty acids, signals in the aromatic region to lignin, and signals in the alkyl region to methylene groups in fatty acids and protein side chains. Upon degradation, NMR signals in the carbonyl region, in the aromatic region, and in the alkyl region increased while the O-alkyl signals attributable to cellulose and hemicellulose decreased. As a result, the ratio of O-alkyl to alkyl groups, which has been employed as an indicator of the extent of natural organic matter degradation (Baldock et al. 1997), decreased upon anaerobic decomposition of the biodegradable materials (Table 4.3).

Table 4.3 Distribution of functional groups in biopolymer-containing materials based on ^{13}C CP-MAS NMR data

Sorbent	Carbonyl[a] (%)	Aromatic[b] (%)	O-alkyl[c] (%)	Alkyl[d] (%)	O-alkyl/alkyl
Fresh office paper	0.9	3.4	94.0	1.7	55.3
Degraded office paper	2.7	8.0	82.8	6.5	12.7
Fresh newsprint	2.1	12.2	82.4	3.3	25.0
Degraded newsprint	2.8	17.1	74.8	5.4	13.9
Fresh rabbit food	7.8	3.4	79.6	9.3	8.6
Degraded rabbit food	8.3	10.9	63.4	17.4	3.6

Chemical shifts: [a] 200-160 ppm; [b] 160-110 ppm; [c] 110-50 ppm; [d] 50-0 ppm

4.2 Sorbate Properties and Leachate Characterization

The characteristics of toluene and *o*-xylene are shown in Table 4.4. *o*-Xylene is more hydrophobic than toluene as indicated by the aqueous solubility and octanol/water partition coefficient.

Table 4.4 Sorbate properties

	toluene	*o*-xylene
Molecular weight (g/mol)	92.1	106.2
Aqueous solubility (mg/L)[a]	518	185
log K_{ow}[a]	2.69	3.12
Solubility parameter δ $(cal/cm^3)^{1/2}$ [b]	8.9	8.8

[a] Schwarzenbach et al. (1993)
[b] Barton (1975)

Leachate characteristics are presented in Table 4.5. The COD, DOC, and pH data are all consistent with previous reports on acidogenic and methanogenic leachate (Barlaz et al. 1990). The COD and DOC of acidogenic leachate are about 40-50 times higher than those of methanogenic leachates. Table 4.5 further shows that laboratory generated methanogenic leachate A exhibited characteristics similar to those of methanogenic leachate B that was collected from an operating landfill. VFA data for acidogenic leachate are summarized in Table 4.6. In acidogenic leachate, VFAs constituted 63% of the COD. The dominant VFA was butyric acid (3300 mg/L), followed by similar concentrations of acetic, propionic, and valeric acid ($\sim$1500 mg/L each). In methanogenic leachate A, no humic acid was present and 57% of the organic matter was fulvic acid (Leenheer, 1981). Compared to the high DOC content of the leachates, UV_{254} absorbance values were small, suggesting that aromatic and unsaturated functionalities were largely absent in both acidogenic and methanogenic leachate organic matter. Consequently, specific UV absorbance values (SUVA = UV_{254}/DOC) were small and about two to three orders of magnitude lower than those of natural waters with significant aquatic humic content (Edzwald et al. 1990). Number-averaged molecular weights (M_n) indicated that relatively low molecular weight organic matter dominated among UV_{254}-absorbing compounds in both leachates. In agreement with prior studies (Harmsen 1983), M_n for acidogenic leachate was smaller than for methanogenic leachate. Weight-averaged molecular weights (M_w) illustrated that high-molecular-weight UV_{254}-absorbing organic matter was present in methanogenic leachate A, but not in acidogenic leachate and methanogenic leachate B.

Table 4.5 Leachate characteristics

Leachate	COD (mg/L)	DOC (mg/L)	UV_{254} (m^{-1})	SUVA (L/mg-m)	pH	Conductivity (µmho/cm)	Average molecular weight (g/mol)	
							M_w	M_n
Acidogenic	22,400	6,620	10.4	0.00157	4.9	6,540	856	181
Methanogenic A	550	115	3.5	0.0304	7.8	1,850	5,849	293
Methanogenic B	660	210	2.4	0.0114	7.9	3,060	579	290

Table 4.6 Volatile fatty acid (VFA) analysis for acidogenic leachate

Sample #	Acetic acid (mg/L)	Propionic acid (mg/L)	i-butyric acid (mg/L)	Butyric acid (mg/L)	2-methyl butyric acid (mg/L)	i-valeric acid (mg/L)	Valeric acid (mg/L)	i-caproic acid (mg/L)	Caproic acid (mg/L)	Heptanoic acid (mg/L)
1[a]	1658	1571	101	3862	52	61	1774	22	337	ND
1	1886	1675	141	3736	56	66	1717	21	317	ND
2	1459	1530	101	3747	48	61	1735	18	351	ND
2	1577	1510	103	3701	48	63	1726	20	318	ND
3	1569	1499	100	3686	45	60	1703	22	330	ND
3	1610	1512	104	3714	47	63	1722	20	317	ND
4	1574	1505	103	3704	45	61	1714	21	334	ND
4	1551	1470	102	3615	44	61	1683	22	307	ND
5	1319	1510	101	3783	53	64	1730	23	b3035	ND
5	1567	1497	105	3640	43	62	1694	21	309	ND
6	1557	1227	76	2940	31	33	1340	16	214	ND
6	1595	1210	80	2842	29	39	1329	12	210	ND
7	2111	1327	118	2859	24	108	1360	22	172	ND
7	1590	1165	73	2621	27	323	1383	20	176	ND
8	1517	1145	65	2612	26	315	1228	11	172	ND
8	1508	1111	66	2485	22	283	1279	18	166	ND
Ave.	1603	1404	96.2	3346.7	40	107.7	1569.8	19.3	251.9	ND
SE	176.65	176.73	19.87	509.63	11.45	100.36	203.59	3.55	72.67	ND

[a] Samples #1-#7 were preserved down at ~pH 2 and #8 at ~pH 12. All these samples were taken at different time points.
[b] The concentrationof caproic acid of sample 5a is an outlier and was removed in the calculation of the average value.

4.3 Single-Solute Sorption Isotherms

4.3.1 Sorption Capacity of MSW Components

Single-solute isotherm parameters describing toluene and *o*-xylene sorption to each model MSW component are summarized in Tables 4.7 and 4.8, respectively. Both the Freundlich model ($q = K_F C_e^n$) and the linear partitioning model ($q = K_p C_e$) were employed to describe the isotherm data. In these models, q ($\mu g/kg$) and C_e ($\mu g/L$) represent the equilibrium solid- and liquid-phase concentrations, respectively. In the two-parameter Freundlich isotherm model, K_F is indicative of sorption capacity at $C_e = 1$ $\mu g/L$ (for the units chosen in this study), and n indicates the site energy distribution of a sorbent, where sorbent heterogeneity increases as n decreases from 1 (Carter and Weber 1995). K_p and $\log K_F$ with 95% confidence limits along with correlation coefficients (R^2), the number of data points for each isotherm (N), the studied equilibrium liquid-phase concentration ranges (C), and the organic carbon-normalized partition coefficients (K_{oc}) are shown in Tables 4.7 and 4.8 for toluene and *o*-xylene, respectively. Normalized partition coefficients (K_{oc}) were calculated by dividing K_p by the calculated f_{oc} value for all materials but PVC. For PVC, K_{oc} was obtained from K_F. As an illustrative example, single-solute *o*-xylene isotherm data for fresh MSW components are depicted in Figure 4.1.

Table 4.7 Isotherm parameters describing toluene sorption to MSW components

Sorbent	N[a]	log K_F[b]	n[c]	R^2	C[d]	K_p[e]	R^2	K_{oc}[f]
Poly(vinyl chloride)	41	3.221(± 0.045)	0.864 (± 0.020)	0.994	1-958	546.6 (± 38.3)	0.912	4,276[g]
High density polyethylene	54	1.826 (± 0.047)	1.012 (± 0.023)	0.993	4-1078	70.7 (± 3.7)	0.946	80.7
Fresh office paper	27	0.642 (± 0.079)	0.923 (± 0.035)	0.991	7-1041	2.7 (± 0.2)	0.957	7.2
Degraded office paper	42	1.400 (± 0.020)	0.988 (± 0.010)	0.999	2-550	23.4 (± 0.3)	0.995	83.1
Fresh newsprint	44	1.220 (± 0.027)	0.961 (± 0.015)	0.998	5-740	13.0 (± 0.2)	0.997	28.8
Degraded newsprint	42	1.464 (± 0.029)	0.980 (± 0.016)	0.997	1-400	25.8 (± 0.4)	0.994	56.7
Fresh rabbit food	46	1.450 (± 0.020)	0.996 (± 0.011)	0.997	2-684	27.5 (± 0.2)	0.999	65.0
Degraded rabbit food	40	1.491 (± 0.067)	0.976 (± 0.027)	0.993	20-2000	27.3 (± 0.9)	0.982	82.9

[a] Number of observations.
[b] K_F units are $(\mu g/kg)(L/\mu g)^n$, 95% confidence interval of log K_F in parentheses.
[c] Dimensionless Freundlich exponent, 95% confidence interval in parentheses.
[d] Concentration range (µg/L)
[e] Partition coefficient units are (µg/kg)(L/µg), 95% confidence interval in parentheses.
[f] K_{oc} units are (µg/kg organic carbon)(L/µg).
[g] Based on K_F, units are $(\mu g/kg \text{ organic carbon})(L/\mu g)^n$.

Table 4.8 Isotherm parameters describing *o*-xylene sorption to MSW components

Sorbent	N[a]	log K_F[b]	n[c]	R^2	C [d]	K_p[e]	R^2	K_{oc}[ef]
Poly(vinyl chloride)	33	3.666 (± 0.056)	0.718 (± 0.034)	0.983	1-770	777.7 (± 58.4)	0.934	11,910[g]
HDPE	48	2.386 (± 0.021)	1.004 (± 0.012)	0.998	1-670	244.1 (± 3.7)	0.996	278.7
Fresh office paper	41	0.782 (± 0.055)	0.985 (± 0.027)	0.993	8-580	5.7 (± 0.1)	0.992	15.3
Degraded office paper	62	1.621 (± 0.033)	1.014 (± 0.019)	0.995	2-370	44.5 (± 1.2)	0.976	160.1
Fresh newsprint	35	1.522 (± 0.024)	0.988 (± 0.012)	0.999	4-540	31.1 (± 0.4)	0.998	69.0
Degraded newsprint	39	1.851 (± 0.021)	0.944 (± 0.012)	0.999	2-400	52.7 (± 0.7)	0.997	115.8
Fresh rabbit food	44	1.837 (± 0.033)	1.010 (± 0.017)	0.996	5-730	76.5 (± 1.4)	0.994	180.9
Degraded rabbit food	39	1.856 (± 0.062)	1.009 (± 0.035)	0.989	4-450	79.3 (± 4.4)	0.954	241.0

[a] Number of observations.
[b] K_F units are (µg/kg)(L/µg)^n, 95% confidence interval of log K_F in parentheses.
[c] Dimensionless Freundlich exponent, 95% confidence interval in parentheses.
[d] Concentration range (µg/L)
[e] Partition coefficient units are (µg/kg)(L/µg), 95% confidence interval in parentheses.
[f] K_{oc} units are (µg/kg organic carbon)(L/µg).
[g] Based on K_F, units are (µg/kg organic carbon)(L/µg)^n.

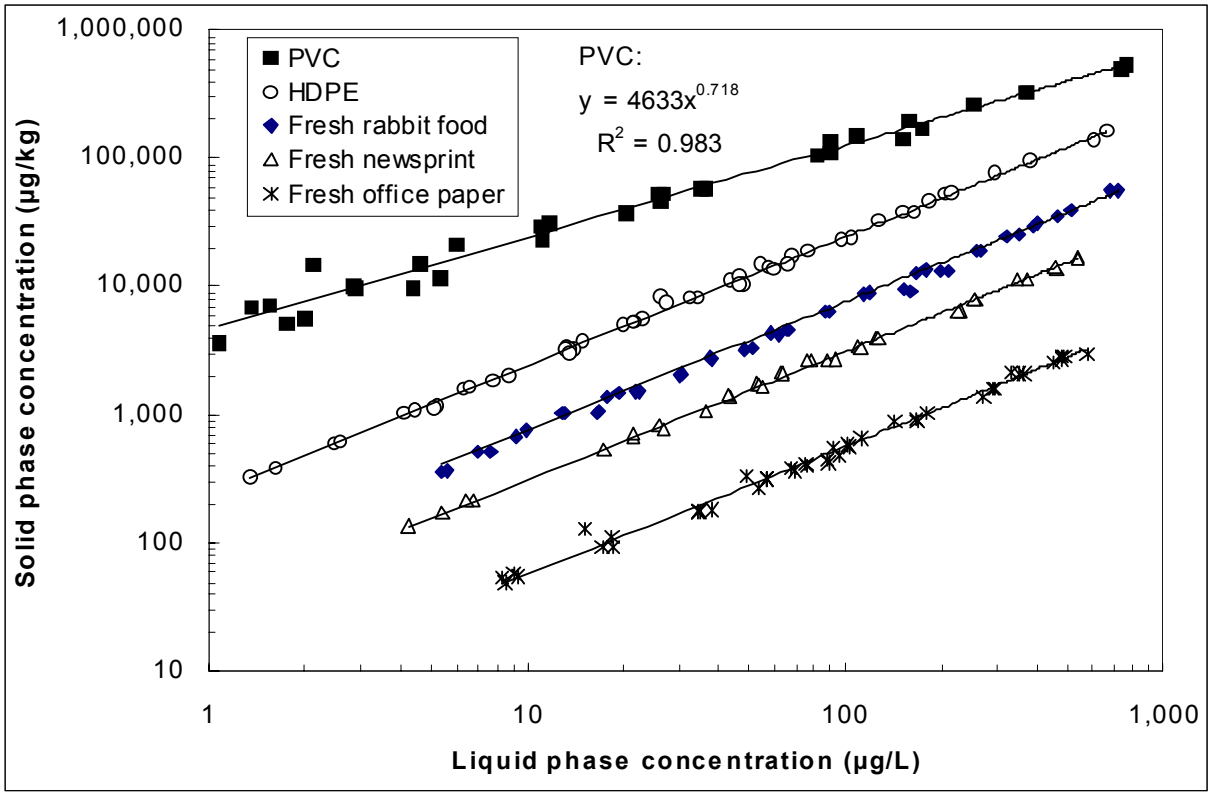

Figure 4-1: Single-solute o-xylene isotherms for model MSW components. Solid lines through all other data sets indicate best fits of the linear partition model, and partition coefficients are shown in Table 4.8.

Equilibrium liquid-phase concentrations (C_e) for each isotherm spanned two to three orders of magnitude, and relative to the aqueous solubility (S_w) of toluene (518 mg/L, Schwarzenbach et al. 1993) and *o*-xylene (185 mg/L, Schwarzenbach et al. 1993), the largest relative concentrations (C_e/S_w) corresponded to about 0.002 and 0.005 for toluene and *o*-xylene, respectively. The tested relative concentration ranges were sufficiently low to assess any isotherm nonlinearity arising from the presence of glassy polymeric domains or high surface area carbonaceous materials (HSACM) in the tested sorbents (Pignatello 1998, Chiou et al. 1998, 2000, Xia and Pignatello, 2001). According to Chiou et al. (1998), HOCs isotherms on soil organic matter tend to display nonlinearity at low C_e/S_w (<0.01-0.015) but exhibit linearity at higher relative concentrations.

Tables 4.7 and 4.8 as well as Figure 4.1 indicate that PVC exhibited the largest sorption capacity for alkylbenzenes and fresh office paper the smallest. The affinity of toluene and *o*-xylene for fresh MSW materials decreased in the order: PVC > HDPE > fresh rabbit food > fresh newsprint > fresh office paper. These results confirmed that sorbent characteristics greatly affect the sorption capacity for HOCs. In addition, the sorption capacity of the tested MSW components for *o*-xylene was about 2 to 3 times higher than for toluene, which is in accordance with the greater hydrophobicity of *o*-xylene.

The relatively high *o*-xylene and toluene sorption capacity of PVC can be explained on the basis of solubility parameters (δ), where sorbate/sorbent systems with matching solubility parameters represent a compatible solute/solvent system (Barton 1975). Solubility parameters are a measure of the cohesive energy of a material, where the cohesive energy is the energy required to hold the constituent atoms or molecules together. The solubility parameter (δ) of a material is defined as the square root of its cohesive energy density (CED); i.e., $\delta = (CED)^{0.5} = (\Delta E_v/V_m)^{0.5}$, where ΔE_v is energy of vaporization, and V_m is the molar volume. When solubility parameters of a solvent, such as an amorphous polymer and a solute, such as an organic pollutant are close, they will be mutually soluble. As a result, PVC [δ = 7.8-11 $(cal/cm^3)^{1/2}$] represented a suitable sorbent (or solvent) for *o*-xylene [$\delta = 8.9\,(cal/cm^3)^{1/2}$] and

toluene [δ =8.8 $(cal/cm^3)^{1/2}$](Barton 1975) because its solubility parameter range includes that of *o*-xylene and toluene. Furthermore, a nonlinear adsorption component on the surfaces of internal nanovoids contributed to *o*-xylene and toluene uptake by the glassy PVC polymer (Xing and Pignatello 1997). Sorption in glassy polymers occurs by partitioning and adsorption, which yields non-linear isotherms. HDPE exhibited a smaller sorption capacity than PVC because the solubility parameter for both *o*-xylene and toluene falls outside of the range for HDPE [δ = 7.7-8.2 $(\text{cal/cm}^3)^{1/2}$(Barton 1975). Moreover, HDPE is a rubbery polymer and partitioning is the sole sorption mechanism. Consequently, the sorption capacity of HDPE is lower than that of PVC as a result of absence of an adsorption component. It is also likely that the high degree of crystallinity of the studied HDPE (∼80%) contributed to the low alkylbenzene sorption capacity.

For the biopolymer-containing sorbents, rabbit food exhibited the largest sorption capacity, which was most likely attributable to its relatively high lipophilic extractives content in comparison with newsprint and office paper. As seen in Table 4.1, the lipophilic extractives content is 4.9% for fresh rabbit food, 1.6% for fresh newsprint and only 0.7% for office paper. The solubility parameter for soybean oil [δ = 8.4-8.9 $(\text{cal/cm}^3)^{1/2}$ (Hancock et al. 1997)], which should be present in rabbit food based on its ingredients, is similar to that of toluene and *o*-xylene. Furthermore, Garbarini and Lion (1986) found that HOC sorption capacities decreased in the order: fats > lignin > protein > humic acids > fulvic acids > cellulose. Therefore, the presence of lignin [δ = 9.8-14.3 $(\text{cal/cm}^3)^{1/2}$ (Barton, 1991)] and protein, which exhibits HOC sorption capacities similar to lignin (Garbarini and Lion 1986), contributed to the high sorption capacity of rabbit food. Consistent with solubility parameters, newsprint with a 22% lignin content exhibited a larger sorption capacity than office paper that contained primarily cellulose [δ = 14.5-16.5 $(\text{cal/cm}^3)^{1/2}$ (Barton 1975)] and hemicellulose.

Overall, the biopolymer composites exhibited lower sorption capacities than plastics because (1) the differences in solubility parameters between sorbates and lignin or cellulose were greater than those between sorbates and PVC or HDPE, and (2) the content of highly compatible sorbent fractions, such as lipophilic extractives, was

small in the biopolymer composites.

4.3.2 Isotherm Linearity

The Freundlich exponents in Tables 4.7 and 4.8 generally varied between 0.94 and 1.01, indicating that the organic sorbents acted primarily as partitioning media. Exceptions are toluene and *o*-xylene isotherms for PVC and the toluene isotherm for fresh office paper, for which smaller Freundlich exponents were obtained. Except for PVC, for which the nonlinear Freundlich isotherm model was more appropriate, the partition model described the isotherm data well over the entire liquid-phase concentration range (Figure 4.1). Because the *o*-xylene isotherm for fresh office paper exhibited a Freundlich exponent (0.985 ± 0.027) that did not differ significantly from 1 ($p < 0.05$), it is doubtful that the Freundlich exponent of 0.92 for toluene sorption to fresh office paper is indicative of true isotherm nonlinearity. Instead, a smaller number of data points and the greater scatter of the toluene isotherm data for this poorly sorbing material may have contributed to this observation. There are two additional reasons why linear toluene sorption to office paper would be expected. First, fresh office paper consists primarily of cellulose, and amorphous regions in cellulose are plasticized by water at room temperature (Akim 1978). Consequently, wet cellulose is a partitioning medium and should exhibit linear isotherms (LeBoeuf and Weber 2000). Second, the presence of small quantities of hydrophobic sizing agents on fresh office paper, such as alkyl ketene dimers of C_{14}-C_{18} unsaturated fatty acids (Roberts 1996), should lead to linear partitioning.

Because lignin constituted a large percentage of fresh and degraded newsprint and lipophilic extractives were low, it can be assumed that lignin controlled alkylbenzene sorption to newsprint. HOC sorption to lignin, a glassy polymer, should be nonlinear, and a Freundlich n-value of about 0.80 was recently obtained for phenanthrene sorption to extracted lignin (LeBoeuf and Weber 2000). The greater isotherm linearity observed in this study with newsprint may have resulted from (1) the topological or covalent bonding between hemicellulose and lignin in wood and wood pulp (Gerasimowicz et al. 1984, Shevchenko et al. 1996, Salmen et al. 1998, Helm 2000) that led

to a new glass transition temperature for the intimately mixed lignin-carbohydrate complex (Kaplan 1976), and/or (2) the introduction of hydrophilic sulfone groups into the lignin structure during the preparation of newsprint (e.g. bisulfite addition during pulping) that enhanced the ability of water to plasticize lignin (Roberts 1996).

In fresh and degraded rabbit food, linear partitioning into phases containing lipophilic extractives was likely dominant and rendered the overall isotherms linear. Furthermore, protein represented a partitioning medium because amorphous protein regions are plasticized by water at room temperature (Green et al. 1994, Sochava 1997). Finally, the behavior of lignin-carbohydrate complexes in rabbit food may have deviated from that of glassy lignin extracts (LeBoeuf and Weber 2000) as explained above. Both toluene and *o*-xylene sorption to PVC was nonlinear, consistent with the dual-mode partitioning and adsorption mechanism that is typically observed for glassy polymers (Xia and Pignatello 2001, Xing and Pignatello 1997). For HDPE, the observation of linear toluene and *o*-xylene isotherms was consistent with previously observed linear partitioning into rubbery polymers (Xing et al. 1996).

4.3.3 Relationship between K_{oc} and K_{ow}

To compare the affinity of the sorbent organic matter for toluene and *o*-xylene, K_{oc} values ($K_{oc} = K_p/f_{oc}$) were calculated from the partition coefficients for all materials but PVC, for which K_{oc} was estimated from $K_{_F}$. Thus, K_{oc} comparisons involving PVC are valid only at an equilibrium liquid-phase concentration of 1 $\mu g/L$. Partition coefficients of organic chemicals are frequently related to their K_{ow} values by the following equation (Chiou et al. 1979, Karickhoff et al. 1979, Brown et al. 1981): $\log K_{oc} = a \log K_{ow} + b$, where K_{ow} is the octanol-water partition coefficient of a given sorbate, and a and b are empirical constants related to sorbent properties. Figure 4.2 depicts the relationship between $\log K_{oc}$ of single-solute isotherms and $\log K_{ow}$ for all tested materials along with the data from Reinhart et al. (1990) who evaluated the sorption capacity of refuse for 9 compounds with different hydrophobicities. Relating K_{oc} values to sorbate K_{ow} values, Figure 4.2 illustrates that K_{oc} values increased with increasing sorbate hydrophobicity (i.e. with increasing octanol/water partition

coefficient, K_{ow}), a trend that is in agreement with that of Reinhart et al. (1990) for mixed MSW as well as for soils and sediments (Schwarzenbach and Westall 1981, Karickhoff 1979). For a given sorbate, the large differences in K_{oc} values between fresh MSW components as well as between fresh and degraded materials (Fig. 4.2, Tables 4.7 and 4.8) illustrate that the chemical nature of the sorbent organic matter greatly influenced HOC sorption and that a unique relationship between $\log K_{oc}$ and $\log K_{ow}$ could therefore not be obtained. Figure 4.2 also shows that, with the exception of PVC, the individually tested MSW components exhibited a smaller sorption capacity than a mixed MSW sample from a prior study (Reinhart et al. 1990). The ethyl ether extractable lipid content of the mixed MSW sample was 4.6% (Reinhart et al. 1990) and thus similar to that of rabbit food evaluated in this study. Consequently, differences in lipophilic extractives content alone could not account for the observed differences in K_{oc} values. Furthermore, differences in equilibration time (24 h for mixed MSW samples, 5 days or longer in the current study) could not explain the comparatively large sorption capacity of mixed MSW. The results in Figure 4.2 therefore illustrate that sorbent organic matter characteristics need to be considered in addition to sorbate hydrophobicity to facilitate the prediction of HOC sorption capacities of complex organic sorbents.

4.3.4 Correlation between Normalized Sorption Parameter and Sorbent Polarity

One sorbent characteristic that controls HOC sorption is the sorbent polarity, as measured by the polarity index [(O+N)/C] (Rutherford et al. 1992, Xing et al. 1996, Xing et al. 1994) or by the percentage of polar organic carbon determined from solid-state ^{13}C CP-MAS NMR spectra (Kile et al. 1999). According to Kile et al. (1999), percent polar organic carbon was calculated as the combined percentage of O-alkyl and carbonyl functional groups. Figure 4.3 depicts the dependence of the normalized sorption parameter [$\log(K_{oc}/K_{ow})$] (Stuer-Lauridsen and Pedersen 1997, Seth et al. 1999) on the polarity of the sorbent organic matter as measured by the

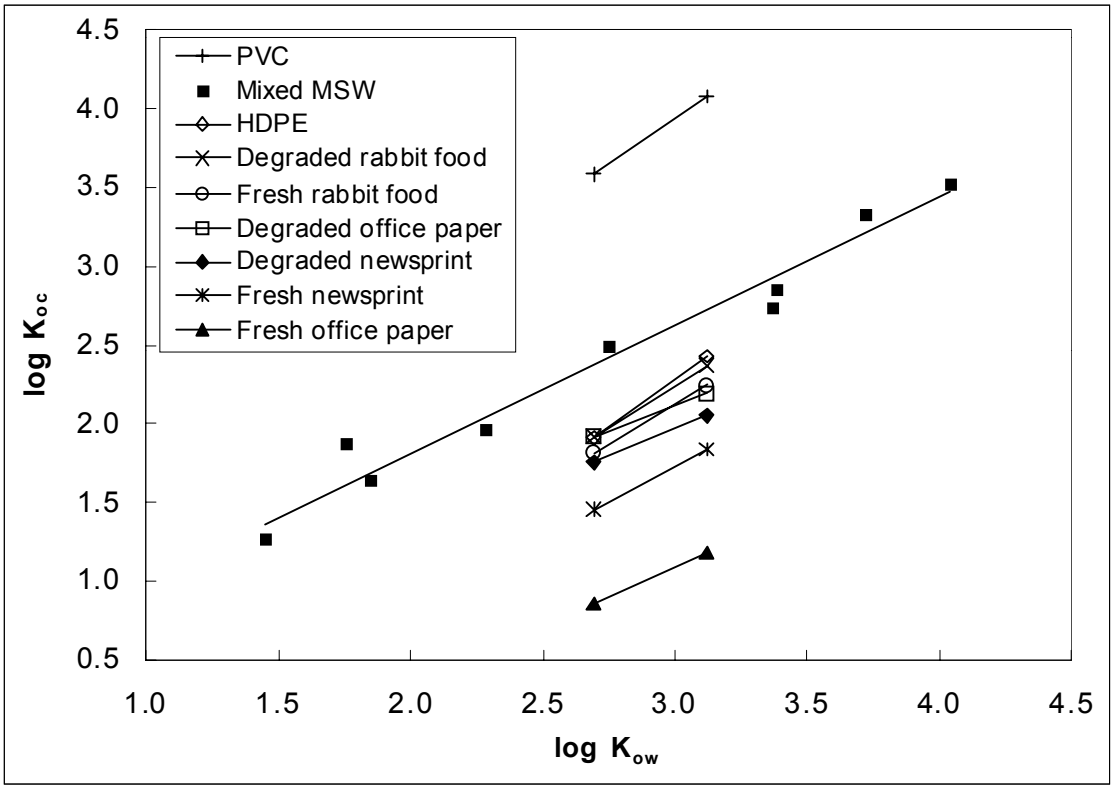

Figure 4-2: Dependence of log K_{oc} on log K_{ow} for individual MSW components and mixed MSW. PVC data represent Freundlich K-values divided by f_{oc} and provide a valid comparison only at an equilibrium liquid-phase concentration of 1 $\mu g/L$. Data for mixed MSW are from ref. 121.

polarity index [(O+N)/C]. In addition to the biodegradable MSW component data from this study, Figure 4.3 depicts HOC sorption data for mixed MSW (Reinhart et al. 1990) and biopolymers (Rutherford et al. 1992, Garbarini and Lion 1986, Xing et al. 1994, summarized by Stuer-Lauridsen and Petersen 1997). The results in Figure 4.3 suggest that HOC sorption to individual MSW components and mixed MSW follows a trend similar to that established by individually tested biopolymers such as lignin, protein, and cellulose, which confirms that sorption capacity decreased with increasing sorbent polarity or decreasing sorbent hydrophobicity. Furthermore, Figure 4.3 illustrates that the polarity index of the mixed MSW sample evaluated by Reinhart et al. (1990) was lower than that of the tested biodegradable MSW components in this study. Thus, sorbent polarity can explain the larger HOC sorption capacity of the mixed MSW samples studied by Reinhart et. al. (1990).

Figure 4.4 depicts the dependence of $\log(K_{oc}/K_{ow})$ on the percentage of polar organic carbon (O-alkyl+Carbonyl) in sorbent organic matter. For reference, Figure 4.4 also includes carbon tetrachloride sorption capacities for soils and sediments (Kile et al. 1999). The latter data suggest that sorbent polarity effectively describes HOC sorption trends of both relatively young sorbent organic matter, such as that in MSW, and more diagenetically altered sorbent organic matter such as that in soils and sediments. Figure 4.4 clearly demonstrates that the normalized sorption parameter decreased as the polar organic carbon percentage increased. Furthermore, the similarity of Figures 4.3 and 4.4 illustrates that the polarity index and percent organic carbon are equivalent descriptors of sorbent polarity.

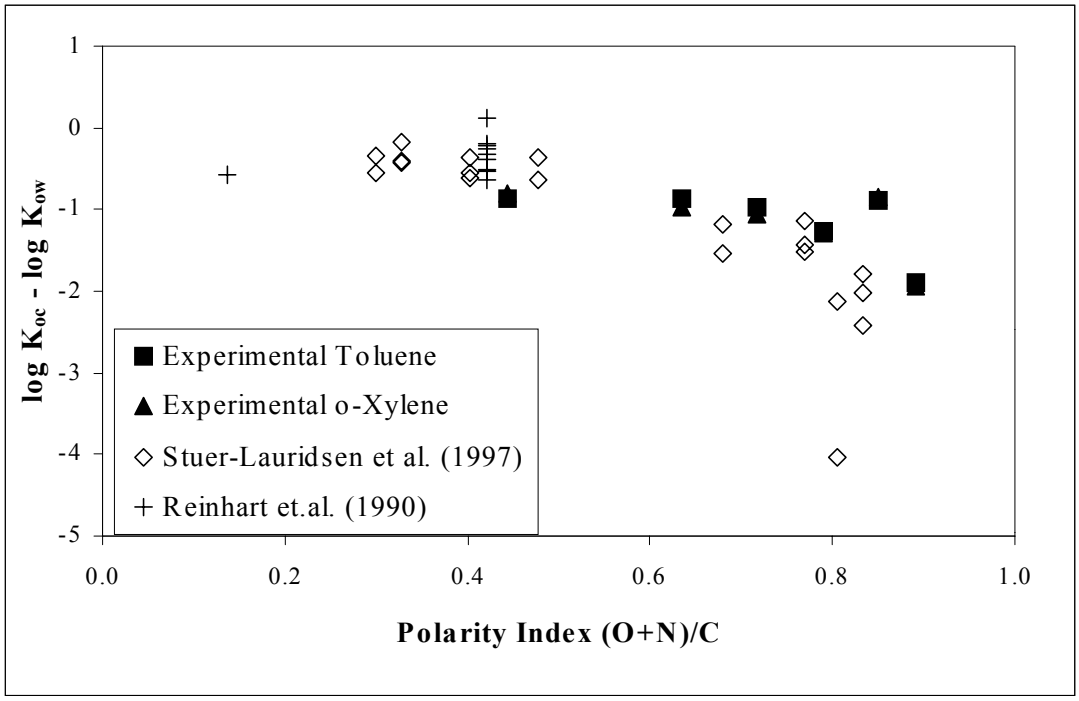

Figure 4-3: Dependence of normalized sorption parameter on sorbent polarity as expressed by the polarity index [(O+N)/C]

Table 4.9 Isotherm parameters describing toluene sorption to lipophilic extracted MSW components

Sorbent	N[a]	K_p[b]	f_{oc}[c]	K_{oc}[d]	R^2
Extracted fresh office paper	6	1.57	0.368	4.269	0.976
Extracted degraded office paper	6	10.245	0.253	40.454	0.996
Extracted fresh newsprint	6	10.304	0.439	23.472	0.975
Extracted degraded newsprint	6	17.93	0.445	40.337	0.952
Extracted fresh rabbit food	20	11.25	0.386	29.126	0.996
Extracted degraded rabbit food	18	16.113	0.295	54.574	0.979

[a] Number of observations
[b] Partition coefficient units are (µg/kg)(L/µg)
[c] Calculated as f_{oc}^{cal}- lipophilic extractives (%)*0.75, where 0.75 refers to f_{oc} of lipid
[d] K_{oc} units are (µg/kg organic carbon)(L/µg).

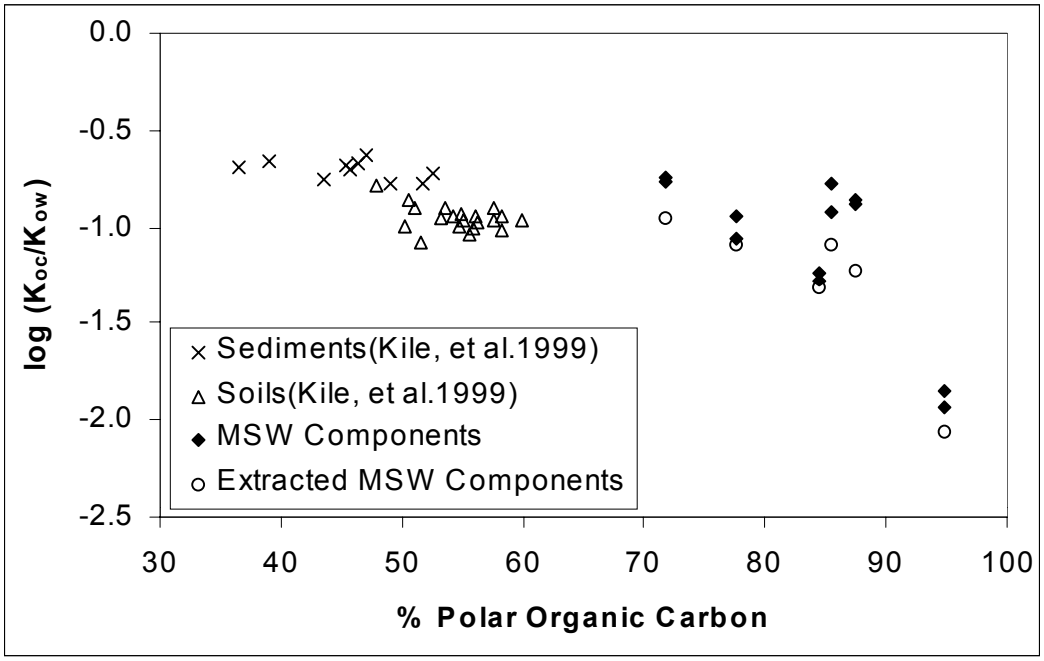

Figure 4-4: Dependence of normalized sorption parameter on sorbent polarity as expressed by % polar organic carbon (= O-alkyl + carbonyl from Table 4.3)

4.3.5 Effect of Sorbent Polarity on Toluene Sorption before and after Removal of Lipophilic Extractives

Although the overall dependence of the normalized sorption parameter on sorbent polarity is clearly established in Figures 4.3 and 4.4, a closer look at the MSW component data illustrates a fair amount of variability. Two sorbents in particular, fresh rabbit food and degraded office paper, exhibited alkylbenzene sorption capacities that were larger than those expected from the trend established by the other biopolymer composites evaluated in this study. To investigate reasons for this observation, single-solute toluene isotherm experiments were conducted for toluene/ethanol extracted biopolymer composites, and the toluene sorption capacities of extracted biopolymer composites are compared to those of non-extracted sorbents in Figure 4.4 and 4.5. Table 4.9 summarizes isotherm parameters describing toluene sorption to extracted MSW components. The toluene partition coefficients depicted in Figure 4.4 and 4.5 indicate that relatively small amounts of lipophilic extractives (<5% of the sorbent

mass) can cause large differences in sorption capacity, and these differences are not captured well by the polarity index or the percentage of polar organic carbon.

To recognize the importance of both sorbent polarity and lipophilic extractives on HOC sorption, the ratio of O-alkyl to alkyl groups, determined from solid-state ^{13}C CP-MAS NMR spectra, was therefore selected as a new sorbent organic matter descriptor. As shown in Figure 4.6, an improved correlation resulted when relating $\log(K_{oc}/K_{ow})$ to the O-alkyl/alkyl ratio. It appears reasonable to focus on the O-alkyl and alkyl regions of the NMR spectra only because these regions unambiguously represent polar and nonpolar regions, respectively. In contrast, carbonyl and aromatic moieties can be present in relatively hydrophilic and hydrophobic compounds. While the O-alkyl/alkyl ratio appears to be a good predictor for sorbents containing relatively young organic matter; i.e., materials with significant cellulose, hemicellulose, and lignin content, it may not be sufficiently sensitive for geosorbents that have undergone more extensive diagenesis and thus contain few O-alkyl groups. In the limit, the correlation in Figure 4.6 predicts a $\log(K_{oc}/K_{ow})$ value of -0.66, which is quite similar to the plateau region [average $\log(K_{oc}/K_{ow})$ = -0.44] established by the eight least polar biopolymers in Figure 4.3 and the largest $\log(K_{oc}/K_{ow})$ value of -0.62 for the sediments shown in Figure 4.4. It should be recognized, however, that HOC sorption to highly diagenetically altered geosorbents such as coals and shale has yielded positive $\log(K_{oc}/K_{ow})$ values (Stuer-Lauridsen and Pedersen 1997, Grathwohl 1990).

4.4 Leachate Effects on Sorption Isotherms

To evaluate the effects of leachate composition on alkylbenzene sorption to MSW components, isotherm data were collected for selected sorbents in acidogenic and methanogenic leachates. Figure 4.7 summarizes isotherm data describing toluene sorption to PVC in organic-free water and in leachates. Toluene isotherms in organic-free water and in methanogenic leachate were statistically similar ($p < 0.05$) with respect to isotherm nonlinearity and differed only slightly with respect to sorption capacity. Thus, the composition of methanogenic leachate had little effect on

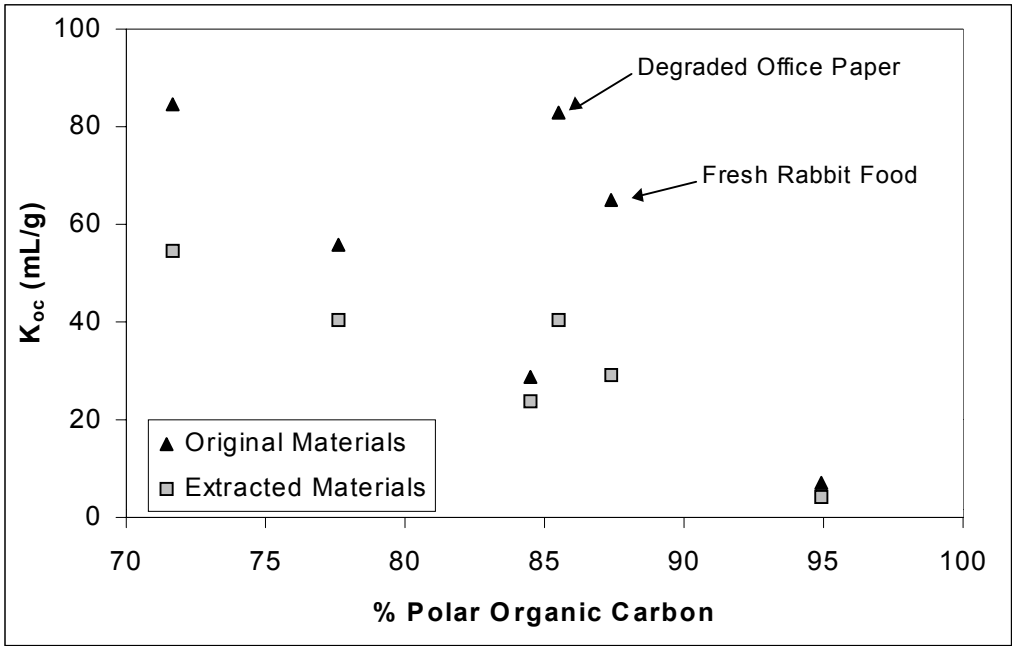

Figure 4-5: Effect of sorbent polarity on toluene sorption to MSW components before and after lipophilic extraction

toluene sorption to PVC. In contrast, the toluene isotherm became linear in acidogenic leachate. This result suggests that organic compounds in acidogenic leachate served as plasticizers that converted PVC from the glassy to the rubbery state. The softening of glassy polymers by high concentrations of cosolutes in multisolute systems has been reported previously (Huang and Weber 1998, White and Pignatello 1999). In acidogenic leachate, propionic and butyric acid may have been the principal plasticizers of PVC because their solubility parameters [$\delta = 9.7$ and 9.1 $(cal/cm^3)^{1/2}$, respectively (Hansen 2000)] fall into the range of δ values given above for PVC. Tables 4.10, 4.11 and 4.12 summarize K_p-values describing toluene and *o*-xylene sorption to sorbents that exhibited linear partitioning in leacheates. A comparison of single-solute K_p-values with those obtained in leachates illustrates that the effects of leachate on toluene and *o*-xylene sorption were small (compared to single-solute values, K_p values in leachates were 11% larger to 26% smaller).

K_p values for toluene isotherms with fresh rabbit food and newsprint conducted

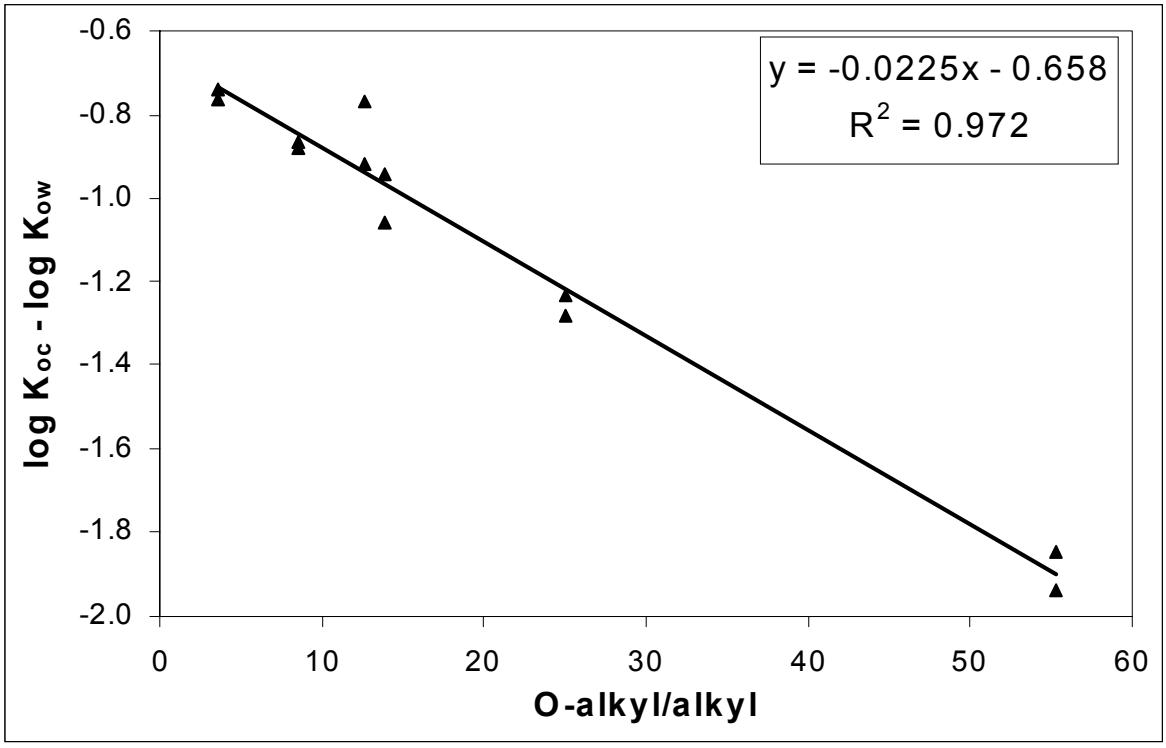

Figure 4-6: Dependence of normalized sorption parameter on sorbent polarity as expressed by O-alkyl/alkyl ratio (from Table 4.3).

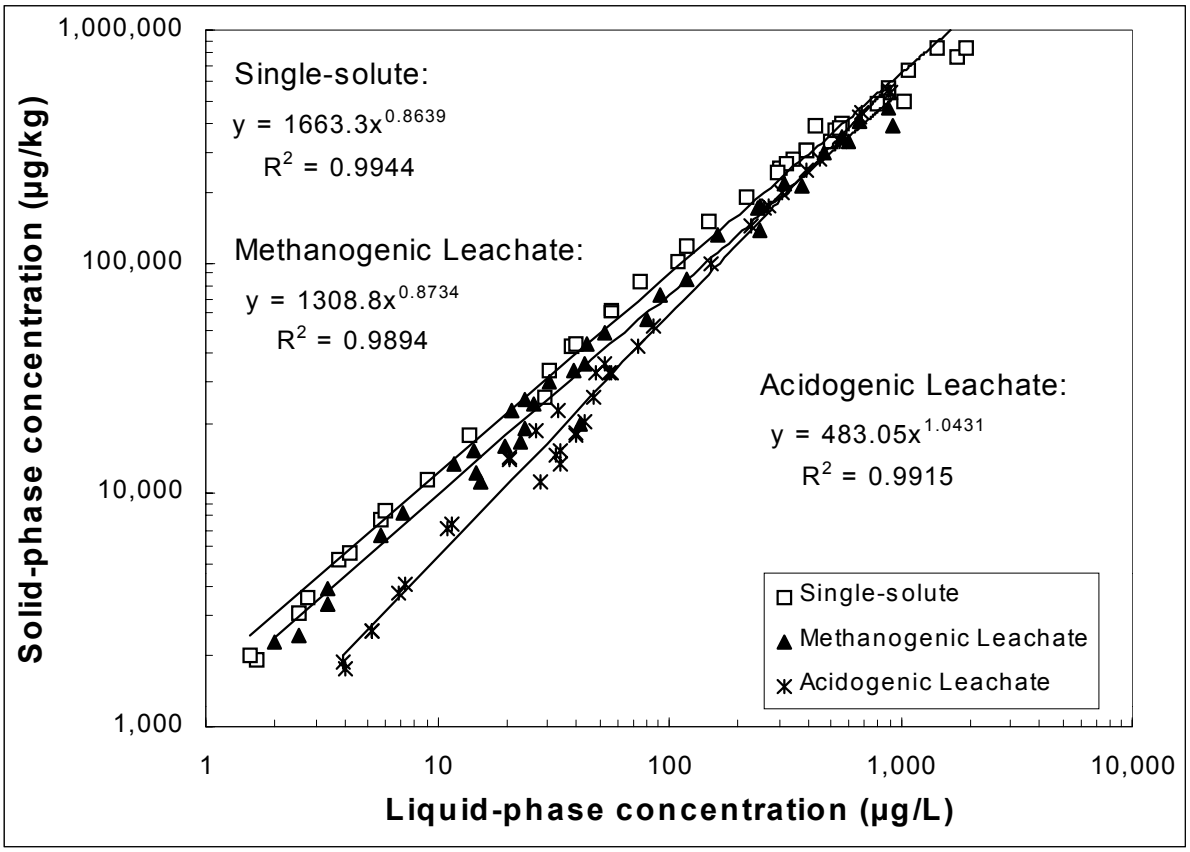

Figure 4-7: Effect of aqueous phase composition on toluene sorption to PVC

in methanogenic leachate B collected from Greensboro landfill site were 14.2±0.6 and 23.5±0.7 (Table 4.11), respectively, which compared well to K_p values obtained in methanogenic leachate A. With the exception of PVC, leachate composition had little influence on toluene and *o*-xylene sorption to MSW, which is consistent with results observed by Reinhart et al. (1990) for sorption of DCB to refuse in distilled water and acidogenic leachate.

Table 4.10 Partition coefficients describing toluene sorption to MSW components in acidogenic leachate and methanogenic leachate A.

Materials	Acidogenic leachate				Methanogenic leachate A			
	K_p[a]	R^2	N[b]	C[c]	Kp (mL/g)	R^2	N	C
HDPE	76.1 (± 1.6)	0.992	44	6-900	72.4 (± 0.8)	0.998	43	6-900
Fresh office paper	2.0 (± 0.1)	0.909	98	6-840				
Degraded office paper	19.9 (± 0.2)	0.997	42	6-790	20.8 (± 0.3)	0.996	36	6-770
Fresh newsprint	13.4 (± 0.4)	0.986	38	4-640	13.3 (± 0.3)	0.991	36	8-960
Degraded newsprint	20.5 (± 0.5)	0.992	42	7-790	22.8 (± 0.2)	0.998	38	8-860
Fresh rabbit food	30.4 (± 0.4)	0.997	47	6-848	24.4 (± 0.4)	0.997	29	20-2100
Degraded rabbit food	31.7(± 0.4)	0.998	29	18-990	24.5 (± 0.5)	0.993	28	18-980

[a] Partition coefficient units are (µg/kg)(L/µg), 95% confidence interval in parentheses.

[b] Number of observations

[c] Concentration range (µg/L)

Table 4.11 Freundlich isotherm parameters and partition coefficients describing toluene sorption to MSW components in methanogenic leachate B.

Materials	Log K_f	N	R^2	n	C	K_p	R^2
Fresh rabbit food	1.408 (±0.024)	0.988 (±0.011)	0.999	34	26-964	23.5 (±0.7)	0.992
Fresh newsprint	1.207 (±0.073)	0.980 (±0.035)	0.989	37	8-780	14.2 (±0.6)	0.987

Table 4.12 Partition coefficients describing *o*-xylene sorption to MSW components in acidogenic leachate and methanogenic leachate A.

Materials	Acidogenic leachate				Methanogenic leachate A			
	K_p[a]	R^2	N[b]	C[c]	Kp (mL/g)	R^2	N	C
Fresh newsprint	34.0 (± 0.3)	0.999	41	8-460	30.1 (± 0.4)	0.998	41	8-460
Degraded newsprint	46.2 (± 0.6)	0.997	41	5-500	46.5 (± 0.6)	0.998	41	5-500
Fresh rabbit food	69.9 (± 0.6)	0.999	38	7-770	58.5 (± 1.6)	0.979	39	7-540

Chapter 5

Results and Discussion - Desorption

5.1 Model Development

The BET surface area of the studied MSW components ranged from 0.5-6.0 m^2/g,and organic carbon contents ranged from 27.8 to 87.6%. Based on these small BET surface area and high organic carbon content of sorbents, it was assumed that the intraparticle porosity was negligible and the mass transfer processes were controlled by intraorganic matter diffusion, in which alkylbenzene diffused through the polymeric organic sorbent matrix. To provide quantitative information that assists in interpreting the release rates of sorbed HOCs from tested MSW components, one-, and two-compartment polymer diffusion models were applied.

5.1.1 One-Compartment Polymer Diffusion Model

In the one-compartment polymer diffusion model, it was assumed that the HOC desorption rate is limited by diffusion through a single polymer phase and each sorbent particle is a homogeneous polymeric sphere. This model was used for simulating the desorption kinetics of alkylbenzenes from homogenous plastics (HDPE and PVC). In radial coordinates, Fick's second law of diffusion yields

$$\frac{\partial q}{\partial t} = \frac{D}{r^2}\frac{\partial}{\partial r}\left(r^2\frac{\partial q}{\partial r}\right) \tag{5.1}$$

where D is the diffusion coefficient [L^2/T], q_r is the solid phase concentration [M_x/M_g], r is solid radius [L], and t is time [T].

To solve the differential equation numerically, two dimensionless variables were introduced:

$$T = \frac{Dt}{a^2} \text{ and } R = \frac{r}{a} \tag{5.2}$$

where a is the mean radius of the sorbent particles.

Introducing the dimensionless variables, governing equation became:

$$\frac{\partial q}{\partial T} = \frac{1}{R^2}\frac{\partial}{\partial R}\left(R^2\frac{\partial q}{\partial R}\right) \tag{5.3}$$

The initial and boundary conditions corresponding to the experimental desorption method are also required to solve equation 5.3. For the initial condition, it was assumed that equilibrium was attained, therefore, the solid phase concentration was uniform throughout the sorbent prior to the initiation of the desorption tests, i.e.,

$$q = q_0 \text{ at } T = 0 \text{ and } 0 \leq R \leq 1$$

The first boundary condition requires that symmetry is maintained at the particle center at all time, i.e.,

$$\frac{\partial q}{\partial R} = 0 \text{ at } R = 0 \text{ and } T > 0$$

The second boundary condition specifies the solid-phase concentration at the external particle surface, and it varied depending on whether the purger was turned on or off. When the purger was on, the aqueous-phase alkylbenzene concentration was zero. Assuming instantaneous equilibrium between the solid- and aqueous-phase concentrations at the external particle surface, the solid-phase concentration at the external particle boundary was therefore also zero, i.e.,

$$q = 0 \text{ at } R = 1 \text{ and times when purger was on}$$

When the purger was off, HOC desorption led to an increase in the aqueous-phase

alkylbenzene concentration. Assuming instantaneous equilibrium at the external particle boundary, application of the linear partition model yielded:

$$q = K_d(\frac{M_j - M_t}{V_e}),\ \text{at } R = 1 \text{ and times when purger was off;} \tag{5.4}$$

while application of the nonlinear Freundlich isotherm model yielded:

$$q = K_F(\frac{M_j - M_t}{V_e})^n, \text{at } R = 1 \text{ and times when purger was off.} \tag{5.5}$$

In equations 5.4 and 5.5, M_j and M_t are the intraparticle solute masses at times t_j and t, respectively. K_d is the partition coefficient for linear isotherms, K_F and n are the Freundlich isotherm parameters for nonlinear isotherms, and Ve is the external volume surrounding the intraparticle zone. Mass flux to the external liquid volume at time t during a given time period (t_j to t_{j+1}) was determined by subtracting the intraparticle solute mass at t_{j+1} from that at time t ($t_j \leq t \leq t_{j+1}$). The intraparticle solute mass is calculated as follows:

$$M_j = \frac{4}{3}\pi\rho \sum_{i=2}^{m} \left[(r_i^3 - r_{i-1}^3)\frac{q_i + q_{i-1}}{2} \right] \tag{5.6}$$

where, ρ is sorbent particle density $[M_s/L^3]$ and m is the number of discretized radial intervals.

The Crank-Nicholson numerical method was applied to solve the one-compartment polymer diffusion model. The Newton-Raphson optimization routine was used to determine the diffusion coefficient such that the mean square error between the model output and the experimental data was minimized.

5.1.2 Biphasic Polymer Diffusion Model

A three-parameter biphasic polymer diffusion model was applied to simulate desorption kinetics of alkylbenzenes from biopolymer composites (office paper, newsprint,

and rabbit food). The assumption of the model is that the sorbent particle is comprised of a fast-desorbing compartment and a slow-desorbing compartment. HOC desorption from each compartment is described by separate diffusion coefficients. By applying Fick's law, a system of two differential equations results:

$$\frac{\partial q^r}{\partial t} = \frac{D_r}{r^2}\frac{\partial}{\partial r}\left(r^2\frac{\partial q^r}{\partial r}\right) \tag{5.7}$$

$$\frac{\partial q^s}{\partial t} = \frac{D_s}{r^2}\frac{\partial}{\partial r}\left(r^2\frac{\partial q^s}{\partial r}\right) \tag{5.8}$$

where, D_s is the diffusion coefficient for the slow-desorbing compartment, D_r is the diffusion coefficient for the rapid-desorbing compartment. q^s and q^r correspond to the intraparticle solute concentration in the slow and rapid-desorbing compartments at time t, respectively.

Similar to the one-compartment model, the governing equations were transformed by incorporating dimensionless variables:

$$\frac{\partial q^r}{\partial T} = \frac{1}{R^2}\frac{\partial}{\partial R}\left(R^2\frac{\partial q^r}{\partial R}\right)$$

$$\frac{\partial q^s}{\partial T} = \frac{1}{R^2}\frac{\partial}{\partial R}\left(R^2\frac{\partial q^s}{\partial R}\right)$$

where

$$T_1 = \frac{D_r t}{a^2}, T_2 = \frac{D_s t}{a^2}, \text{and } R = \frac{r}{a}.$$

The corresponding initial conditions are:

$$q^r = \phi_r q_0, \text{and } q^s = \phi_s q_0 \text{ at } T_1 = T_2 = 0, \text{ for all } 0 \leq R \leq 1.$$

where q_0 is the initial solid-phase concentration, ϕ_s is the slowly desorbing fraction, $\phi_r (= 1 - \phi_s)$ the rapidly desorbing fraction,

The boundary conditions at the center of the particle are:

$$\frac{\partial q^r}{\partial R} = 0 \tag{5.9}$$

$$\frac{\partial q^s}{\partial R} = 0 \tag{5.10}$$

The boundary conditions at the external sorbent surface are:

$$\begin{aligned} q^r(r &= a) = q^s(r = a) = 0, \text{ when purger is on;} \\ q^r(r &= a) = K_d \frac{M_j^r - M_t^r}{V_e},\ q^s(r = a) = K_d \frac{M_j^s - M_t^s}{V_e}. \end{aligned}$$

The definitions of M_j and M_t are the same as those in one-compartment diffusion model.

The coupled system of differential equations was solved using Crank-Nicholson numerical method, and the values of D_r, D_s and Φ_r were obtained with a modified Levenberg-Marquardt nonlinear optimization technique (IMSL C numerical libraries, Visual Numericals, Inc., Houston, TX).

5.2 Model Verification and Interpretation

5.2.1 Model Verification

The validity of the finite difference models was verified by comparing the numerical solutions to the analytical solutions provided by Crank (1975) for the one-compartment diffusion model and Carroll et al. (1994) for the two-compartment model (Figure 5.1). Table 5.1 summarizes the relevant MSW component properties used in model simulation. One of the numerical solutions in Figure 5.1 was obtained by assuming that the purger was always on while the second numerical solution was based on experimental purging conditions used in this study. Figure 5.1 illustrates representative comparisons of the numerical and analytical solutions for one- and two-compartment models. Toluene desorption from the homogenous polymeric sorbent (HDPE) was described by the one-compartment model while toluene desorption from the biopolymer composite fresh rabbit food was described by the two-compartment model. For toluene desorption from HDPE, the value of D was $4.75*10^{-11}$ cm^2/s. For toluene desorption from fresh rabbit food, D_r was $4.09*10^{-9}$ cm^2/s, D_s was $4.29*10^{-11}$ cm^2/s,

and Φ_r was 0.8227. As shown in Figure 5.1, the numerical results assuming continuous purge were in good agreement with the analytical results for the two models, which implied that the numerical solutions were accurate and good approximations of the exact model solutions. Numerical models were more flexible than analytical ones, however, because they permitted the incorporation of experiment-specific boundary conditions.

Additionally, Figure 5.1 shows that differences in toluene desorption rates for continuous and intermittent purge scenarios were small. From a standpoint of experimental method development, an intermittent purge was cheaper and more feasible than a continuous purge. However, the results in Figure 5.1 suggest that the intermittent purge technique maintained a concentration gradient between the solid and liquid phases that closely approximated the maximum concentration gradient, i.e., that obtained for an infinite bath.

Table 5.1. Properties of model MSW components

Materials	Particle density (g/cm^3)	Mean particle diameter (μm)
Fresh rabbit food	1.50	320
Degraded rabbit food	1.78	289
Fresh newsprint	1.32	298
Degraded newsprint	1.81	213
Fresh office paper	1.44	278
Degraded office paper	2.13	210
HDPE	0.962	500
PVC	1.4	140

5.2.2 Model Interpretation

One-Compartment Polymer Diffusion Model

One compartment polymer diffusion model was applied to simulate the desorption kinetics of toluene and *o*-xylene from HDPE and PVC at different aging times. The diffusion coefficients are listed in Table 5.2. As mentioned previously, HDPE is a homogenous rubbery polymer and PVC a homogeneous glassy polymer. However, prior

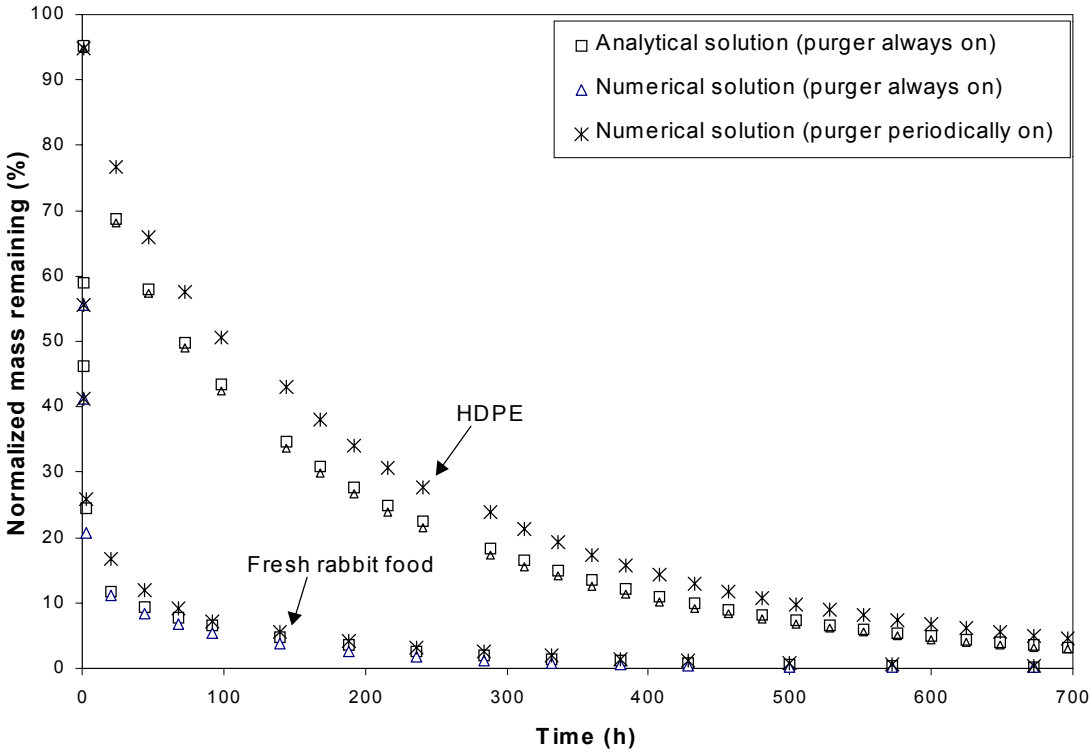

Figure 5-1: Comparison of analytical and numerical solutions for one and two-compartment models

research (Wu et al. 2001) showed that PVC is plasticized by acidogenic leachate constituents. Therefore, the isotherm model employed to describe the boundary condition at the external particle surface was linear for HDPE and for PVC in acidogenic leachate but non-linear for PVC in methanogenic leachate. Figure 5.2 depicts the one-compartment model fitting for experimental toluene desorption data from HDPE , PVC, and rabbit food in acidogenic leachate after aging time of 8 months . As seen in Figure 5.2, toluene desorption rates from HDPE and PVC were well described by the one-compartment model, and diffusion coefficients yielding the best fits of experimental data were $3.85*10^{-11}\ cm^2/s$ and $4.78*10^{-14}\ cm^2/s$ for HDPE and PVC, respectively. However, the one-compartment model underestimated early release and overestimated later release for fresh rabbit food. The same trend was consistently observed for all other tested biopolymer composites such as fresh and decomposed newsprint and office paper. Hence, the one-compartment diffusion model is only appropriate to describe desorption kinetics for homogenous polymers such as HDPE and PVC. In contrast, rabbit food and paper materials are complex biopolymer composites that exhibit two-stage desorption behavior. Therefore, a biphasic polymer diffusion model was employed to simulate HOC desorption rates from fresh and degraded biopolymer composites.

Table 5.2. Diffusion coefficient estimates for the one-compartment polymer diffusion model

sample	Toluene				*o*-xylene	
	Acidogenic leachate		Methanogenic leachate		Acidogenic leachate	
	D (cm^2/s)	MSE	D (cm^2/s)	MSE	D (cm^2/s)	MSE
HDPE (30 days)	4.72E-11	0.019	4.53E-11	0.014	N/A	N/A
HDPE (250 days)	3.85E-11	0.010	4.72E-11	0.011	1.06E-11	0.011
PVC (30 days)	3.74E-14	0.003	1.78E-14	0.004	N/A	N/A
PVC (250 days)	4.78E-14	0.004	1.94E-14	0.004	1.39E-14	0.002

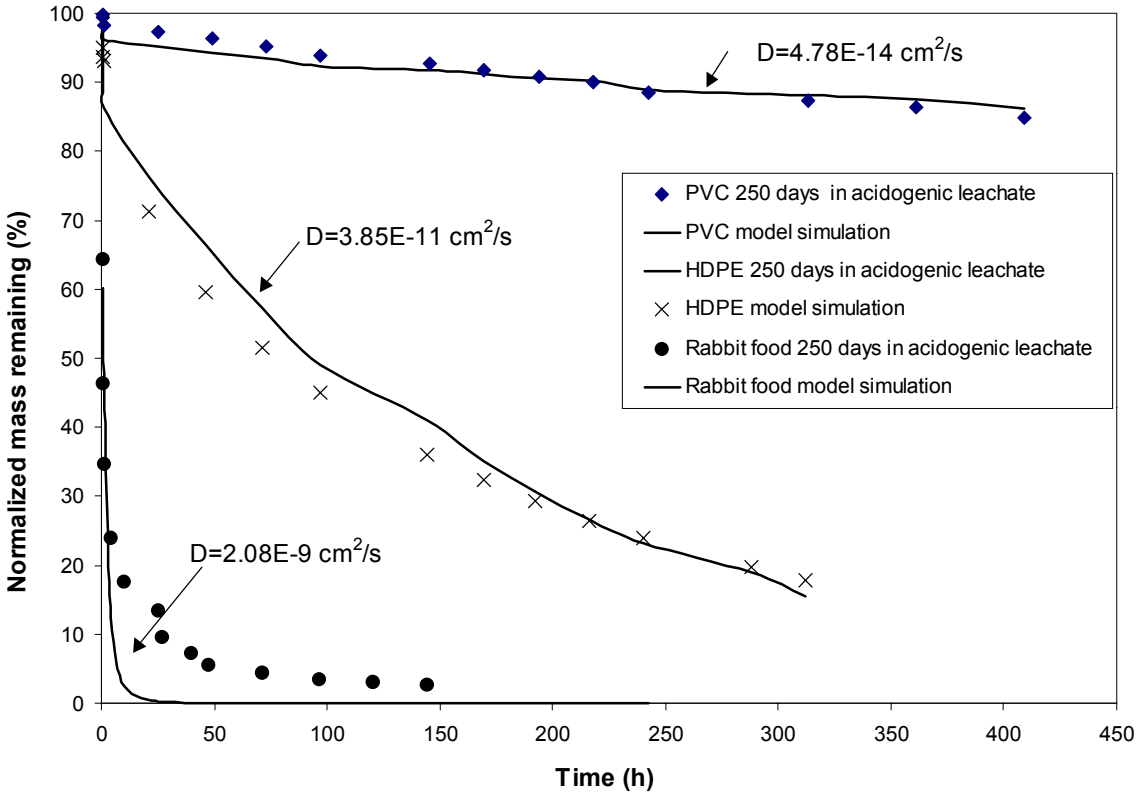

Figure 5-2: Experimental toluene desorption data and one-compartment polymer diffusion model simulations for MSW components in acidogenic leachate after 250 days aging

Biphasic Polymer Diffusion Model

Model simulations for toluene desorption from degraded rabbit food at two aging times (30 days and 250 days) are depicted in Figure 5.3. As shown in Figure 5.3, the biphasic polymer diffusion model successfully described the two-stage desorption behavior observed for biopolymer composites. As mentioned earlier, the basic assumption for the model is that solid-phase HOC concentrations in slow and rapid-desorbing compartments of the sorbents are in equilibrium with the liquid-phase HOC concentration prior to desorption. The assumption of true equilibrium might in some cases be inappropriate for short aging periods, however, in which case, the fitting routine tends to bias desorption rate parameters by assuming initial equilibration. If equilibration is not attained before desorption starts, bi-directional diffusion will develop, i.e., sorption continues in an inward direction and desorption in an outward direction. The improper assumption of equilibrium at the start of a desorption test will result in an underestimation of desorption rate, because the measured HOC mass released at any given time is smaller than that if equilibrium existed at the start of experiment. In addition, the nonequilibrium condition may also lead to an overestimation of the desorption rate. The latter occurs if the outer region of sorbent is oversaturated with the sorbate before reaching equilibrium. In that case, the mass desorbed during the early purge period will be greater than that if true equilibrium existed at the start of the experiment. Consequently, the model yields an overestimation of the rate parameter to fit the early desorption data.

In this study, it was assumed that a contact time of 250 days was sufficient to reach sorption equilibrium for biopolymer composites. Consequently, it was assumed that the diffusion coefficients D_s and D_r obtained from model fitting are reflections of the true diffusion coefficients associated with the slow- and rapid-desorbing compartments. These diffusion coefficients should not vary with aging time, but the HOC fractions in slow- and rapid-desorbing compartments of the sorbents can vary. In this study, the optimal parameter estimates for Φ_s, D_r and D_s were first obtained by a non-linear least-square optimization routine for desorption data after 250 days

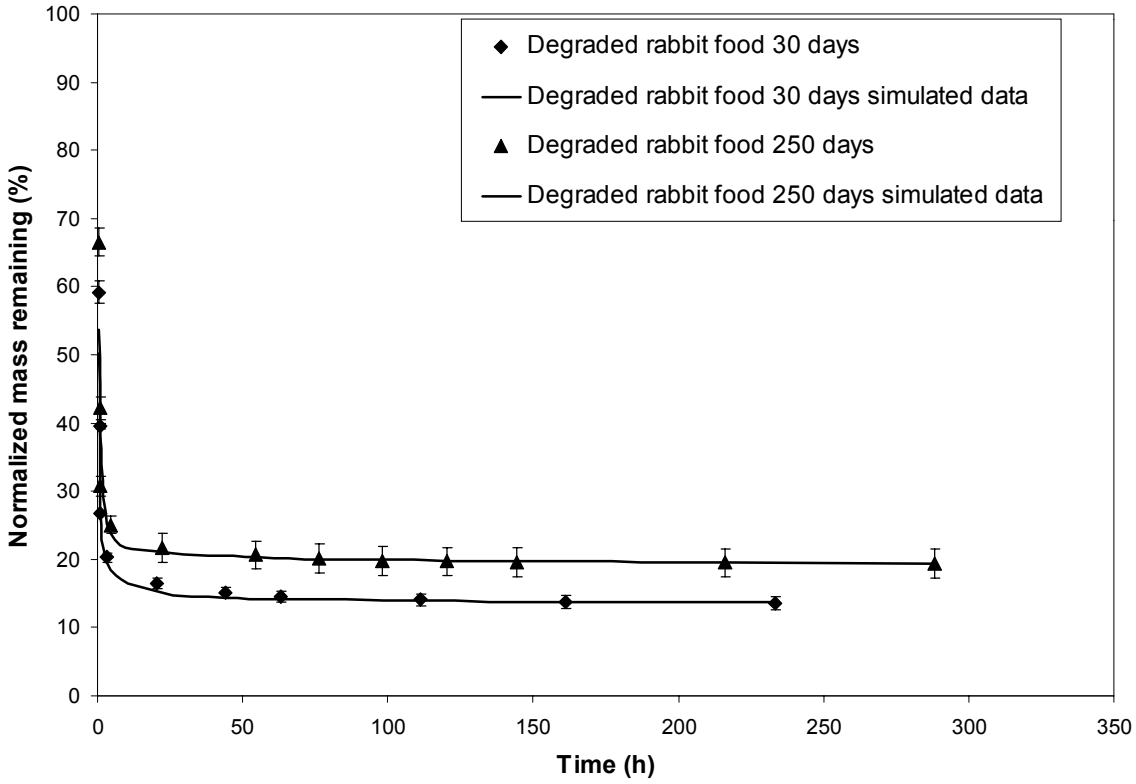

Figure 5-3: Experimental toluene desorption data for degraded rabbit food in acidogenic leachate and biphasic polymer diffusion model simulations

aging. The D_r and D_s values calculated from the desorption data obtained after 250 days of aging were subsequently used to simulate desorption rates at shorter aging times. Only the HOC fraction in the slow-desorbing compartment (Φ_s) was adjusted by the search routine to obtain model fits for desorption data after an aging time of 30 days. Therefore, aging effects on desorption rate were assessed by changes in the HOC fractions residing in the slow- and rapid-desorbing compartments at different aging times. Parameter estimates describing toluene and *o*-xylene desorption from biopolymer composites in acidogenic leachate at two aging times are summarized in Table 5.3.

Table 5.3. Desorption rate parameter estimates for the two-compartment polymer diffusion model in acidogenic leachate

	Toluene				*o*-xylene			
sample	Φ_r	Φ_s	Dr (cm^2/s)	Ds (cm^2/s)	Φ_r	Φ_s	Dr (cm^2/s)	Ds (cm^2/s)
Fresh newsprint (30 days)	0.9517	0.0483	3.76E-9	4.79E-14				
Fresh newsprint (250 days)	0.8786	0.1214	3.76E-9	4.79E-14	0.8992	0.1008	3.74E-9	5.27E-16
Degraded newsprint (30 days)	0.8806	0.1194	1.56E-9	2.48E-14				
Degraded newsprint (250 days)	0.8073	0.1927	1.56E-9	2.48E-14	0.8248	0.1752	1.32E-9	3.38E-13
Fresh rabbit food (30 days)	0.8706	0.1294	4.04E-9	4.29E-11				
Fresh rabbit food (250 days)	0.8227	0.1773	4.04E-9	4.29E-11	0.7378	0.2622	3.71E-10	1.03E-11
Degraded rabbit food (30 days)	0.8539	0.1461	5.17E-9	9.19E-14				
Degraded rabbit food (250 days)	0.7918	0.2082	5.17E-9	9.19E-14	0.7728	0.2272	6.07E-10	6.09E-12
Fresh office paper (30 days)	0.8414	0.1586	2.62E-10	2.26E-11				
Fresh office paper (250 days)	0.5591	0.4409	2.62E-10	2.26E-11	0.4727	0.5273	4.88E-10	2.47E-12
Degraded office paper (30 days)	0.5539	0.4461	1.76E-9	7.83E-12				
Degraded office paper (250 days)	0.4221	0.5779	1.76E-9	7.83E-12	0.4320	0.5681	1.62E-9	1.87E-12

5.3 Effects of Sorbent Type on Desorption Rate

In Figure 5.4, the normalized toluene mass remaining in the solid phase is depicted as a function of time for all tested MSW components after an aging time of 30 days in aciodgenic leachate. For heterogeneous biopolymer composites (sorbents other than PVC and HDPE), the desorption curves suggest that a fast initial desorption step during the first 20 hours, was followed by a slow desorption period. In contrast, toluene desorption rates were more uniform during the entire test period from HDPE and PVC. Figure 5.4 also shows that desorption rates and extents were strongly related to sorbent type. Overall, PVC showed the slowest desorption rate while fresh rabbit food and fresh newsprint showed the fastest.

As shown in Table 5.2, the diffusivity of alkylbenzene in PVC, a glassy polymer, is

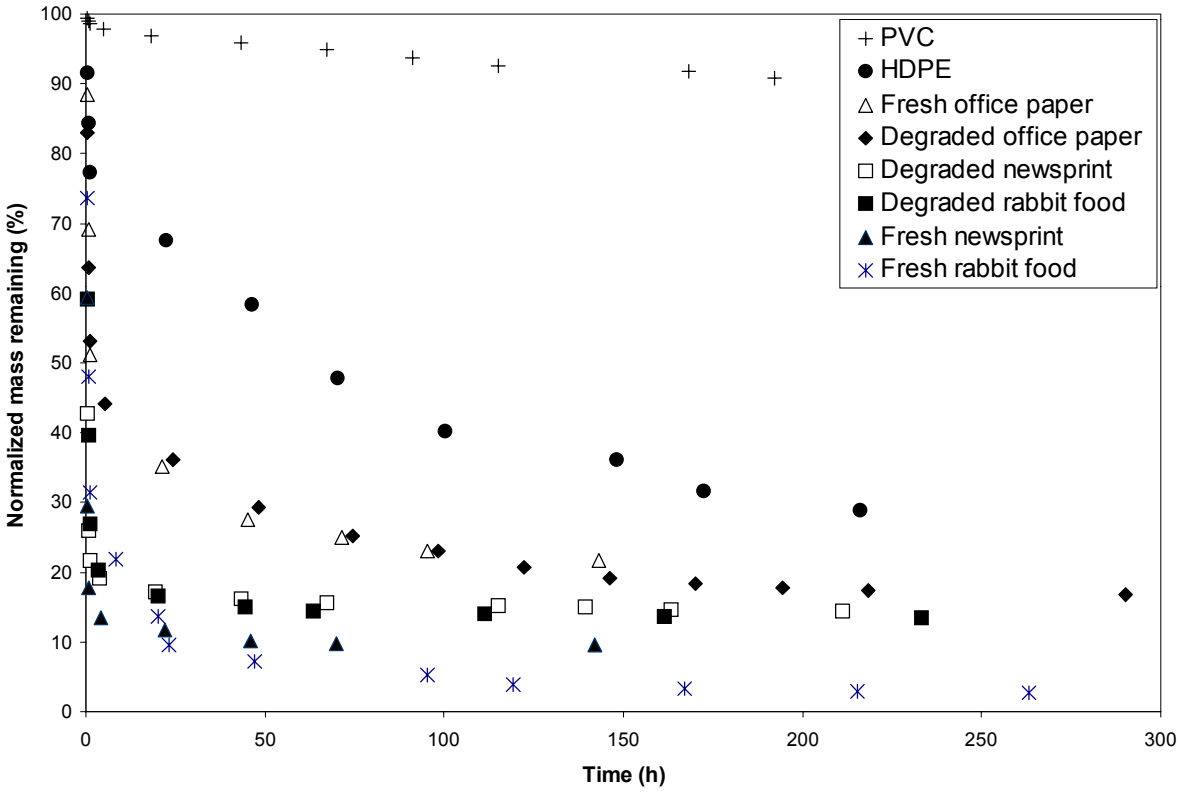

Figure 5-4: Experimentally determined toluene desorption rates from MSW components after aging of 30 days in acidogenic leachate

on the order of $10^{-14} cm^2/s$, and that in HDPE, a rubbery polymer, is on the order of $10^{-11} cm^2/s$, which are in consistent with the values reported from literature (Berens 1989, Rogers et al. 1960). Diffusion in glassy polymers is generally much slower than in rubbery polymers, the ratio of $D_{rubbery}/D_{glassy}$ may be 10^2 –10^8 (Berens 1989, Carroll et al. 1994, Leboeuf et al. 1997). The polymeric organic matrix within glassy polymers is more rigid than within rubbery polymers, which explains the smaller diffusivities in glassy polymers. Additionally, nanovoids contained within glassy polymer matrices provide strong adsorption sites that further reduce desorption rates.

For toluene desorption from biopolymer composites, the HOC diffusion coefficients from the rapid-desorbing compartment range from 10^{-10} –$10^{-9} cm^2/s$ while those for slow-desorbing compartment range from 10^{-14}–$10^{-11} cm^2/s$. The range of rapid diffusion coefficients are in close agreement with HOC diffusion coefficients for soils and sediments obtained by one-compartment intraparticle diffusion models (10^{-8} –10^{-10} cm^2/s, Harmon and Roberts et al. 1994, 10^{-9} –10^{-10} cm^2/s, Werth et al. 1997). Very little information is available on diffusion coefficients based on two-compartment diffusion models. Johnson et al. (2002) reported D_r/a^2 and D_s/a^2 values for phenathrene desorption from geosorbents, which ranged from 0.00031 to 0.032 day^{-1} for D_r/a^2 and from 0.000011 to 0.0010 day^{-1}for D_s/a^2. Table 5.4 summarized the calculated D_r/a^2 and D_s/a^2 values for toluene desorption from biopolymer composites after aging for 250 days, where diffusional length scale is assumed to be equal to mean solid particle radius. D_r/a^2 values for toluene desorption from biopolymer composites are several orders of magnitude larger than that for phenanthrene desorption from geosorbents, whereas D_s/a^2 values in this study are close to literature values. Carroll et al. (1994) reported that diffusion coefficients for PCBs in rubbery and glassy sediment organic matter were 2.6*10^{-18} and 7.3*10^{-21} cm^2/s, respectively. These values are several orders of magnitude smaller than the diffusion coefficients obtained in this study. Those differences between values from literature and this study may be in part due to differences in sorbate properties (phenanthrene and PCBs are longer and more

hydrophobic than alkylbenzenes) and sorbent properties. Piatt et al. (1998) studied the sorption of homologous series of polycyclic aromatic hydrocarbons, alkylated benzenes, chlorinated benzenes and chlorinated alkenes to two soils and indicated that the diffusion coefficients for the most soluble HOCs (benzene, toluene and DCB) were almost two orders of magnitude higher than phenanthrene and pyrene. Their results also confirmed that the diffusion within SOM matrix was highly dependent on sorbate shape/structure. The D/a^2 values for HDPE and PVC in methanogneic leachate after 250 days aging were 0.0065 and $3.42*10^{-5}$ day^{-1}, respectively, indicating that slow-desorbing compartments are glassy-like organic matter. In addition, uncertainty in diffusion length scales affect diffusivity estimates. The slow-desorbing fraction varied from 0.0483 for fresh newsprint to 0.5779 for degraded office paper (Table 5.3). Furthermore, as seen in Figure 5.4, the mass fraction of toluene remaining on the sorbents after a desorption time period of 200 hours was between 5% (rabbit food) and 20% (fresh and degraded office paper). These results suggest that a large fraction of HOC sorbed to biopolymer composites was released rapidly. However, the remaining HOC fraction was released very slowly (the diffusivities for the slowly desorbing fractions were up to 5 orders of magnitude smaller than those for the rapidly desorbing fractions), suggesting that mass transfer processes largely control the long-term fate and transport of remaining HOC fraction.

Table 5.3 also shows that the Φ_s values increased as fresh biopolymer composites were anaerobically degraded, suggesting that alkylbenzene sequestration to biopolymer composites was enhanced during anaerobic biodegradation in landfill. Similar observation has been reported previously for sediments; i.e., biologically mediated increases in sorbent hydrophobicity can lead to enhanced HOC sequestration (Guthrie et al. 1999).

To investigate the effects of sorbent organic matter characteristics on alkylbenzene desorption rates, the relationship between log (Φ_r/Φ_s) and O-alkyl/alkyl ratio of the sorbent organic matter was plotted for toluene and *o*-xylene after 250 days equilibration. The plot shows that the ratio of the rapid fraction to the slow fraction increases with increasing sorbent polarity. However, the trend observed for fresh

and degraded office paper differed from that observed for the remaining biopolymer composites. One mechanistic interpretation for relationship between sorbent polarity and log (Φ_r/Φ_s) is that HOC desorption rates are dependent on the surface energy of sorbent organic matter. For newsprint and rabbit food, lipophilic extractives and lignin primarily controlled HOC sorption (Wu et al. 2001). According to Reinhart et al. (1990), the surface energy of lipophilic extractives is lower than that to lignin, and sorption affinity of HOC is inversely related to surface energy. The lipophilic extractives content of fresh and degraded rabbit food was approximately 5%, while that of fresh and degraded newsprint was approximately 1.5%, therefore, a large fraction of sorbed alkylbenzenes was likely associated with lipophilic extractives in fresh and degraded rabbit food than in fresh and degraded newsprint. It is thus plausible that the slowly desorbing HOC fraction is associated with a strongly hydrophobic environment such as that offered by liphophilic extractives.

Table 5.4. Dr/a^2 and Ds/a^2 values for toluene desorption from biopolymer composites

	Dr (cm^2/s)	Ds (cm^2/s)	Dr/a^2 (day^{-1})	Ds/a^2 (day^{-1})
Fresh newsprint (250 days)	3.76E-09	4.79E-14	1.46	1.86E-05
Degraded newsprint (250 days)	1.56E-09	2.48E-14	0.61	9.65E-06
Fresh rabbit food (250 days)	4.04E-09	4.29E-11	1.57	0.017
Degraded rabbit food (250 days)	5.17E-09	9.19E-14	2.01	3.58E-05
Fresh office paper (250 days)	2.62E-10	2.26E-11	0.10	0.0088
Degraded office paper (250 days)	1.76E-09	7.83E-12	0.68	0.0030

The different trend established by fresh and degraded office paper is difficult to interpret. One possible hypothesis for comparatively large slow desorption compartments in fresh and degraded office paper is that conformational changes within the organic matrix of office paper materials occurred during or after the uptake of solute such that diffusional pathways were blocked to some extent, e.g., Barrer et al. (1957) suggested that ethyl cellulose chains formed an ordered or immobilized configuration with penetrants such as benzene. Some recent findings also support the hypothesis

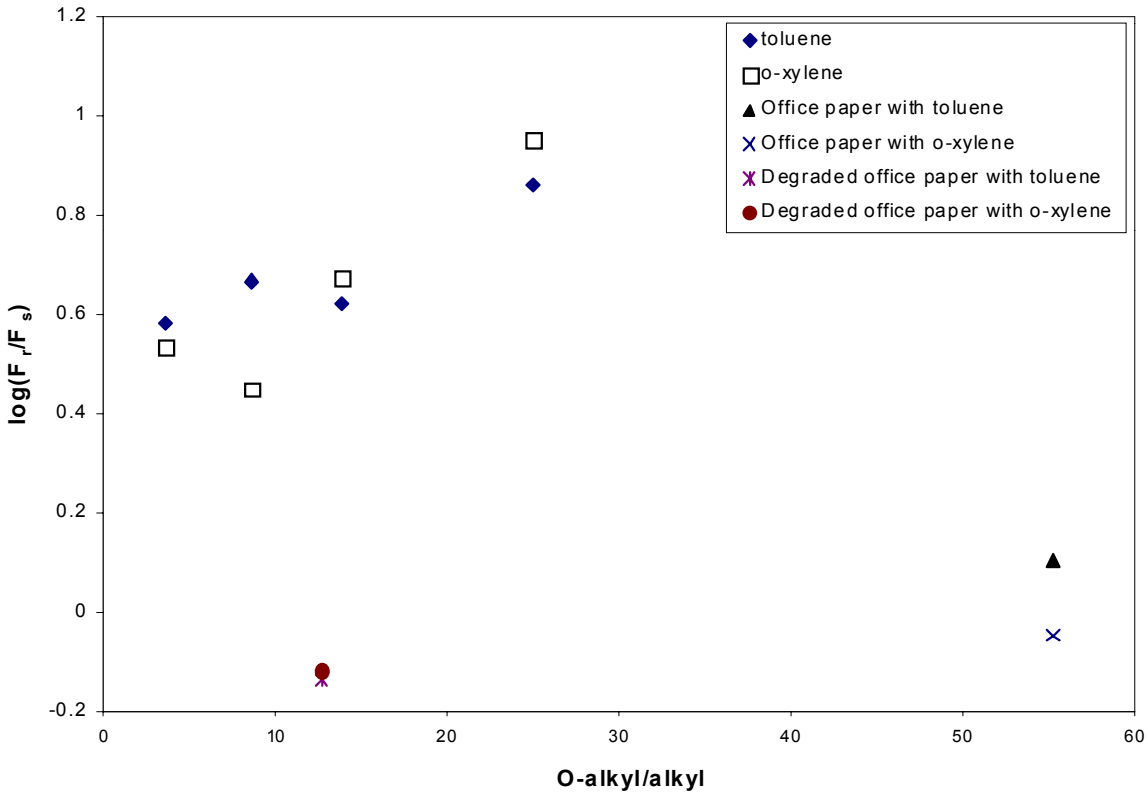

Figure 5-5: The relationship between log (Φ_r/Φ_s) and O-alkyl/alkyl ratio of sorbent organic matter

that conformational change in the organic matter of solid may affect the mass transfer rate of solute (Deitsch et al. 1998, 2000, Kan et al. 1997). Their studies support the hypothesis that rearrangement of SOM may obstruct or destruct diffusional pathway. Another possible explanation is that a fraction of sorbed alkylbenzenes are strongly associated with sizing agent in office paper. Sizing agents such as alkyl ketene dimers are hydrophobic compounds that lower the surface energy of paper. Further research such as NMR analysis is needed to provide the mechanistic information about how and where alkylbenzenes are associated with organic matter in office paper materials.

5.4 Aging Effects

The HOC fraction residing in the rapid-desorbing compartment (ϕ_r) decreased with increasing aging time from 30 days to 250 days for all biopolymer composites (Table 5.3 and Figure 5.6). The aging effects suggest that alkylbenzenes had not fully penetrated into the slow-desorbing compartment of sorbents at the end of the shorter aging period. Hence, the increase in Φ_s between 30 and 250 days demonstrates an aging effect that can be explained by continued diffusion into the slow-desorbing compartment.

No aging effects were observed for HDPE (Figure 5.6) because of its homogeneous rubbery polymeric structure. For PVC, toluene diffusivities after 250 days were similar to those after 30 days aging samples in both acidogenic and methanogenic leachates (Table 5.2). These results are fortuitous given the assumption that sorption equilibrium was reached after the 30 days of aging. Based on sorption kinetic tests performed earlier, sorption equilibrium was only attained after a contact time of about 250 days. Recognizing that the sorption sites located at the center of PVC particles were not fully occupied after 30 days of aging, bi-directional diffusion occurred at the initiation of the desorption test. Given that a uniform concentration profile was assumed in the model, the occurrence of bi-directional diffusion should yield an underestimate of the true diffusion coefficient. Furthermore, the oversaturation of the outer region of PVC with toluene before reaching equilibrium tends to yield an overestimate of the

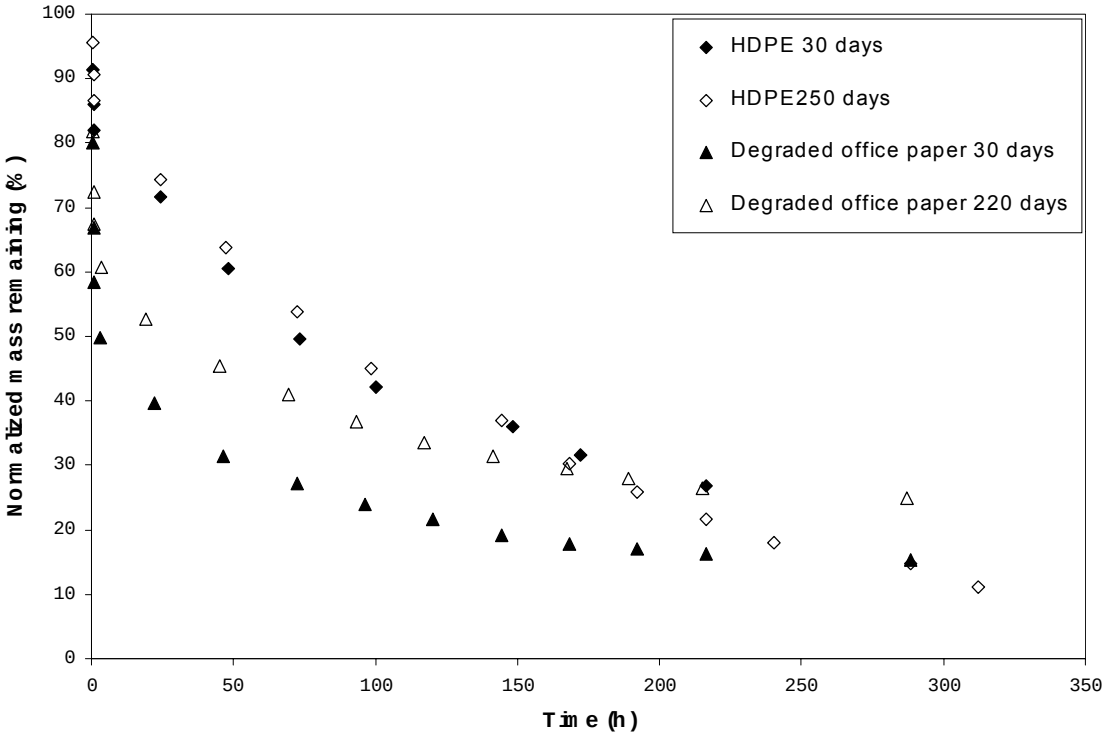

Figure 5-6: Toluene desorption from HDPE and degraded office paper in methanogenic leachate at two aging times

diffusion coefficient when a uniform concentration profile is assumed. However, it appears that the effects of oversaturation and bi-directional diffusion on the diffusivity estimate cancelled each other such that the toluene diffusivity after 30 days of contact with PVC was similar to that after 250 days of contact. Also, at a given initial spiked toluene mass and PVC dose, the solid phase toluene concentration increased by only about 10% as aging time increased from 20 to 250 days. Thus, the relatively small change in the solid phase concentration is another explanation for the similar toluene diffusivities obtained after 30 and 250 days aging.

5.5 Solute Effects

Two solutes were studied in this research, toluene and *o*-xylene. The comparisons of desorption kinetics between toluene and *o*-xylene for HDPE, fresh rabbit food and newsprint are depicted in Figure 5.7. Figure 5.7 shows that desorption rates of *o*-xylene were slower than toluene given rabbit food and HDPE as sorbents, and same trend was also observed for degraded rabbit food as well as for fresh and degraded office paper. However, the desorption rate of *o*-xylene is same as that of toluene for fresh and degraded newsprint.

Table 5.2 shows that the diffusivities of *o*-xylene for PVC and HDPE are approximately 3.5 times smaller than those of toluene. Comparing D_s and D_r values of toluene and *o*-xylene for fresh and degraded rabbit food in Table 5.3, *o*-xylene D_r values are $\sim$10 times smaller than that of toluene. Since the rapid-desorbing fraction constitutes a major part of rabbit food materials ($\sim$80%), the decrease of desorption rate of *o*-xylene was mainly attributable to desorption from the rapid-desorbing fraction. For fresh and degraded office paper, the D_r values of *o*-xylene and toluene differed only slightly, but the D_s values of *o*-xylene were 9.1 times smaller for fresh office paper and 4.2 times smaller for degraded office paper than those of toluene. The slow-desorbing fraction within office paper materials ranged up to 50%, so the slow-desorbing compartment likely contributed to slower desorption rate of *o*-xylene.

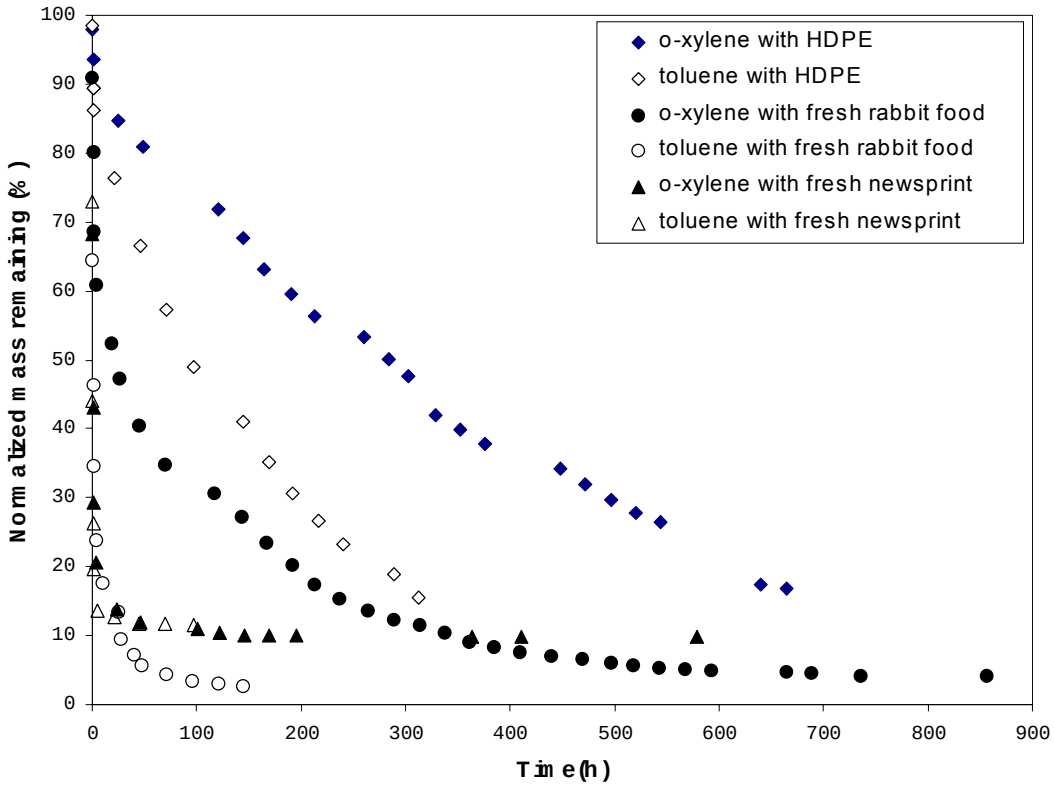

Figure 5-7: Toluene and *o*-xylene desorption from HDPE, fresh rabbit food and fresh newsprint in acidogenic leachate after 250 days aging

Given that *o*-xylene is a larger molecule than toluene (the molecular diameters of *o*-xylene and toluene are 0.68 and 0.585 nm, respectively, Baertsch et al. 1996), the inverse relationship between molecular size and desorption rates for the two solutes are attributed to the diffusional resistances that increase with molecular size (Ball and Roberts 1991, Deitsch et al. 1998, Berens 1989). Sorbates with a larger molecular size or a more complex structure exhibit increased potential for entanglement with the sorbent organic matter matrix; therefore, diffusion is hindered.

For fresh and degraded newsprint, desorption rates of toluene and *o*-xylene differed only slightly. The reason for this observation is not clear and no explanation can be offered at this time.

Additionally, the slow and rapid fractions obtained for *o*-xylene and toluene for a given sorbent are quite similar, a result that is consistent with the assumption that intraorganic matter diffusion controlled HOC desorption rates. The two solutes differ only slightly in their solubility parameters (8.8 $(cal/cm^3)^{1/2}$ for toluene and 8.9 $(cal/cm^3)^{1/2}$ for *o*-xylene) and are likely sorbed to the same organic matter phases, therefore, similar Φ_r and Φ_s can be expected.

5.6 Leachate Effects

The effects of two leachate phases on the rates of alkylbenzene desorption from MSW components were also investigated (Figures 5.8 and 5.9). Except for fresh office paper and PVC, leachate composition did not affect alkylbenzene desorption rates. For fresh office paper, toluene and *o*-xylene desorption rates were faster in acidogenic leachate than in methanogenic leachate. As suggested by other researchers, environmental factors such as pH, ionic strength and temperature can alter the polymeric structure of sorbent organic matter (Kan et al. 1994, Carroll et al. 1994, Deitsch et al. 1999). One difference between the two leachate phases was pH (pH 4.9 for acidogenic leachate and 7.8 for the methanogenic leachate). To determine whether pH was responsible for the differences in toluene desorption rate between the two leachates, the desorption tests for toluene with fresh office paper were also performed in phosphate-buffered (1mM)

DI water at pH 5 and pH 7 (Figure 5.9). The desorption curves of toluene in neutral DI water and in methanogenic leachate were almost identical as were the desorption curves in acidified DI water and acidogenic leachate. These data illustrate that the pH difference between acidogenic and methanogenic leachate caused the different desorption rates. Fresh office paper primarily consists of cellulose and hemicellulose and may undergo hydrolysis due to the existence of acidic compounds in acidogenic leachate (Esteghlalian et al. 1997, Maloney et al. 1985, Lipinsky 1979). Under dilute acidic conditions, the hydrogen bond between carbohydrate polymers may be broken and cellulose may dissociate partially as a result. In addition, hemicellulose associated with cellulose is vulnerable to acid attack and may be hydrolyzed to its monomeric constituents (Maloney et al. 1985). Consequently, the hydrolysis of cellulose and hemicellulose in acidogenic leachate altered the organic matrix of office paper such that toluene desorption rates were enhanced.

The diffusivity of toluene in PVC that was in contact with acidogenic leachate was approximately 2 times larger than that in methanogenic leachate (Table 5.2). Initially, it was assumed that organic compounds such as propionic and butyric acids in acidogenic leachate plasticized PVC and converted it from the glassy to the rubbery state (Wu et al. 2001). As a result, the toluene sorption isotherm on PVC was linear and plasticization would also explain enhanced toluene diffusivities. To verify the plasticization hypothesis, volatile fatty acid (VFA) analyses were performed for acidogenic leachate samples (20 ml) that were contacted with 1 g PVC for 3 months and for acidogenic leachate containing no PVC (Table 5.5). The VFA results showed negligible changes in VFA concentrations between blank samples and mixture containing PVC. Nonetheless, the plasticization of PVC by VFAs cannot be ruled out. One possible explanation is that the analytical method used for VFA analysis was not sufficiently accurate to detect small VFA concentration changes (the variation of VFA concentrations between duplicate samples was up to 200 mg/L). The solid phase concentration of VFA would be about 2 mg/g if the difference between initial and equilibrium VFA concentration was 100 mg/L. Xia and Pignatello (2001) determined that solid-phase concentrations of $\sim$5 mg/g for 1,2-DCB and $\sim$1 mg/g for

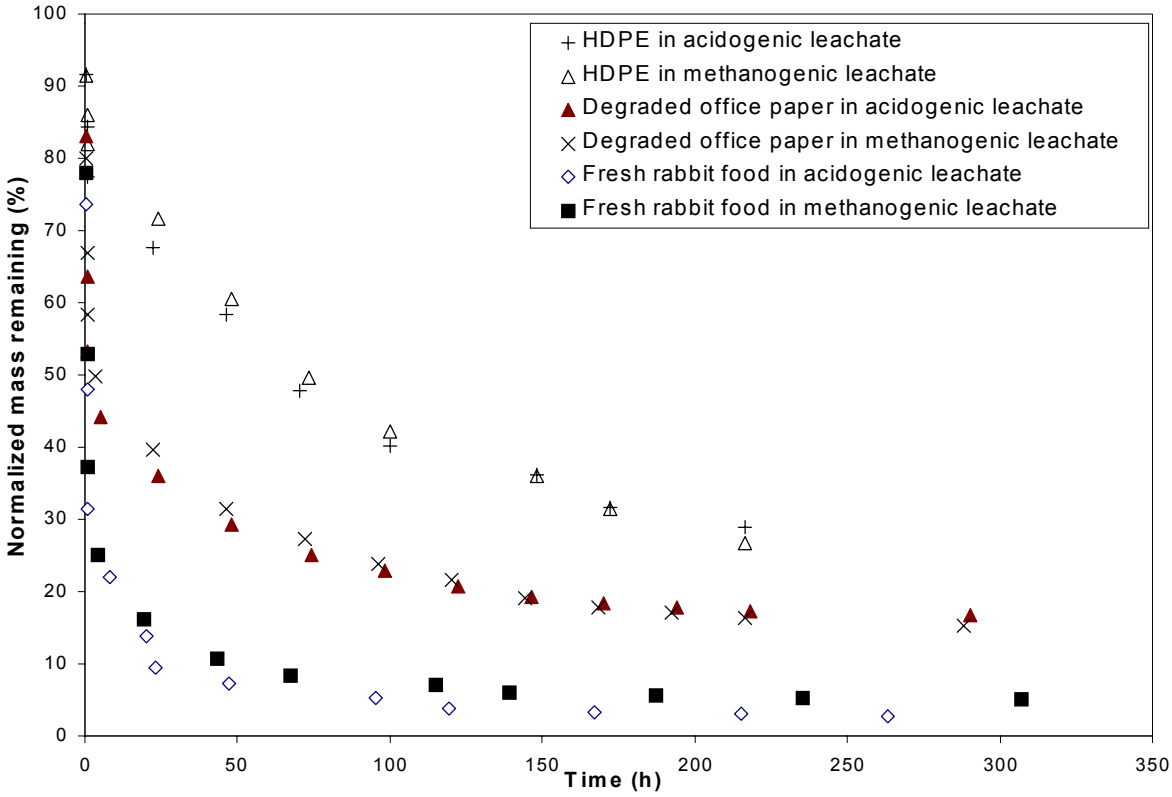

Figure 5-8: Toluene desorption from HDPE and biopolymer composites in two leachate phases after 30 days of aging

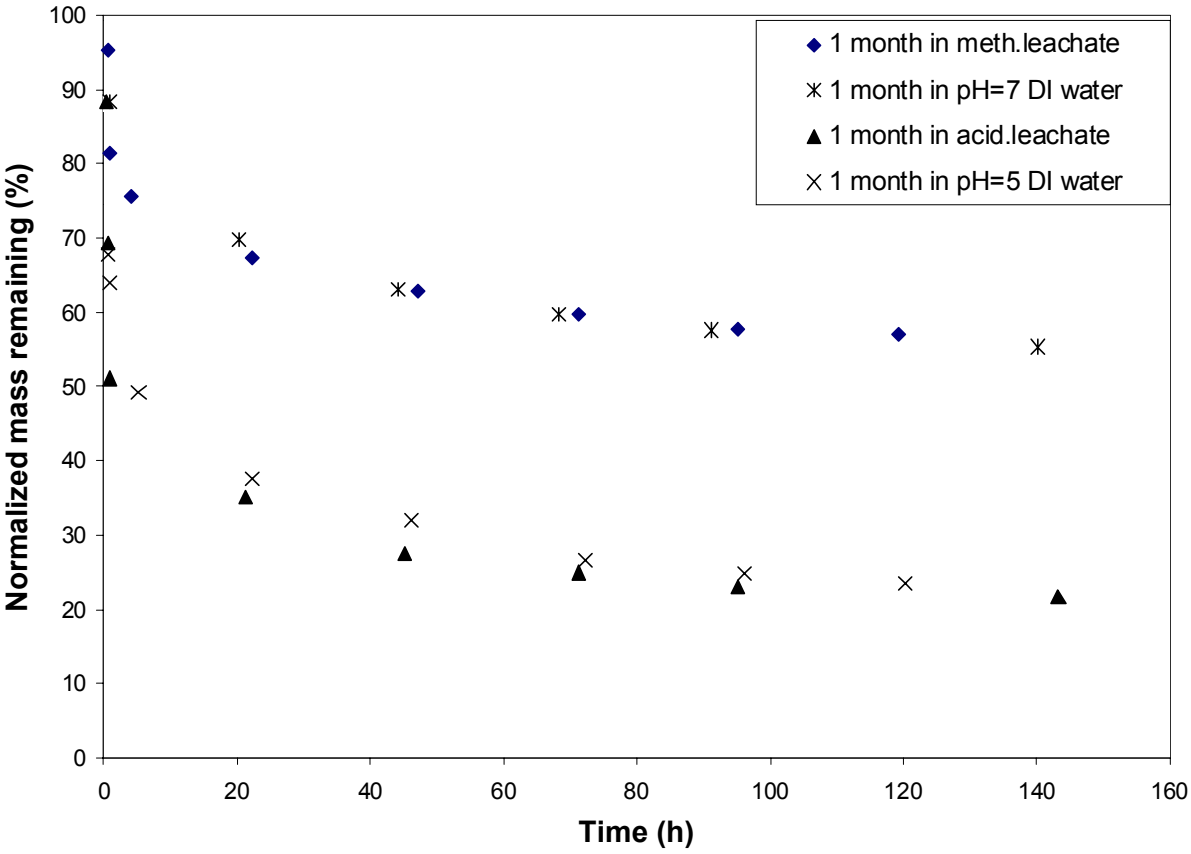

Figure 5-9: pH effects on toluene desorption rates for fresh office paper

1,2,4-TCB could plasticize PVC. Therefore, it is possible that PVC was softened by VFAs in acidogenic leachate but the employed analytical technique could not detect the resulting VFA concentration changes. Another possible explanation is that the softening of PVC was caused by other factors such as the pH or ionic strength of acidogenic leachate. Factors such as pH and high ionic strength may alter sorbent organic matter (Kan et al. 1994) although no direct evidence is available to date to support this hypothesis. Further investigation is therefore required to fully understand the effects of acidogenic leachate on alkylbenzene sorption to and desorption from PVC.

Table 5.5. VFA analysis for acidogenic leachate with/without PVC

Volatile fatty acids	PVC+acidogenic leachate after 3month aging (mg/L)		Acidogenic leachate after 3month aging (mg/L)	
	sample 1	sample 2	sample 1	sample 2
Acetic acid	2000	1963	1970	1962
Propionic acid	834	876	861	803
i-butyric acid	47.1	47.2	47.1	47.2
Butyric acid	2104	2198	2202	1940
2-methyl butyric acid	51	50	49	52
Valeric acid	811	841	795	890
i-caproic acid	39	47	51	60
Caproic acid	94	99	102	115
Heptanoic acid	47	46	45	45

5.7 Mass Balances

Mass balances were measured for three sorbate/sorbent systems (toluene sorbed to degraded rabbit food, *o*-xylene sorbed to degraded newsprint, and degraded office paper, all after 250 days aging) and results are provided in Table 5.6. Overall, recoveries for the three materials were between 98% and 102%, indicating that HOC losses in batch reactors were negligible and the experimental procedure was reliable for measuring desorption kinetics. It was hypothesized that benzyl alcohol extraction swelled

the sorbent organic matrix and opened diffusive pathways in those regions of the sorbent organic matter from which alkylbenzene partially desorbed (Deitsch and Smith 1999). About 5-10% of the initial alkylbenzene mass was recovered by benzyl alcohol extractions. The fraction of alkylbenzenes associated with humic and fulvic materials (0-3%) was recovered in 0.1N NaOH. The remaining non-extractable alkylbenzene fraction in MSW components (∼4-6%) may have been associated with humins. These alkylbenzene residues are likely sequestered as a result of strong non-covalent interactions with non-extractable sorbent organic matter. Non-covalent interactions such as van der Waals forces and hydrogen bonding can be sufficiently strong to prevent HOC removal by solvent extraction (Guthrie et al. 1999)

Table 5.6. Mass balance analysis

Solid		Chemical	Desorbed fraction %)	Benzyl Alcohol exacted (%)	0.1 N NaOH exacted (%)	Non-solvent extracted (%)	Total mass (%)
Degraded rabbit food	Sample 1	Toluene	89.03	4.79	2.58	5.56	101.96
	Sample 2	Toluene	87.87	4.68	1.42	6.35	100.02
Degraded office paper	Sample 1	*o*-xylene	81.38	8.82	0.05	4.23	98.71
	Sample 2	*o*-xylene	82.12	9.87	0.06	4.35	100.75
Degraded newsprint	Sample 1	*o*-xylene	90.22	6.51	0.09	5.87	102.38
	Sample 2	*o*-xylene	88.2	6.31	0.09	5.03	99.75

5.8 Model Prediction for Desorption Kinetics from Mixture of MSW Components

Having measured alkylbenzene sorption isotherms (Wu et al. 2001) and desorption rates for individual MSW components, it is possible to simulate HOC desorption rates from mixed MSW. The results presented herein as well as the work of Kjeldsen and Christensen (2001), suggest that the long-term fate of HOC in landfills is controlled by the waste properties. The composition of waste buried in landfill has changed over the past 30 years. Prior to ∼1970, the plastics component of MSW was small

due to limited production and use of plastics. Since 1960, the plastics component of MSW increased continuously from 0.5% to 13.0% in 1997. Consequently, two landfill scenarios were evaluated. For the old landfill scenario, the mass distribution of waste categories was based on material discarded in 1960. For the new new landfill scenario, the mass distribution of waste categories was based on material discarded in 1997 after taking into account recycling (EPA, 1999).

Table 5.7 summarizes the sorbent organic matter composition of mixed MSW in 1997. The plastic wastes were classified as rubbery and glassy polymer based on their glass transition termperatures (T_g) (Table 5.8). Table 5.8 further shows that the solubility parameters of polystyrene (PS) and polyethylene terephthalate (PET) are similar to that of PVC while that of polypropylene (PP) is similar to HDPE (Barton 1991). Therefore, the K_F value of PVC was used for glassy plastics and the K_p value of HDPE was used for rubbery plastics. Half of the corrugated boxes and magazine waste was assigned to the newsprint category and the other half to the office paper category because the lignin contents of these wastes fall between those of newsprint and office paper (Eleazer et al. 1997). The mass percentage for each waste category was calculated by dividing the mass of each waste category by the amount of total discarded waste. The fraction of sorbed toluene in MSW for each waste listed in Table 5.7 represents the HOC percentage associated with each sorbent organic matter category and was calculated as: $K_i * M_i / \sum(K_i * M_i) * 100\%$, where K_i is the sorption parameter for each waste category, and M_i is the mass percentage of each waste category. Table 5.9 gives the sorbent organic matter composition of mixed MSW in 1960.

Table 5.7. Composition of sorbent organic matter in municipal solid waste (1997)

Waste category		Discards (tons*10^3)[a]	Mass percentage (%)	Sorption capacity parameter for toluene [b]	Fraction of sorbed toluene in hypothetical MSW (%)
Total newsprint	Newsprint	5,730	18.58	13.0	1.99
	Telephone book	570			
	Corrugated Boxes+Magazines	6335			
Total office paper	Folding cartons	5,380	20.42	2.7	0.45
	Office paper	3,630			
	Books	920			
	Third class mails	4,330			
	Corrugated Boxes+Magazines	6,335			
	Commercial printing	4,580			
Glassy plastics	Polyvinyl chloride (PVC)	1,450	5.86	1663	80.09
	Polystyrene (PS)	2,270			
	Polyethylene terephthalate (PET)	1,960			
Rubbery plastics	HDPE	4,850	14.11	70.7	8.20
	LDPE/LLDPE	5,890			
	Polypropylene	2,940			
Food + yard waste	Yard waste	15,170	41.03	27.5	9.27
	Food waste	24,610			
Total waste		96,950	100		100

[a] From EPA(1999).
[b]For glassy plastics, the K_f value of PVC was used, for other materials, K_p values were used (Wu et al. 2001)

Table 5.8. Properties of plastics

Polymer	T_g (°C) [a]	Solubility parameter ($cal^{1/2}cm^{-3/2}$) [b]
Polyvinyl chloride (PVC)	80	8.5-11.0
Polystyrene (PS)	100	8.5-10.6
Polyethylene terephthalate (PET)	70	9.3-10.8
HDPE	-80	7.7-8.2
Polypropylene	-10	7.9

[a] The classification of polymer state is based on T_g values and definitions (Troloar, 1974).
[b] From Barton (1991).

The particle diameter for each MSW component was based on the thickness of representative materials for each waste category as shown in Table 5.10. The thickness of newsprint is 0.09 *mm* per sheet and the average number of sheets for each section is about 3. Therefore, 0.27 *mm* was used as the diameter of newsprint assuming that the same section of newspaper is likely disposed together. Drinking water, milk and orange juice bottles are typical HDPE containers, and the average thickness of these containers is 1.85 *mm*. Another large source of HDPE waste is plastic bags with a thickness of 0.02 *mm*. According to EPA (1999), the amount of HPDE container waste buried in landfills is about 1670 thousand tons, and the amount of plastic bags is 2350 thousand tons. Therefore, the mass ratio of container waste to bag waste is about 0.71:1. Toluene desorption curves were obtained separately for HDPE container and bag wastes, and the overall toluene desorption curve for HDPE was obtained by summing up the two curves with appropriate sorbed toluene fraction. For glassy polymers, a 0.4 *mm* thick material was assumed based on the thickness of packaging with newly purchased shirts.

Table 5.9. Composition of sorbent organic matter in municipal solid waste (1960)

Waste category	Mass percentage (%)	Fraction of sorbed toluene (%)
Total Newsprint	20.64	11.91
Total office paper	22.68	2.72
Glassy plastics	0.21	15.5
Rubbery plastics	0.507	1.59
Food+yard waste	55.95	68.28

Table 5.10. Thickness of MSW components used in model prediction

Waste category	Sample	Thickness (mm)
Newsprint	News & observer	0.09/sheet
Office paper	Printing paper	0.106/sheet
HDPE	Drinking water bottles	1.33
	Milk bottles	1.98
	Orange juice bottles	2.25
	Plastic bags	0.02
PVC	Plastic support in shirts	0.4

Assuming an infinite dilution scenario (i.e., a constant zero concentration at the external particle surface), toluene desorption curves were predicted for each waste category, and the individual desorption curves were summed to obtain an overall desorption curve for the MSW mixture based on the fraction of sorbed toluene for each waste category. To determine the model sensitivity to particle size, overall desorption curves for the old and new MSW mixtures were obtained by varying the particle size of individual waste categories by a factor of 2 (Figure 5.10). Figure 5.10 shows that toluene desorption rates from mixed MSW decreased with increasing particle size and increasing plastics contents. If particle sizes of each waste category are doubled, the half life of toluene, $t_{0.5}$, increases from 5.83 to 24 days for the old landfill scenario and from 3.97 to 16 years new landfill scenario. Figure 5.10 stresses that the overall toluene desorption rate and extent was controlled by the size of MSW

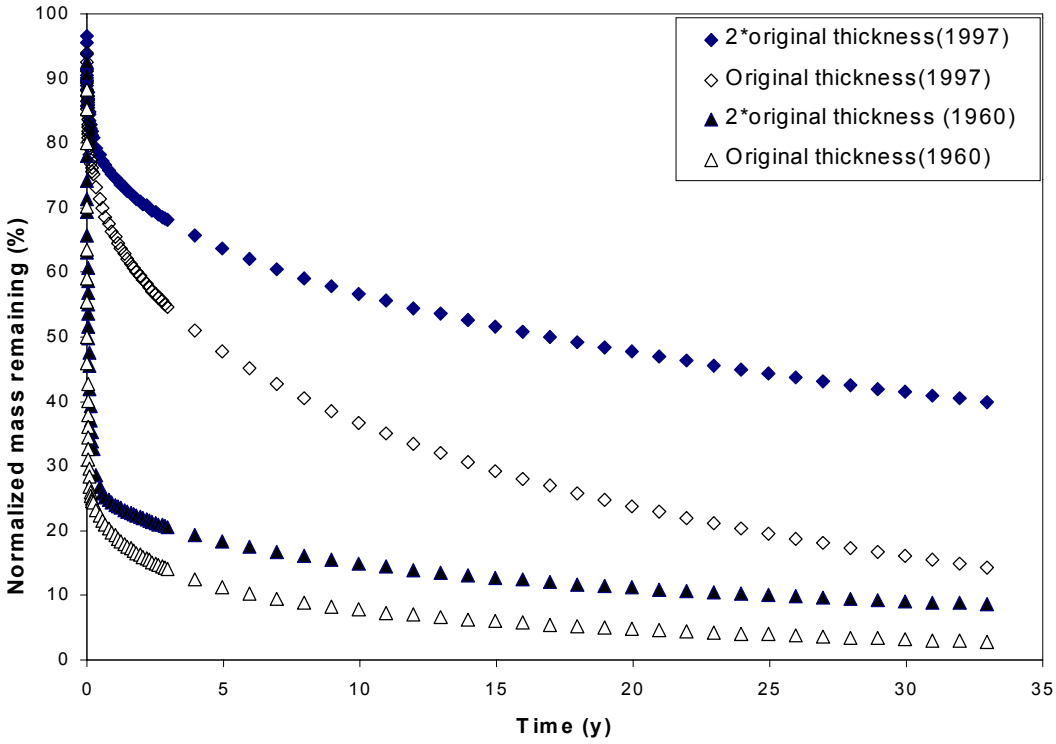

Figure 5-10: Model prediction for toluene desorption from mixed MSW components as a function of solid size

components and especially by the presence of plastic waste as demonstrated by the longer half-lives for the new landfill scenario.

In landfills, the mineralization of sorbed HOCs is dependent on the HOC desorption rate if microorgansims are only able to degrade aqueous-phase compounds. Desorption becomes the rate-limiting step of bioremediation if the desorption rate is slower than the biodegradation rate. The half-life of toluene biodegradation under methanogenic conditions was reported to be 34 days in aquifer sediments (Suarez and Rifai 1999) and approximately 100 days in decomposing refuse (Sanin et al. 2000). These half-lives are slightly longer than those associated with toluene desorption from MSW with low plastics (1960). Consequently, the mineralization of toluene in old landfills should be controlled by the biodegradation rate. In contrast, desorption is the limiting factor for toluene bioremediation in landfills receiving MSW with

higher plastics, primarily because of slow toluene desorption from glassy polymers. From a bioremediation perspective, the slow release of HOC from glassy polymers like PVC will render contaminants less available for interaction with microorganisms in landfills and will limit the bioremediation rate. Consequently, the HOC residence time at the contaminated site is prolonged. On the other hand, slow desorption of HOCs from glassy polymers will retard the movement of HOCs into the subsurface and reduce the risk associated with potential ground water contamination by landfill leachate. In terms of enviromental release, the plastics in landfill waste are helpful.

Chapter 6

Conclusions and Future Research

6.1 Conclusions

This study evaluated the sorption and desorption of toluene and *o*-xylene from individual municipal solid waste (MSW) constituents [office paper, newsprint, model food and yard waste, high density polyethylene (HDPE), and poly(vinyl chloride) (PVC)]. Effects of sorbent decomposition and solvent composition on alkylbenzene sorption and desorption were studied by evaluating biodegradable sorbents in both fresh and anaerobically decomposed form and by conducting single-solute sorption isotherm tests and batch desorption tests in acidogenic and methanogenic leachate. To determine the effects of aging on alkylbenzene desorption rates, desorption tests were performed for samples that were contacted with toluene for 30 and 250 days. Selected samples containing *o*-xylene were analyzed after an aging time of 250 days. One- and two-compartment polymer diffusion models were applied to quantify desorption rate data from MSW components. The conclusions based on this study include:

1. Linear isotherms showed that alkylbenzene uptake by HDPE, office paper, newsprint, and model food and yard waste occurred by partitioning ("dissolution") into sorbent organic matter.

2. Alkylbenzene isotherms on PVC were nonlinear in organic-free water and methanogenic leachate but linear in acidogenic leachate. The isotherm nonlinearity can be explained by alkylbenzene adsorption on the surfaces of internal nanovoids

of this glassy polymer. In acidogenic leachate, volatile fatty acids likely plasticized PVC, which led to linear partitioning.

3. Except for PVC, isotherms in organic-free water and in both acidogenic and methanogenic leachates showed small differences. These results showed that even though the dissolved organic carbon contents of acidogenic and methanogenic leachates were 6620 and 115 mg/L, respectively, these high DOC levels had little effect on HOC sorption to MSW components.

4. Sorption of toluene and *o*-xylene generally decreased with increasing sorbent polarity as evidenced by the correlation of the normalized sorption parameter with the polarity index [(O+N)/C]. An improved relationship was obtained when correlating the normalized sorption parameter [$\log K_{oc}/K_{ow}$] with the O-alkyl/alkyl ratio that recognizes the importance of both sorbent polarity and lipophilic extractives on the sorption of hydrophobic organic contaminants.

5. Alkylbenzene sorption in landfills is strongly influenced by the presence of plastics and lipophilic compounds. The recalcitrance of these compounds increases the sorbent organic matter affinity for hydrophobic organic contaminants as biologically mediated sorbent degradation proceeds in the landfill.

6. Desorption kinetic tests showed that desorption rates of alkylbenzene varied significantly for different MSW components. The slowest desorption rates were observed for PVC while the fastest desorption rates were observed for biopolymer composites.

7. Desorption rates decreased as aging time increased for all tested sorbents except HDPE. Aging had no effect on toluene desorption from HDPE and PVC.

8. A single-parameter spherical diffusion model successfully described alkylbenzene desorption rate data for PVC and HDPE but failed to simulate desorption rate data for biopolymer composites such as rabbit food, newsprint and office paper.

9. A three-parameter biphasic polymer diffusion model successfully described the two-stage desorption curves that were observed for biopolymer composites.

10. The effects of aging on alkylbenzene desorption rates were quantified by ϕ_s, the HOC fraction residing in the slowly desorbing compartment. As aging time increased from 30 to 250 days, ϕ_s increased for all biopolymer composites. The largest increase

(30%) was observed for degraded office paper.

11. Toluene desorption rates from mixed MSW in two landfill scenarios were predicted and model results showed that the half life of toluene desorption was 5.83 days for the old landfill scenario containing little plastics waste and 3.97 years for the new landfill containing more plastics. Consequently, the bioremediation of toluene was controlled by biodegradation rate in old landfills since the biodegradation rate is higher than the desorption rate. In contrast, desorption is the limiting factor for toluene bioremediation in relatively young landfills because of slow toluene desorption rate from glassy plastics.

The results of this study illustrate that toluene and *o*-xylene sorption and desorption in MSW components is strongly affected by the presence of plastics. The existence of plastics will increase the fraction of HOC sorbed to MSW waste and reduce the rate and extent of HOC desorption, thus limiting the rate of HOC leaching and biodegradation.

Since landfills are dynamic and interdependent system comprised of MSW, contaminants and microorganisms, building a biodegradation model must combine the abiotic mechanisms governing sorption/desorption with the mechanisms governing cell growth and substrate utilization. Therefore, the quantification of the release rates of alkylbenzene under abiotic conditions in this study can provide useful information to bioavailability research to assess whether desorption rates or biodegradation rates control the biodegradation of alkylbenzene in landfills.

6.2 Future Research

1. Based on the isotherm studies conducted with individual MSW components and correlation between $\log(K_{oc}/K_{ow})$ and to O-alkyl/alkyl ratio, it is possible to estimate HOC sorption capacities for mixed MSW samples. Such estimates should be verified experimentally for mixed MSW components. The experimental studies with mixed waste will be more applicable to actual landfill simulation than studies with individual waste fraction.

2. The current model was developed for batch desorption experiments. However, HOCs in landfill may be transported with percolating moisture and desorbed HOCs from waste located at the top of a landfill cell may be resorbed by waste buried below. Therefore, dynamic column tests should be conducted in future work to simulate the concurrent processes of advection, hydrodynamic dispersion and sorption/desorption in landfills. Also, the presented models should be modified to describe HOC transport in fixed beds, which would permit simulation of column test data.

3. To understand the mechanisms reponsible for sorption/desorption of HOCs in biopolymer composites, particularly for explaining the unusual alkylbenzene desorption behavior with office paper and newsprint, spectroscopic analyses such as ^{13}C-NMR are necessary. ^{13}C-NMR analysis will be able to characterize the association between ^{13}C-labeled sorbate and sorbent organic matter.

Bibliography

[1] Akim, E.L., "Cellulose-bellwether or old hat", *Chemtech*, Vol. 8, pp. 676-682,1978.

[2] Alexander, M., "Research needs in bioremediation", *Environ. Sci. Technol.*, Vol. 25, No. 12, pp. 1972-1973,1991.

[3] Ball, W.P., Buehler, CH., Harmon, T.C., Mackay, D.M., Roberts, P.V., "Characterization of a sandy aquifer materials at the grain scale", *J. Contam. Hydrol.* Vol. 5, pp. 253-295, 1990.

[4] Ball, W.P., Roberts, P.V., In: Organics substances and sediments in water, Lewis Publishers: Chelsea, MI, pp. 273, 1991.

[5] Ball, W.P., Roberts, P.V., "Long-term sorption of halogenated organic chemicals by aquifer materials: 1. Equilibrium", *Environ. Sci. Technol.*, Vol. 25, pp. 1223-1237, 1991.

[6] Ball, W.P., Roberts, P.V., "Long-term sorption of halogenated organic chemicals by aquifer materials: 2. Intraparticle diffusion", *Environ. Sci. Technol.*, Vol. 25, pp. 1237-1249, 1991.

[7] Baldock, J.A., Oades, J. M., Nelson, P. N., Skene, T. M., Golchin, A., Clarke, P., "Changes in soil carbon under long-term maize in monoculture and legume-based rotations", *Aust. J. Soil Res.* Vol. 35, pp. 1061-1083, 1997.

[8] Baertsch, C.D., Funke, H.H., Falconer, J. L., Nobel, R.D., "Permeation of

aromatic hydrocarbon vapors through silicalite-zeolite membranes", *J. Phys. Chem.*, Vol. 100, pp. 7676-7679, 1996.

[9] Barrer, R.M., Barrie, J.A., "Sorption and diffusion in ethyl cellulose: Part II: Quantitative examination of settled isotherms and permeation rates", *J. Poly. Sci.*, Vol. XXIII, pp. 331-344, 1957.

[10] Barlaz, M.A., Ham, R.K., Schaefer, D. M., "CRC Crit. Rev.", *Environ. Control*, Vol.19, pp. 557-584, 1990.

[11] Barton, A. F. M., "Solubility parameters", *Chemical Reviews*, Vol. 75, pp. 731-753, 1975.

[12] Barton, A. F. M. *CRC Handbook of Solubility Parameters and Other Cohesion Parameters*, 2nd ed., CRC Press: Boca Raton, FL, 1991.

[13] Bauer, M.J., and R. Herrman, "Dissolved organic carbon as the main carrier of phthalic acid esters in municipal landfill leachates", *Waste Management and Research*, Vol. 16, pp. 446-454, 1998.

[14] Bertran, M.S., Dale, B.E., "Enzymatic hydrolysis and recrystallization behavior of initially amorphous cellulose", *Biothechnol. Bioeng.,* Vol. 27, pp. 177-181, 1985.

[15] Bennett, A.E., Rienstra, C. M., Auger, M., Lakshmi, K. V.; Griffen, R. G., "Heteronuclear decoupling in rotating solids", *J. Chem. Phys.* Vol.103, pp. 6951-6958, 1995.

[16] Berens, A.R., Huvard, G.S., "Particle size distribution of polymer powders by analysis of sorption kinetics", *J. Disper. Sci. & Tech.*, Vol. 2, pp. 359-378, 1981.

[17] Berens, A.R., "Transport of organic vapors and liquids in poly(vinyl chloride)", *Markromol. Chem. Maracomol. Symp.*, Vol. 29, pp. 95-108, 1989.

[18] Bhandari A., Novak, J.T., Berry, D.F. "Binding of 4-mono chlorophenol to soil". *Environ. Sci. Technol.,* Vol. 30, No. 7, pp. 2305-2311, 1996.

[19] Bollag, J.M., Loll, M.J., "Incorporation of xenobiotics into soil humus", *Experimental,* Vol. 39, pp. 1221-1231, 1983.

[20] Bosma, T.N.P, Middeldorp P.J.M., Schraa G., Zehnder A.J.B., "Mass transfer limitation of biotransformation quantifying bioavailability", *Environ. Sci. Technol.*, Vol. 31, No. 1, pp. 248-252, 1997.

[21] Brady, N.C., *The Nature and Properties of soils.* 8th edn. MacMillan Publishing Co., New York, 1974.

[22] Brandup, J., Immergnt, E.H., Grulke, E.A., *Polymer Handbook*, pp. 206, New York: Wiley, 1989.

[23] Bristow, J.A, Kolseth, P., *Paper Structure and Properties*, International Fiber Science and Technology Series/8, 1986.

[24] Brutsaert, W., "Probability laws for pore-size distributions", *Soil Science*, Vol. 101, No. 2, pp. 85-92, 1966.

[25] Brusseau, M.L., Rao, P. S. C., "The influence of sorbate-organic matter interactions sorption nonequilibrium", *Chemosphere*, Vol. 18, pp. 1691-1706, 1989.

[26] Brusseau, M. L., Jessup, R. E., Rao, P. S. C., "Nonequilibirum sorption of organic chemicals: elucidation of rate-limiting processes", *Environ. Sci. Technol.*, Vol. 25, pp. 134-142, 1991.

[27] Brusseau, M.L, "Influence of sorbate structure on nonequilibrium sorption of organic compounds", *Environ. Sci. Technol.*, Vol. 25, pp. 1501-1508 1991.

[28] Brusseau, M.L., Wood, L.A., Rao, P.S.C., "Influence of organic cosolvents on the sorption kinetics of hydrophobic organic chemicals", *Environ. Sci. Technol.*, Vol. 25, No. 5, pp. 903-910, 1991.

[29] Burgos, W.D., Novak, J.T., Berry, D.F., "Reversible sorption and irreversible binding of naphthalene and a-Naphthol to soil: Elucidation of processes", *Environ. Sci. Technol.*, Vol. 30, No.4, pp. 1205-1211, 1996.

[30] Carra, J.S., Cossu, R. In: International Perspectives on Municipal Solid Wastes and Sanitary Landfilling; Carra, J. S., Cossu, R., Eds.; Academic Press: London, U.K., pp 1-14, 1990.

[31] Carroll, K.M., Harkness, M.R., Bracco, A.A., Balcarcel, R.R., "Application of a permenant / polymer diffusional model to the desorption of polychlorinated biphenyls from Hudson River sediment". *Environ. Sci. Technol.* Vol. 28, No. 2, pp. 253-258, 1994.

[32] Carter, M. C.; Kilduff, J. E.; Weber, W. J., Jr., "Site energy distribution analysis of preloaded adsorbents", *Environ. Sci. Technol.* Vol. 29, No. 7, pp. 1773-1780, 1995.

[33] Caulfield, D.F., Moore, W.E., "Effect of varying crystallinity of cellulose on enzymic hydrolysis", *Wood Science*, Vol. 6, No. 4, pp. 375-378, 1974.

[34] Caulfield, D.F., Steffes, R.A., "Water-induced recrystallization of cellulose", Vol. 52, No. 7, pp. 1361-1366, 1969.

[35] Chen, W., Wagenet, R.J., "Solute transport in porous media with sorption-site heterogeneity", *Environ. Sci. Technol.*, Vol. 29, No. 11, pp. 2725-2734, 1995.

[36] Chian E. S. K., De Walle F. B., "Characterization of soluble organic matter in leachate", *Environ. Sci. Technol.*, Vol. 10, pp. 158-163, 1977.

[37] Chiou, C.T., McGroddy, S.E., Kile, D.E.,"Partition characteristics of polycyclic aromatic hydrocarbons on soils and sediments", *Environ. Sci. Technol.* Vol.32, 264-269,1998.

[38] Chiou, C.T., Kile, D.E.,"Deviations from sorption linearity on soils of polar and nonpolar organic compounds at low relative concentrations", *Environ. Sci. Technol.* Vol.32, No.3, pp.338-343,1998.

[39] Christensen, T. H., Kjeldsen, P. L, Holm, P. E., "Attentuation of landfill leachate pollutants in aquifers", Crit.Rev. In *Environ. Sci. Technol.*, Vol. 24, pp. 119-202, 1994.

[40] Connaughton, D.F., "Sorption kinetics of polynuclear aromatic hydrocarbons on aquifer material: A investigation of long-term exposure effects", Master Thesis, Cornell University, 1992.

[41] Connaughton, D.F., Stedinger, J.R., Lion, L.W., and Shuler, M.L., "Description of time-varying desorption kinetics", *Environ. Sci. Technol.*, Vol. 27, No. pp. 2397-2403, 1993.

[42] Cornelissen, G., Paul, C.M., Noort, V.C., Govers, H.A.J., "Desorption kinetics of chlorobenzenes, polycyclic aromatic hydrocarbons and polychlorinated biphenyls: Sediment extraction with TeNAX and effects of contact time and solute hydrophobicity", *Environ. Toxicol. Chem.*, Vol. 16, No.7, pp. 1351-1357, 1997.

[43] Crank, J., *The mathematics of diffusion*, Clarendon press, Oxford, UK, 1975.

[44] Crawford, R.C., *Lignin biodegradation and transformation*, Viley-Interscience, New York, 1981.

[45] Culver, T.B., Hallisey, S.P., Sahoo, D., Deitsch, J.J., and Smith, J.A., "Modeling the desorption of organic contaminants from long-term contaminated soil using distributed mass transfer rate", *Environ. Sci. Technol.*, Vol.31, No. 6, pp. 1581-1588, 1997.

[46] Dec, J., and Bollga, J.M.,"Microbial release and degradation of catechol and chlorophenols bound to synthetic humic acid", *Soil. Sci. Soc. Am. J.* Vol 52, No.5, pp. 1366-1371, 1988.

[47] Dec, J., Shuttleworth, K.L., and Bollag, J.M.,"Microbial release of 2,4-dichlorophenol boudn to humic acid or incorporated during humification", *J. Environ.Qual.*, Vol. 19, pp. 546-551, 1990.

[48] Dec, J., Bollag, J.M., "Determination of covalent and noncovalent binding interactions between xenobiotic chemicals and soil", *Soil Sci.*, Vol. 162, No. 12, 1997.

[49] Deitsch, J.J., Smith, J.A., "Sorption and desorption rate comparisons for 1,2-Dichlorobenzene to a peat soil", *Environ. Sci. Technol.*, Vol. 18, No. 8, pp. 1701-1709, 1999.

[50] Deitsch, J.J., Smith, J.A., Culver, T.B., Brown, R.A., and Riddle, S.A., "Distributed-rate model analysis of 1,2-Dichlorobenzene batch sorption and desorption rates for five natural sorbents", *Environ. Sci. Technol.*, Vol. 34, No. 8, pp. 1469-1476, 2000.

[51] Demeyer, D.I., Henderson, C., Prins, R.A., "Relative significance of exogenous and de novo fatty acid synthesis in formation of rumen microbial lipids in vitro", *Appl. Environ. Microbiol.*, Vol. 35, pp. 24-31, 1998.

[52] Dinel, H., Schnitzer, M., Dumontet, S., "Compost maturity chemical characteristics of extractable lipids", *Compost Sci. Util.* Vol. 4, pp. 16-25, 1996.

[53] Di Toro, D.M., Horzempa, L.M., "Reversible and resistant components of PCB adsorption-desorption isotherms. *Environ. Sci. Technol.* Vol. 16, No. 9, pp. 594-602, 1982.

[54] Division of Physical Chemistry, International Union of Pure and Applied Chemistry. *Pure Appl. Chem.*, Vol. 31, pp. 537-638, 1972.

[55] Douglas. J.Jr., "The application of stability analysis in the numberical solution of quasi-linear parabolic differential equations", *Thransactions of the American Mathematical Society*, Vol. 89, pp. 484-518, 1958.

[56] Edzwald, J.K., van Benschoten, J. E. In *Chemical Water and Wastewater Treatment*, Hahn, H. H., Klute, R., Eds.; Springer-Verlag: Berlin, Germany, pp. 341-359, 1990.

[57] Eleazer,W.E., Odle, W.S., Wu, Y.S., Barlaz,M.A., "Biodegradability of municipal solid waste components in laboratory-scale landfills", *Environ. Sci. Technol.*, Vol. 31, No. 3, pp. 911-917, 1997.

[58] Esteghlalian, A., Hashimoto, A.G., Fenske, J.J., Penner, M.H., "Modelling and optimization of dilute-sulfuric-acid pretreatment of corn stover, poplar and switch grass", *Bioresour. Technol.*, Vol. 59, pp. 129-136, 1997.

[59] Garbarini , D. R, Lion, L. W., "Influence of the nature of soil organics on the sorption of toluene and trichloroethylene", *Environ. Sci. Technol.*, Vol. 20, pp. 1263-1269, 1986.

[60] Gerasimowicz, W.V., Hicks, K.B., Pfeffer, P.E., "Evidence for the existence of associated lignin-carbohydrate polymers as revealed by carbon-13 CPMAS solid-state NMR spectroscopy", *Macromolecules*,Vol. 17, pp. 2597-2603, 1984.

[61] Grathwohl, P., "Influence of organic matter from soils and sediments from various origins on the sorption of some chlorinated aliphatic hydrocarbons: Implications on Koc correlations", *Environ. Sci. Technol.*, Vol. 24, No. 11, pp. 1687-1693, 1990.

[62] Graber, E.R., Borisover, M.D., "Evaluation of the glassy/rubbery model for soil organic matter", *Environ. Sci. Technol.* Vol. 32, No. 21, pp. 3286-3292, 1998.

[63] Green, J.L., Fan, J., Angell, C.A., "The protein-glass analogy: some insights from homopeptide comparisons", *J. Phys. Chem.* Vol. 98, pp.13780-13790, 1994.

[64] Gschwend, P. M., Wu, S.C., "On the constancy of sediment-water partition coefficients of hydrophobic organic pollutants", *Environ. Sci. Technol.*, Vol.19, No. 1, pp. 90-96, 1985.

[65] Guthrie,E.A., Bortiatynski, J.M., Van Heemst, J.D.H., Richman, J.E., Hardy, K.S., Kivach, E.M.,and Hatcher, P.G. "Determination of 13C Pyrene Sequestration in Sediment Microcosms Using Flash Pyrolysis-GC-MS and 13C NMR", *Environ. Sci. Technol.* Vol. 33, No. 1, pp. 119-125, 1999.

[66] Hancock, B. C., York, P., Rowe, R. C., "The use of solubility parameters in pharmaceutical dosage from design", *Int. J. Pharmac.* Vol. 148, pp. 1-21, 1997.

[67] Harmsen, J., "Identification of organic compounds in leachate from a waste tip", *Wat. Res.*, Vol. 17, No. 6, pp. 699-705, 1983.

[68] Harmon, T.C., "Comparison of intraparticle sorption and desorption rates for a halogenated Alkene in a sandy aquifer material." *Environ. Sci. Technol.* Vol. 28, pp. 1650-1656, 1994.

[69] Harmon, T.C., Roberts, P.V., "Determining and modeling mass-transfer rate limitations in heterogeneous aquifers", *Water Sci. Technol.* Vol. 26, pp. 71-77, 1992.

[70] Harmon, T.C., Roberts, P.V., "The effect of equilibration of time on desorption rate measurements with chlorinated alkenes and aquifer particles", *Environ. Prog.*, Vol. 13, No. 1, 1994.

[71] Hatzinge, P.B., Alexander, M, "effect of aging of chemicals in soil on their biodegradability and extractability". *Environ. Sci. Technol.*, Vol. 29, No. 2, pp. 537-545, 1995.

[72] Hayes, M.H.B.,"Adsorption of triazine herbicides on soil organic matter, including a short review on soil organic matter chemistry", *Res. Rev.* Vol. 31, pp 131-174, 1970.

[73] Helm, R.F., "Lignin-polysaccharide interactions in woody plants", In *Lignin: Historical, Biological, and Materials Perspectives*; ACS symposium Series 742, Glasser, W.G., Northey, R.A., Schultz, T.P., Eds., American Chemical Society: Washington, DC, pp 161-171, 2000

[74] Huang, W.L., Walter J. Weber Jr. "A distribution reactivity model for sorption by soils and sediments. 10. Relationships between desorption, hysteresis, and the chemical characteristics of organic domains". *Environ. Sci. Technol.* Vol. 31, No. 9, pp. 2562-2569,1997.

[75] Huang, W.L., Walter J. Weber Jr., "A distribution reactivity model for sorption by soils and sediments. 11. Slow concentration-dependent sorption rates", *Environ. Sci. Technol.* Vol. 32, No. 22, pp. 3549-3555, 1998.

[76] Huang, W.L., Yu, H., Weber, W.J., "Hysteresis in the sorption and desorption of hydrophobic organic contaminants by soils and sediments. 1. A comparative analysis of experimental protocols.", *Journal of contaminant Hydrology.* Vol. 31, pp. 129-148, 1998.

[77] Huang, W.L., Weber W.J., "Distributed reactivity model for sorption by soils and sediments.11. Slow concentration-dependent sorption rates", *Environ. Sci. Technol.,* Vol. 32, No. 22, pp. 3549-3555,1998.

[78] Imai, A., K. Onuma, Y. Inamori, R. Sudo, "Biodegradation and adsorption in refractory leachate treatment by the biological activated carbon fluidized bed process", *Wat. Res.*, Vol. 29, No. 2, pp. 687-694, 1995.

[79] Isaacson, P.J., Frink C.R. "Nonreversible sorption of phenolic compounds by sediment fractions: The role of sediment organic matter", *Environ. Sci. Technol.,* Vol. 18, pp. 43-48,1984.

[80] Johnson, M.D., Keinath T.M.,Weber, J.W.Jr., "A distributed reactivity model for sorption by soils and sediments 14. Characterization of phenanthrene desorption rates", *Environ. Sci. Technol.* Vol. 35, No. 8, pp. 1688-1695, 2001.

[81] Kan, A.T., Fu, G., Hunter, M.A., and Tomson M.B., "Irreversible adsorption of naphthalene and tetrachlorobiphenyl to Lula and surrogate sediments", *Environ. Sci. Technol.*, Vol. 31, No. 8, pp. 2176-2184, 1997.

[82] Kan, A.T., Fu, G., Tomson, M.B., "Adsorption /desorption hysteresis in organic pollutants and soil/sediment interaction", *Environ. Sci. Technol.* Vol. 28, No. 5, pp. 859-867,1994.

[83] Kan, A.T., Fu, G., Hunter, M.A., Chen, W, Ward, C.H., and Tomson M.B.,

"Irreversible sorption of neutral hydrocarbons to sediments: Experimental observations and model predictions", *Environ. Sci. Technol.*, Vol.32, No. 7, pp. 892-902, 1998.

[84] Kaplan, D.S., "Structure-property relationships in copolymers to composites: Molecular interpretation of the glass transition phenomenon", *J. of Appl. Polym. Sci.*, Vol. 20, pp. 2615-2629, 1976.

[85] Karickhoff, S.W., "Sorption kinetics of hydrophobic pollutants in natural sediments", *Contaminants and Sediments,* Baker, R.A., Ed., Science/Butterworth: Ann Arbor, MI, pp. 193-205, 1980.

[86] Karickhoff, S.W., Brown, D.S., "Paraquat sorption as a function of particle size in natural sediments", *J. Environ. Qual.*, Vol. 7, No. 2, pp 246-252,1978.

[87] Karickhoff, S.W., Brown, D.S., Scott, T.A, "Sorption of hydrophobic pollutants on natural sediments", *Water Research*, Vol. 13, pp. 241-248, 1979.

[88] Karickhoff, S.W., "Semi-empirical estimation of sorption of hydrophobic pollutants on natural sediment and soils", *Chemosphere*, Vol. 10, No. 8, pp. 833-846, 1981.

[89] Karickhoff, S.W., Morris, K.R.,"Sorption of hydrophobic pollutants in sediment suspensions", *Environ. Toxicol. Chem.* Vol. 4, pp. 469-479, 1985.

[90] Kazano, H., Kearney, P.C., Kaufman, D.D., "Metabolism of methylcarbamate insecticides in soils", *J. of Agric. Fd Chem.*, Vol. 20, pp. 975-979, 1972.

[91] Kile, D.E., Chiou, C T., Zhou, H., Li, H., Xu, O., "Partition of nonpolar organic pollutants from water to soil and sediment organic matters", *Environ. Sci. Technol.*, Vol. 29, No. 5, pp. 1401-1406, 1995.

[92] Kile, D.E., Wershaw, R.L., Chiou, C.T, "Correlation of soil and sediment organic matter polarity to aqueous sorption of noionic compounds", *Environ. Sci. Technol.* Vol. 33, No. 12, pp. 2053-2056, 1999.

[93] Kjeldson, P., Christensen, T.H., "A simple model for the distribution and fate of organic chemicals in a landfill: MOCLA", *Waste Management & Research*, Vol. 19, pp. 201-216, 2001.

[94] Lambert, S. M., Porter, P. E., Schieferstein, R. H., "Movement and sorption of chemicals applied to the soil", *Weeds*, Vol. 13, pp. 185-190, 1965.

[95] Laor,Y., Strom, P.F., Farmer, W.J., "The effect of sorption on phenanthrene bioavailability", *Journal of Biotechnology*, Vol. 51, pp. 227-234, 1996.

[96] Larsen,T., Christensen, T.H, Pfeffer, F.M., Enfield, G.G, "Landfill leachate effects on sorption of organic micropollutants onto aquifer materials", *Journal of Contaminant Hydrology*, Vol. 9, pp. 307-324, 1992.

[97] Leenheer, J.A., "Comprehensive approach to preparative isolation and fractionation of dissolved organic carbon from natural waters and wastewaters", *Environ. Sci. Technol.* Vol. 15, No.5, pp.578-587, 1981.

[98] LeBoeuf, E.J., Weber, W.J. Jr., "A distributed reactivity model for sorption by soils and sediments. 8.Sorbent organic domains: Discovery of a humic acid glass transition and an argument for a polymer-based model", *Environ. Sci. Technol.*, Vol. 31, No. 6, pp. 1697-1702, 1997.

[99] LeBoeuf, E.J., Weber, W.J., Jr., "Macromolecular characteristics of natural organic matter. 2. Sorption and desorption behavior", *Environ. Sci. Technol.* Vol. 34, No. 17, pp. 3632-3640, 2000.

[100] Lerch, R.N., Thurman, E.M., Kruger, E.L., "Mixed-mode sorption of hydroxylated atrazine degradation products to soil: A mechanism for bound residue", *Environ. Sci. Technol.*, Vol. 31, No. 5, pp 1539-1546, 1997.

[101] Lipinsky, E. S., " Perspectives on preparation of cellulose for hydrolysis", Hydrolysis of Cellulose: Mechanisms of Enzymatic and Acid Catalysis, Advances in chemistry series 181, American Chemical Society, Washington, D.C.

[102] Maloney, M.T., Chapman, T.W., Baker, A.J., "Dilute –acid hydrolysis of paper birch: kinetic studies of xylan and acetyl group between hydrolysis", *Biotechnol. Bioengng*, Vol. 27, pp. 355-361, 1985.

[103] McCarthy, J.F., Jimenez, D.D., Southworth, G.R., DiToro, D.M., and Black, M.C., "Anomalous binding of organic contaminants may be artifactual due to radiochemical impurities", *Water Res.*, Vol. 20, No. 10, pp. 1251-1254, 1986.

[104] McGroddy, S.E., and Farrington, J.W., "Sediment porewater partitioning of polycyclic aromatic hydrocarbons in three cores from Boston harbor, Massachusetts", *Environ. Sci. Technol.*, Vol. 29, No. 6, pp. 1542-1550, 1995.

[105] McGroddy, S.E., Farrington, J.W., and Gschwend, P.M., "Comparison of the in situ and desorption sediment-water partitioning of polycyclic aromatic hydrocarbons and polychlorinated biphenyls", *Environ. Sci. Technol.*, Vol. 30, No. 1, pp. 172-177, 1996.

[106] Means, J.C., Wood, S.G., Hassett, J. J., Banwart, W. L., "Sorption of polynuclear aromatic hydrocarbons by sediments and soil", *Environ. Sci. Technol.*, Vol. 14, pp. 1524-1528, 1980.

[107] Michel, F.C., Jr., Reddy, C.A., Forney, L.J., "Microbial degradation and humification of the lawn care pesticide 2,4-Dichlorophenoxyacetic acid during the composting of yard trimmings". *Appl.Environ. Microiol.* Vol. 61, No. 7, pp. 2566-2571,1995.

[108] Miller, C.T., Pedit, J.A., "Use of a reactive surface-diffusion model to describe apparent sorption desorption hysteresis and degradation of lindane", *Environ. Sci. Technol.*, Vol. 26, No. 7, pp. 1417-1427, 1992.

[109] Nam, K., Alexander, M., "Role of nanoporosity and hydrophobicity in sequestion and bioavailability: Tests and model solids", *Environ. Sci. Technol.* Vol. 32, No. 1, pp. 71-74, 1998.

[110] Nkedi-Kizza, P., Brusseau, M.L, Rao, P.S.C., Hornsby, A.G., "Nonequilibrium sorption during displacement of hydrophobic organic chemicals and 45Ca through soil columns with aqueous and mixed solvents", *Environ. Sci. Technol.*, Vol. 23, No. 7, pp. 814-820, 1989.

[111] Odier, E., Monties, B., "Absence of microbial mineralization of lignin in anaerobic enrichment cultures", *Appl. Environ. Microbiol.*, Vol. 40, pp. 601-605, 1983.

[112] Öman C., Camilla S., "Sorption of neutral organic compounds to solid waste", *Waste Management and Research.,* Vol. 17. No. 4, pp. 275-287, 1999.

[113] Öman C., "Comparison between the predicted fate of organic compounds in landfills and the actual emissions", *Environ. Sci. Technol.*, Vol. 35, pp.232-239, 2000.

[114] Ogram, A.V., R.E. Jessup, L.T. Ou, P.S.C.Rao, "Effects of Sorption on Biological Degradation Rates of (2,4-Dichlorophenoxy) acetic Acid in Soils." *Appl. Environ. Microbiol.,* Vol. 49, No. 3, pp. 582-587, 1985

[115] Pavlostathis, S.G. and Jaglal K., "Desorptive behavior of trichloroethylene in contaminated soil". *Environ. Sci. Technol.,* Vol. 25, No. 2, pp. 274-279, 1991.

[116] Pavlostathis, S.G. and Matharan, "Desorption kinetics of selected volatile organic compounds from field contaminated soils", *Environ. Sci. Technol.,* Vol. 26, No. 3, pp. 532-538, 1992.

[117] Pedit, J.A., Miller, C.T., "Heterogeneous sorption processes in subsurface systems: 1. model formulations and applications", *Environ. Sci. Technol.,* Vol. 28, pp. 2094-2104, 1994.

[118] Pelekani, C., Newcombe, G., Snoeyink,V.L, Hepplewhite, C., Assemi, S., Beckett,R, "Characterization of natural organic matter using high performance size exclusion chromatography", *Environ. Sci. Technol.,* Vol. 33. No.6, pp. 2807-2813, 1999.

[119] Piatt, J.J, Brusseau, M.L, "Rate-limited sorption of hydrophobic organic compounds by soils with well-characterized organic matter", *Envir. Sci. Tech.*, Vol. 32, pp. 1604-1608, 1998.

[120] Pichler, M., Kögel_knabener, I., "Chemolytic analysis of organic matter during aerobic and anaerobic treatment of municipal solid waste", *J. Environ. Qual.*, Vol. 29, pp 1337-1344, 2000.

[121] Pignatello, J. J., "Soil organic matter as a nanoporous sorbent of organic pollutants", *Adv. Colloid Interface Sci.*, Vol. 76-77, pp. 445-467,1998.

[122] Pignatello, J.J., Ferrandino, F.J., and Huang, L.Q., "Elution of aged and freshly added herbicides from a soil", *Environ. Sci. Technol.*, Vol. 27, pp. 1563-1571, 1993.

[123] Pignatello, J.J., and Huang, "Sorptive reversibility of atrazine and metolachlor residues in field soil samples", *J. Environ. Qual.*, Vol. 20, pp. 222-228, 1991.

[124] Pignatello, J.J and Xing, B.S, "Mechanism of slow sorption of organic chemicals to natural particles", *Environ. Sci. Technol.,* Vol 30, No. 1, pp. 1-10, 1996.

[125] Poirrer, M.A., Bordelon, B.R., and Laseter, J.L., "Adsorption and concentration of dissolved carbon-14 DDT by coloring colloids in surface waters. *Environ. Sci.Technol.,* Vol. 6, pp. 1033-1035, 1972.

[126] Rao, P.S.C., Lee, L.S., and Pinal R., "Cosolvency and sorption by hydrophobic orgnanic chemicals", *Environ. Sci. Tech.,* Vol. 24, No. 5, pp.647-654, 1990.

[127] Rebhun, M., Kalalbo, R., Grossman, L., Manka, J, Rav-acha, C. H., " Sorption of organics on clay and synthetic humic-clay complexes simulating aquifer processes", *Wat. Res.*, Vol. 26, No. 1, pp. 79-84, 1992.

[128] Reinhart, D.R., Gould, J.P., Wendall, H.C., Pohland, F.G. In *Emerging Technologies in Hazardous Waste management*, ACS Symposium Series 422, Tedder,

D.W., Pohland, F.G., Eds.; American Chemical Society: Washington, DC, pp. 292-310,1990.

[129] Reinhart, D.R., Pohland, F.G., Gould, J.P., Cross, W. H., "The fate of selected organic pollutants codisposed with municipal refuse", *J.Water Pollut. Cont. Fed.,* 63, 780-788, 1991.

[130] Roberts, J.C., *The Chemistry of Paper*, The Royal Society of Chemistry: Herts, U.K., 1996.

[131] Rogers, C.E., Stannett, V., Szwarc, M., "The sorption diffusion and erpmeation of organic vapors in polyethylene", *J. Polymer Sci.*, Vol. XLV, pp. 61-82, 1960.

[132] Rutherford, D.W., Chiou, C. T., Kile, D. E., "Influence of soil organic matter composition on the partition of organic compounds", *Environ. Sci. Technol.*, Vol. 26, pp. 336-340, 1992.

[133] Sakata, I., Senju, R., "Thermoplastic behavior of lignin with various synthetic plasticizers", *J. of Appl.Poly. Sci.*, Vol. 19, pp. 2799-2810, 1975.

[134] Salmėn, L., Olsson, A.M., "Interaction between hemicellulose, lignin and cellulose: structure-property relationships", *J. of Pulp and Paper Sci.*, Vol. 24, No. 3, pp. 99-103, 1998.

[135] Sanin, F.D., Knappe, D.R.U., Barlaz, M.A., "Biodegradation and humification of toluene in simulated landfill", *Water Res.*, Vol. 34, pp. 063-3074, 2000.

[136] Sahoo, D., Smith, J.A., "Enhanced trichloroethene desorption from long-term contaminated soil using triton X-100 and pH increases", *Environ. Sci. Technol.*, Vol. 31, No. 7, pp. 1910-1915, 1997.

[137] Sahoo, D., Smith, J.A., imbrigiotta, T.E., and Mclellan, H.M., "Surfactant-enhanced remediation of a trichloroethene-contaminated aquifer. 2. Transport of TCE", *Environ. Sci. Technol.*, Vol. 32, No. 11, pp. 1686-1693, 1998.

[138] Sarkar, J.M., Malcolm, R.C., Bollag, J.M., "Enzymatic coupling of 2,4-dichlorophenol to stream fulvic acid in the presence of oxidoreductases", *Soil Sci.. Soc. Am. J.*, Vol. 52, pp. 688-694, 1988.

[139] Schwarzenbach, R. P., Westall, J., "Transport of nonpolar organic compounds from surface water to groundwater. Laboratory sorption studies", *Environ. Sci.Technol.*, Vol. 15, pp. 1360-1367, 1981.

[140] Schultz, B., P. Kjelesen, "Screening of organic matter in leachate from sanitary landfills using gas chromatography combined with mass spectrometry", *Wat. Res.*, Vol. 20, pp. 965, 1986.

[141] Schwab, B.S.,"Characterization of compost from a pilot plant-scale composter utilizing simulated solid waste", *Waste Manage. Res.,* Vol. 12, pp. 289-303, 1994.

[142] Scow, K.M., "Effect of sorption-desorption and diffusion processes on the kinetics of biodegradation of organic chemicals in soil". In: *Linn, D.M., Carski, T.H., Brusseau, M.C., and Chang, F.H.(Eds). Sorption and degradation of pesticides and organic chemicals in soils. Spec.* Publ.3, Soil Science Society of America, Madison, 1993.

[143] Scow, K.M., Alexander, M., "Effect of diffusion on the kinetics of biodegradation: Experimental results with synthetic aggregates", *Soil Sci.Soc. Am.J.*, Vol.56, pp 128-134, 1992.

[144] Seth, R., MacKay, D., Muncke, J., "Estimating the organic carbon partition coefficient and its variability for hydrophobic chemicals", *Environ. Sci. Technol.,* Vol. 33, No. 14, pp. 2390-2394, 1999.

[145] Shaw, L.J. beaton Y., Glover L .A, Killham K., Osborn, D., Meharg, A.A, " Bioavailability of 2,4-Dichlorophenol associated with soil water-soluble humic materials". *Environ. Sci. Technol.,* Vol. 34, No. 22, pp. 4721-4726, 2000.

[146] Sochava, I. V., "Heat capacity and thermodynamic characteristics of denaturation and glass transition of hydrated and anhydrous proteins", *Biophys. Chem.,* Vol. 69, pp. 31-41, 1997.

[147] Soil Science Society of America, *Glossary of Soil Science Terms*, Soil Science of Society of American, Madison, WI, 1997.

[148] Steinberg, S.M., Pignatello, J.J. and Sawhey, B.J., "Persistence of 1,2-dibromoehtane in soils: Entrapment in intraparticle micropores", *Environ. Sci. Technol.*, Vol. 21, No. 12, pp. 1201-1208, 1987.

[149] Stuer-Lauridsen, F. and Pedersen, F, "On the Influence of the Polarity Index of Organic Matter in Predicting Environmental Sorption of Chemicals", *Chemosphere*. Vol. 35. No. 4, pp. 751-773, 1997.

[150] Suarez, M.P., Rifai, H.S., "Biodegradation rates for fuel hydrocarbons and chlorinated solvents in groundwater", *Bioremediation Journal,* Vol. 3, No. 4, pp. 337-362, 1999.

[151] Sweeney, R. A., "Generic combustion method for determination of crude protein in feed", *J. Assoc. Off. Anal. Chem.* Vol. 72, pp. 770-774, 1989.

[152] Tobolsky, A.V., Mark, H.F., *Polymer Science and Material*, Robert E.Krieger Publishing Company, Huntington, New York, 1980.

[153] Treloar, L.R.G., *Introduction to Polymer Science*, Wykeham Publications (London) LTD, London and Winchester, 1974.

[154] U.S. EPA. *Characterization of Municipal Solid Waste in the United States: 1998 Update*; *US EPA/530-R-99-021; Office of Solid Waste*, U.S. Environmental Protection Agency: Washington, DC, 1999.

[155] Wang, Y.S., Odle, W., Eleazer, W.E., Barlaz, M.A., "Methane Potential of Food Waste and Anaerobic Toxicity of Leachate Produced During Food Waste Decomposition," *Waste Manage. Res.*, Vol. 15, No. 2, pp. 149-167, 1997.

[156] Weber, W.J., Huang, H, "A distributed reactivity model for sorption by soils and sediments. 4. Intraparticle heterogeneity and phase-distribution relationships under nonequilibrium conditions", *Environ. Sci. Technol.,* Vol. 30, No 3, pp. 881-888, 1996.

[157] Weber,W.J., Jr., McGinley, P.M., Katz, L.E., "A distributed reactivity model for sorption by soils and sediments: 1. Conceptual basis and equilibrium assessment", *Environ. Sci. Technol.*, Vol. 26, pp. 1955-1962, 1992.

[158] Weber,W.J., McGinley, P.M., Lynn E. K, "Distributed reactivity in the sorption of hydrophobic organic contaminants in natural aquatic systems", *Aquatic Chemistry*, American Chemical Society, Washington DC.,1995.

[159] Weber, W. J., Jr., Miller, C.T, "Modeling the sorption of hydrophobic contaminants by aquifer materials-I", *Water Res.*, Vol. 22, pp. 457-464, 1988.

[160] Werth, C.J., Reinhard, M., "Effects of temperature on trichloroethylene desorption from silica gel and natural sediments. 2. kinetics", *Environ. Sci. Technol.,* Vol. 31, No. 3, pp. 697-703, 1997.

[161] White, J.C., Pignatello, J.J., "Influence of bisolute competition on the desorption kinetics of polycyclic aromatic hydrocarbons in soil", *Environ. Sci. Technol.,* Vol. 33, No. 23 , pp. 4292-4298, 1999.

[162] Wolf, D.C., Martin, J.P., "Decomposition of fungal mycelia and humic type polymers containing carbon-14 from ring and side-chain labeled 2,4-D and chloropropham", *Soil Sci. Soc. Am. Proc.*, Vol. 40, pp. 700-704, 1976.

[163] Wu, B., Taylor, C.M., Knappe, D.R.U., Nanny, M.A., Barlaz, M.A., "Factors controlling alkylbenzene sorption to municipal solid waste", *Environ. Sci. Technol.*, Vol. 35, pp. 4569-4576, 2001.

[164] Wu, S.C., Gschwend, P.M., "Sorption kinetics of hydrophobic organic compounds to natural sediments and soils", *Environ. Sci. Technol.*, Vol. 20, pp. 717-725, 1986.

[165] Wu, Q., Schleuss, U., Blume, H.P.Z., "Investigation on soil lipid extraction with different organic solvents", *Pflanzenernaehr. Bodenk.* Vol. 158, No. 4, pp. 347-350, 1995.

[166] Xia, G., Pignatello, J. J., "Detailed sorption isotherms of polar and a polar compounds in a high-organic soil", *Environ. Sci. Technol.* Vol.35, No. 1, pp. 84-94, 2001.

[167] Xing, B.S., McGill, W.B., Dudas, M.J., "Sorption of phenol by selected biopolymers: isotherms, energetics and polarity", *Environmental Science and Technology.*, Vol. 28, pp. 466-473, 1994.

[168] Xing, B.S., McGill, W.B., Dudas, M.J, "Cross-correlation of polarity curves to predict partition coefficients of nonionic organic contaminants", *Environ. Sci. Technol.* Vol. 28, No.11, pp. 1929-1933, 1994.

[169] Xing, B. S., Pignatello, J. J., "Dual-mode sorption of low-polarity compounds in glassy poly(vinyl chloride) and soil organic matter", *Environ. Sci. Technol.* Vol.31, No. 3, pp. 792-799, 1997.

[170] Xing, B.S., Pignatello, J.J., Gigliotti B., "Bisolute competitive sorption between atrazine and other organic compounds in soils and model sorbents", *Environ. Sci. Technol.*, Vol. 30, pp. 2432-2440,1996.

[171] Young, T.M, Weber, W.J. Jr., "A distributed reactivity model for sorption by soils and sediments. 3. Effects of diagenetic processes on sorption energetics", *Environmental Science and Technology*, Vol. 29, No. 1, pp. 92-97, 1995.

[172] Young, L.Y., Frazer, A.C., "The fate of lignin and lignin-derived compounds in anaerobic environments", Geomicrobiology Journal, Vol. 5, No. 314, 1987.

[173] Zhang, S., Czekaj, C, Ford, W. T., "Enhancement of polarization transfer under high-speed MAS using a quasi-adiabatic cross-polarization sequence", *J. Magn. Reson., Ser. A* Vol. 111, pp. 87-92, 1994.

[174] Zhao, D., Pignatello, J.J., White J.C., Braida, W. and Ferrandino, F., "Dual-mode modeling of competitive and concentration-dependent sorption and desorption of kinetics of polycyclic aromatic hydrocarbons in soils", unpublished article, 2000.

[175] Zhou, Q.H., Caraniss S.E., Maurice, P.A., "Considerations in the use of higher-pressure size exclusion chromatography (HPSEC) for determining molecular weights of aquatic humic substances", *Wat. Res.,* Vol. 34, No. 14, pp. 3503-514, 2000.

[176] Zief, M., Mitchell J.W., *Chemical Analysis.* Elving, P.J., Ed., John Wiley & Sons: NewYork, 1976.

Appendices

A. Mathematical model

A.1 Crank-Nicholson Implicit Finite Difference Scheme

$$
\begin{aligned}
\frac{\partial q}{\partial T} &= \frac{1}{R^2}\frac{\partial}{\partial R}(R^2\frac{\partial q}{\partial R}) \\
\frac{\partial q}{\partial T}|_{t=j+\frac{1}{2}}^{R=i} &= (\frac{1}{R^2}\frac{\partial}{\partial R}(R^2\frac{\partial q}{\partial R}))|_{t=j+\frac{1}{2}}^{R=i} \\
&\Rightarrow \frac{q_{i,j+1}-q_{i,j}}{\Delta t} = \frac{1}{R_i^2}\frac{R_{i+\frac{1}{2}}^2\frac{\partial q}{\partial R}|_{t=j+\frac{1}{2}}^{R=i+\frac{1}{2}} - R_{i-\frac{1}{2}}^2\frac{\partial q}{\partial R}|_{t=j+\frac{1}{2}}^{R=i-\frac{1}{2}}}{R_{i+\frac{1}{2}}-R_{i-\frac{1}{2}}} \\
&\Rightarrow \frac{q_{i,j+1}-q_{i,j}}{\Delta t} = \frac{1}{R_i^2}\frac{R_{i+\frac{1}{2}}^2\frac{q_{i+\frac{1}{2},j+\frac{1}{2}}-q_{i,,j+\frac{1}{2}}}{R_{i+1}-R_i} - R_{i-\frac{1}{2}}^2\frac{q_{i,j+\frac{1}{2}}-q_{i-1,,j+\frac{1}{2}}}{R_i-R_{i-1}}}{\Delta R} \\
&\Rightarrow \frac{q_{i,j+1}-q_{i,j}}{\Delta t} = \frac{1}{\Delta R^2}\left\{\begin{array}{c} \{[\frac{1}{8}(\frac{R_{i+1}+R_i}{R_i})^2][(q_{i+1,j+1}+q_{i+1,j})-(q_{i,j+1}+q_{i,j})]\} \\ -\{[\frac{1}{8}(\frac{R_{i-1}+R_i}{R_i})^2][(q_{i,j+1}+q_{i,j})-(q_{i-1,j+1}+q_{i-1,j})]\} \end{array}\right\} \\
\text{Let } \alpha &= \frac{\Delta t}{\Delta R^2} \\
A_i &= \frac{1}{8}(\frac{R_{i+1}+R_i}{R_i})^2 = \frac{1}{8}(2+\frac{1}{i})^2 \\
B_i &= \frac{1}{8}(\frac{R_{i-1}+R_i}{R_i})^2 = \frac{1}{8}(2-\frac{1}{i})^2 \\
&\Rightarrow -\alpha A_i q_{i+1,j+1} + [1+\alpha(A_i+B_i)]q_{i,j+1} - \alpha B_i q_{i-1,j+1} \\
&= \alpha A_i q_{i+1,j} + [1-\alpha(A_i+B_i)]q_{i,j} + \alpha B_i q_{i-1,j}
\end{aligned}
$$

A.2 Derivation of the Intraparticle Solute Mass Remaining M_j

Left point rule:

$$\Delta M_j = q_{i-1}\rho_a \Delta V_i$$

Right point rule:

$$\Delta M_j = q_i \rho_a \Delta V_i$$

$$\Delta V_i = \frac{4}{3}\pi(r_i^3 - r_{i-1}^3)$$

Trapezoid rule:

$$\Delta M_j = \frac{q_i + q_{i-1}}{2}\rho_a \Delta V_i$$

$$M_j = \sum_{i=2}^{m} \Delta M_j = \frac{4}{3}\pi\rho_a \sum_{i=2}^{m} \left[(r_i^3 - r_{i-1}^3)\frac{q_i + q_{i-1}}{2}\right]$$

where

M_j = the total solute mass at time t_j;
ρ_a = particle density of the immobile phase $[M_s/L^3]$;

A.3 One-compartment polymer diffusion model

Input file (HDPE as example)

```
1.0                    // Linearity indicator
11                     // Number of data points
60                     // Numer of iteration
13.510                 // Total simulation time (days)
1.0                    // Timestep size (min)
0.025                  // Particle radius (cm)
100                    // Spatial interval per particle
1.2                    // Solid density
128                    // Kd
0.631                  // Fractional uptake
0     0.677    0.922   // time for purger on (days)   purger off (days) observed mass remainig
1.667 1.677    0.885
2.5   2.510    0.851
3.333 3.3434   0.827
4.583 4.594    0.807
5.833 5.844    0.784
7.917 7.927    0.764
8.917 8.927    0.748
9.5   9.510    0.735
11.5  11.510   0.717
13.5  13.510   0.691
```

C++ One-compartment polymer diffusion model program listing

```
#include <stdio.h>
#include <stdlib.h>
#include <math.h>
int num_iter;          // the total number of iterations to estimate Ds value
int num_data;          // the total number of data points to be fitted
```

```
    double simulation_time; // the simulation time (in days)
    double delta_t;            // time step size: delta t (in minutes)
    int num_t; // the number of time steps; the number of time index is (num_t+1):
0,1,...,num_t
    int num_r;      // the number of radial intervals; the number of spatial index is (num_r+1):
0,1,...,num_r
    double delta_r;           // the size of radial interval along the radial direction
    double radius;              // the radius of particle
    double rho_a;              // the apparent density of the particle [Ms/L^3]
    double k_d;                  //
    double fractional_uptake;     //
    double d_s;                  // the Ds value used in Crank-Nicolson method
    double R_int;               //
    double exponent;           // the index for linearity: 1.0 - linear, nonlinear otherwise
    int purge_index;      // the index of purges
    double *r;                   // the position of each radial grid; (num_r + 1) elements
    double *estimate;          // estimated values for Ds; (num_iter) elements
    double *mse;               // averaged MSE between the actual_data[] and sim_data[];
(num_iter) elements
    double *q;
    double *time_purge_on;     // the time when the purge i is turned on (in days)
    double *time_purge_off;     // the time when the purge i is turned off (in days)
    double *actual_data;      // the actual data to be fitted with
    double *sim_data;          // the simulation output data
    FILE *fp_out;
    extern void CrankLinear();
    extern double ComputeVe();
    extern bool IsPurgeOn(double t_day);
    extern double ComputeMj(double *q);
    extern void Initialize();
    extern void CleanUp();
    extern void EstimateDs(int n_iter);
    extern void Output();
    void main()
    {
        Initialize();
        for (int k=0; k<num_iter; k++)
        {
            CrankLinear();
            EstimateDs(k);
            printf("Iteration #%d\n", k+1);
        }
        Output();
        CleanUp();
    }
```

```
void Initialize()
{
    FILE *fp;
    int i;
    fp = fopen("input.dat", "r");
    fscanf(fp, "%lf\n", &exponent);
    fscanf(fp, "%d\n", &num_data);
    fscanf(fp, "%d\n", &num_iter);
    fscanf(fp, "%lf\n", &simulation_time);
    fscanf(fp, "%lf\n", &delta_t);
    num_t = int(simulation_time*24*60/delta_t);
    fscanf(fp, "%lf\n", &radius);
    fscanf(fp, "%d\n", &num_r);
    delta_r = radius / num_r;
    fscanf(fp, "%lf\n", &rho_a);
    fscanf(fp, "%lf\n", &k_d);
    fscanf(fp, "%lf\n", &fractional_uptake);
    time_purge_on = new double [num_data];
    time_purge_off = new double [num_data];
    actual_data = new double [num_data];
    sim_data = new double [num_data];
    for(i=0; i<num_data; i++)
    {
        fscanf(fp, "%lf %lf %lf\n", &(time_purge_on[i]), &(time_purge_off[i]), &(ac-
tual_data[i]));
    }
    q = new double [num_r+1];
    fclose(fp);
    r = new double [num_r+1];
    for(i=0; i<=num_r; i++)
    {
        r[i] = i * delta_r;
    }
    estimate = new double [num_iter];
    mse = new double [num_iter];
    purge_index = 0;
    d_s =0.2e-7;      // initialize Ds to be 0.2e-7
    fp_out = fopen("output.dat", "w");
}
void CleanUp()
{
    fclose(fp_out);
    delete time_purge_on;
    delete time_purge_off;
    delete actual_data;
```

```
    delete sim_data;
    delete r;
    delete estimate;
    delete mse;
    delete q;
}
/*************************************************************************
* use Crank-Nicolson method to solve Linear PDE:
*          dq/dT = (1/R^2) * d(R^2*dq/dR)/dR
* the PDE is discretized to:
*          a[i]q[i+1] + b[i]q[i] + c[i]q[i-1] = d[i], i=1,2,...,num_r-1
* the boundary conditions are:
*          (1) (dq/dR|R=0) = 0 => q[0] = q[1]
*          (2) q[num_r] = 0 if purge on; = (m_i - m_t)/v_e if purge off
* the initial condition is:
*          at time t=0, the concentration q=1.0 at everywhere in the sphere
*************************************************************************/

void CrankLinear()
{
    int i;      /* i is used for the index of grid */
    int j;      /* j is used for the index of time */
    double *a, *b, *c, *d, *e, *f;
    a = new double [num_r+1];
    b = new double [num_r+1];
    c = new double [num_r+1];
    d = new double [num_r+1];
    e = new double [num_r+1];
    f = new double [num_r+1];
    /* transform from dimensional data (r, t) to non-dimensional data (R, T) */
    double delta_R = delta_r / radius;
    double delta_T = d_s * delta_t/(radius * radius);
    /* the initial condition: at time t=0, q[i] is 1.0 at every grid point */
    for(i=0; i<=num_r; i++)
        q[i] = 1.0;
    /* compute the initial solute mass at the beginning of the experiment */
    double ini_m_j = ComputeMj(q);      // initial m_j
    /* the boundary condition at the center of the sphere:
        (dq/dR|R=0)=0 => q[0] = q[1].
    since q[0] = e[0]*q[1] + f[0], we have */
    e[0] = 1.0;
    f[0] = 0.0;
    /* compute the coefficiencies for the equation */
    /* a[i]*q[i+1] + b[i]*q[i] + c[i]*q[i-1] = d[i] */
    double alpha = delta_T/(8*delta_R*delta_R);
```

```
        for(i=1; i<=num_r; i++)
        {
            a[i] = -alpha*(2+1.0/i)*(2+1.0/i);
            c[i] = -alpha*(2-1.0/i)*(2-1.0/i);
            b[i] = 1 - a[i] - c[i];
        }
        double v_e = ComputeVe();
        for(j=0; j<=num_t; j++)
        {
            double t_day = j*delta_t / (24*60);      // the current time grid (in days)
            double old_m_j, new_m_j;
            /* compute the solute mass at the current time */
            new_m_j = ComputeMj(q);
            /* set the boudary condition at the border of the sphere */
            if(IsPurgeOn(t_day) == true)
            {
                if(t_day < 1e-6)
                    q[num_r] = 1.0;      // at time 0, the boundary concentration should
be 1.0
                else
                    q[num_r] = 0.0;      // at any other time point, when purger is on,
the boundary concentration should be 0.0
                /* to see if at the next time step, we enter another purge or
                    the current purge is turned off.
                if it is true, then save the current solute mass as
                the solute mass after this purge being turned off */
                double next_t_day = (j+1)*delta_t / (24*60);      // the next time grid (in
days)
                if(IsPurgeOn(next_t_day) == false)
                {
                    old_m_j = new_m_j;
                    sim_data[purge_index] = new_m_j/ini_m_j;      // record the actual
simulation output ????
                    purge_index++;
                    if(purge_index >= num_data)
                        purge_index = 0;
                }
            }else{
                /* compute the boundary condition when purge is off;
                note that new_m_j is the current solute mass;
                old_m_j is the solute mass after the last purge being turned off */
                q[num_r] = (old_m_j-new_m_j)*k_d / v_e;
            }
            /* caculate the coefficiencies d[i], e[i], f[i] */
            for(i=1; i<=num_r; i++)
```

```
            {
                /* update the new values of d[i] */
                d[i] = -a[i]*q[i+1] + (2-b[i])*q[i] - c[i]*q[i-1];
                /* forward propagation to get all the values of e[i] and f[i] */
                e[i] = -a[i]/(b[i] + c[i]*e[i-1]);
                f[i] = (d[i] - c[i]*f[i-1])/(b[i] + c[i]*e[i-1]);
            }
            /* backward calculate the values of all q[i] */
            for(i=num_r-1; i>=1; i–)
            {
                q[i] = e[i]*q[i+1] + f[i];
            }
        }
        delete a;
        delete b;
        delete c;
        delete d;
        delete e;
        delete f;
}
/************************************************
*
* Compute m_j - the total solute mass at the current time j
*
************************************************/
double ComputeMj(double *q)
{
        double tmp = 4.0/3.0 * 3.14159 * rho_a;
        double total_m = 0;
        for(int i=1; i<=num_r; i++)
        {
                total_m += (r[i]*r[i]*r[i] - r[i-1]*r[i-1]*r[i-1]) * (q[i] + q[i-1])/2;
        }
        return tmp * total_m;
}
/************************************************
*
* Compute v_e - the volume external to the particle
*
************************************************/
double ComputeVe()
{
        return 4.0*radius*radius*radius/3.0 * 3.14159 * rho_a*k_d *
      (1 - fractional_uptake)/fractional_uptake;
}
```

```
    /***********************************************
    *
    * To test if the purge is on at a given time t_day
    *
    ***********************************************/
    bool IsPurgeOn(double t_day)
    {
        if( (t_day >= time_purge_on[purge_index]) && (t_day < time_purge_off[purge_index])
)
            return true;
        else
            return false;
    }
    /***********************************************
    *
    * Compute the average MSE between the actual data and simulatioin output data
    *
    ***********************************************/
    double ComputeMSE()
    {
        double error = 0;
        for(int k=0; k<num_data; k++)
        {
            error += (actual_data[k] - sim_data[k]) * (actual_data[k] - sim_data[k]);
        }
        return sqrt(error)/num_data;
    }
    /***********************************************
    *
    * Estimate new Ds value based on the MSE
    *
    ***********************************************/
    void EstimateDs(int n_iter)
    {
        mse[n_iter] = ComputeMSE();
        estimate[n_iter] = d_s;
        fprintf(fp_out, "\nIteration #%d \t Ds: %e \t MSE: %e", n_iter, d_s, mse[n_iter]);
        if(n_iter == 0)       // if it is the first iteration, set the next Ds to be (1.2 times the
current Ds)
        {
            d_s = 1.2 * d_s;
            return;
        }
        double slope = (mse[n_iter] - mse[n_iter-1]) / (estimate[n_iter] - estimate[n_iter-1]);
        double coef_p, coef_n;
```

```
        if(mse[n_iter] < 0.01)
        {
            coef_p = 1.1;
            coef_n = 0.9;
        }else{
            coef_p = 1.2;
            coef_n = 0.8;
        }
        if(slope < 0)
            d_s *= coef_p;
        else
            d_s *= coef_n;
    }
    void Output()
    {
        int k;
        for(k=0; k<num_data; k++)
        {
            fprintf(fp_out, "\nactual data: %e \t simulation data: %e", actual_data[k],
sim_data[k]);
        }
        fprintf(fp_out, "\nFinal q[i] values:\n");
        for(k=0; k<=num_r; k++)
        {
            fprintf(fp_out, "%.3lf ", q[k]);
        }
    }
```

A.4 Biphasic polymer diffusion model for searching Φ_s, D_s, D_r.

Input file (fresh rabbit food as an example)

```
12                  //Number of data points
100                 // Numer of iteration
12.80208333  // Total simulation time (days)
1.0                  // Timestep size (min)
0.016               // Particle radius (cm)
60                  // Spatial interval per particle
1.5                 // Solid density
22.38           // Kd
0.472           // Fractional uptake
// purger on (days)    time for purger off (days) observed normalized mass remainig
0                       0.020833333       0.779848126
0.020833333       0.03125             0.528446038
0.03125             0.041666667       0.373236597
0.166666667       0.177083333       0.250354027
```

0.791666667	0.802083333	0.161909444
1.791666667	1.802083333	0.107555165
2.791666667	2.802083333	0.083993416
4.791666667	4.802083333	0.070016454
5.791666667	5.802083333	0.060485188
7.791666667	7.802083333	0.056053361
9.791666667	9.802083333	0.052466218
12.79166667	12.80208333	0.050716152

C++ Program Listing

```
#include <stdio.h>
#include <stdlib.h>
#include <math.h>
#include <imsl.h>
int num_iter;            // the total number of iterations to estimate Ds value
int num_data;            // the total number of data points to be fitted
double simulation_time; // the simulation time (in days)
double delta_t;                  // time step size: delta t (in minutes)
int num_t; // the number of time steps; the number of time index is (num_t+1):
0,1,...,num_t
int num_r;      // the number of radial intervals; the number of spatial index is (num_r+1):
0,1,...,num_r
double delta_r;           // the size of radial interval along the radial direction
double radius;                // the radius of particle
double rho_a;                // the apparent density of the particle [Ms/L^3]
double k_d;                    //
double fractional_uptake;      //
double *r;                    // the position of each radial grid; (num_r + 1) elements
double *time_purge_on;      // the time when the purge i is turned on (in days)
double *time_purge_off;      // the time when the purge i is turned off (in days)
double *actual_data;      // the actual data to be fitted with
FILE *fp_out;
extern void CrankLinearTwoParts(int m, int n, double x[], double f[]);
extern void CrankLinear(double diff_coef, double phi, double *out_q);
extern double ComputeVe();
extern bool IsPurgeOn(double t_day, int purge_index);
extern double ComputeMj(double *q);
extern void Initialize();
extern void CleanUp();
void main()
{
    Initialize();
    int m = num_data; // dimension of function values
    int n = 3;            // dimension of variable
    double *result_x;
```

```
        double xguess[3]; //= {0.0001, 0.01, 0.6}; //1: d_s; 2: d_r; 3:phi_s;
        printf("d_s:");
        scanf("%lf", &xguess[0]);
        printf("\nd_r:");
        scanf("%lf", &xguess[1]);
        printf("\nphi_s:");
        scanf("%lf", &xguess[2]);
        xguess[0] = 1e+6*xguess[0];
        xguess[1] = 1e+6*xguess[1];
        fprintf(fp_out, "d_s: %lf\n", xguess[0]);
        fprintf(fp_out, "d_r: %lf\n", xguess[1]);
        fprintf(fp_out, "phi_s: %lf\n", xguess[2]);
        double xlb[3] = {0, 0, 0};
        double xub[3] = {1, 1, 1};

        result_x = imsl_d_bounded_least_squares(CrankLinearTwoParts, m, n, 0, xlb, xub,
            IMSL_XGUESS, xguess, IMSL_MAX_ITN, 500, IMSL_MAX_FCN, 2000, 0);
        CleanUp();
    }
    void Initialize()
    {
        FILE *fp;
        int i;
        fp = fopen("input.dat", "r");
        fscanf(fp, "%d\n", &num_data);
        fscanf(fp, "%d\n", &num_iter);
        fscanf(fp, "%lf\n", &simulation_time);
        fscanf(fp, "%lf\n", &delta_t);
        num_t = int(simulation_time*24*60/delta_t);
        fscanf(fp, "%lf\n", &radius);
        fscanf(fp, "%d\n", &num_r);
        delta_r = radius / num_r;
        fscanf(fp, "%lf\n", &rho_a);
        fscanf(fp, "%lf\n", &k_d);
        fscanf(fp, "%lf\n", &fractional_uptake);
        time_purge_on = new double [num_data];
        time_purge_off = new double [num_data];
        actual_data = new double [num_data];
        for(i=0; i<num_data; i++)
        {
            fscanf(fp, "%lf %lf %lf\n", &(time_purge_on[i]), &(time_purge_off[i]), &(ac-
tual_data[i]));
        }
        fclose(fp);
        r = new double [num_r+1];
```

```
    for(i=0; i<=num_r; i++)
    {
        r[i] = i * delta_r;
    }
    fp_out = fopen("output.dat", "w");
}
void CleanUp()
{
    fclose(fp_out);
    delete time_purge_on;
    delete time_purge_off;
    delete actual_data;
    delete r;
}
void CrankLinearTwoParts(int m, int n, double x[], double f[])
{
    double d_s = x[0];
    double d_r = x[1];
    double phi_s = x[2];
    double phi_r = 1 - phi_s;
    double *out_q_s = new double [num_data];
    double *out_q_r = new double [num_data];
    CrankLinear(d_s, phi_s, out_q_s);
    CrankLinear(d_r, phi_r, out_q_r);
    printf("d_s:%e d_r:%e phi_s:%lf\n", 1e-6*d_s, 1e-6*d_r, phi_s);
    fprintf(fp_out, "d_s:%e d_r:%e phi_s:%lf\n", 1e-6*d_s, 1e-6*d_r, phi_s);
    double mse = 0;
    for(int k=0; k<num_data; k++)
    {
    //      f[k] = (actual_data[k]-out_q_s[k]-out_q_r[k])/actual_data[k];
//      mse = mse + f[k]*f[k]*actual_data[k]*actual_data[k];
        f[k] = (actual_data[k]-out_q_s[k]-out_q_r[k]);
        mse = mse + f[k]*f[k];
        printf("%lf\n", out_q_s[k]+out_q_r[k]);
        fprintf(fp_out, "%lf\n", out_q_s[k]+out_q_r[k]);
    }
    //imsl_d_write_matrix("the solution is", 1, n, x, 0);
    //imsl_d_write_matrix("the function value is", 1, m, f, 0);
    printf("mse: %lf\n\n", mse);
    fprintf(fp_out, "mse: %lf\n\n", mse);
    delete out_q_s;
    delete out_q_r;
}
/*************************************************************************
* use Crank-Nicolson method to solve Linear PDE:
```

```
*           dq/dT = (1/R^2) * d(R^2*dq/dR)/dR
* the PDE is discretized to:
*           a[i]q[i+1] + b[i]q[i] + c[i]q[i-1] = d[i], i=1,2,...,num_r-1
* the boundary conditions are:
*           (1) (dq/dR|R=0) = 0 => q[0] = q[1]
*           (2) q[num_r] = 0 if purge on; = (m_i - m_t)/v_e if purge off
* the initial condition is:
*           at time t=0, the concentration q=1.0 at everywhere in the sphere
**************************************************************************/

void CrankLinear(double diff_coef, double phi, double *out_q)
{
    int i;      /* i is used for the index of grid */
    int j;      /* j is used for the index of time */
    int purge_index=0;      // the index of purges
    double *a, *b, *c, *d, *e, *f, *q;
    q = new double [num_r+1];
    a = new double [num_r+1];
    b = new double [num_r+1];
    c = new double [num_r+1];
    d = new double [num_r+1];
    e = new double [num_r+1];
    f = new double [num_r+1];
    /* transform from dimensional data (r, t) to non-dimensional data (R, T) */
    double delta_R = delta_r / radius;
    double delta_T = 1e-6 * diff_coef * delta_t/(radius * radius);
    //printf("delta_T:%lf", delta_T);
    /* the initial condition: at time t=0, q[i] is phi at every grid point */
    for(i=0; i<=num_r; i++)
        q[i] = phi;
    /* compute the initial solute mass at the beginning of the experiment for part 1*/
    double ini_m_j1 = ComputeMj(q);      // initial m_j
    /* compute the initial solute mass at the beginning of the experiment for part 2*/
    double *q2;
    q2 = new double [num_r+1];
    for(i=0; i<=num_r; i++)
        q2[i] = 1-phi;
    double ini_m_j2 = ComputeMj(q2);      // initial m_j
    delete q2;
    /* the initial solute mass is the summation of those for part 1 and part 2 */
    double ini_m_j = ini_m_j1 + ini_m_j2;
    /* the boundary condition at the center of the sphere:
        (dq/dR|R=0)=0 => q[0] = q[1].
    since q[0] = e[0]*q[1] + f[0], we have */
    e[0] = 1.0;
```

```
        f[0] = 0.0;
        /* compute the coefficiencies for the equation */
        /* a[i]*q[i+1] + b[i]*q[i] + c[i]*q[i-1] = d[i] */
        double alpha = delta_T/(8*delta_R*delta_R);
        for(i=1; i<=num_r; i++)
        {
            a[i] = -alpha*(2+1.0/i)*(2+1.0/i);
            c[i] = -alpha*(2-1.0/i)*(2-1.0/i);
            b[i] = 1 - a[i] - c[i];
        }
        double v_e = ComputeVe();
        for(j=0; j<=num_t; j++)
        {
            double t_day = j*delta_t / (24*60);      // the current time grid (in days)
            double old_m_j, new_m_j;
            /* compute the solute mass at the current time */
            new_m_j = ComputeMj(q);
            /* set the boudary condition at the border of the sphere */
            if(IsPurgeOn(t_day, purge_index) == true)
            {
                if(t_day < 1e-6)
                    q[num_r] = phi;      // at time 0, the boundary concentration should
be phi
                else
                    q[num_r] = 0.0;      // at any other time point, when purger is on,
the boundary concentration should be 0.0
                /* to see if at the next time step, we enter another purge or
                    the current purge is turned off.
                if it is true, then save the current solute mass as
                the solute mass after this purge being turned off */
                double next_t_day = (j+1)*delta_t / (24*60);      // the next time grid (in
days)
                if(IsPurgeOn(next_t_day, purge_index) == false)
                {
                    old_m_j = new_m_j;
                    out_q[purge_index] = new_m_j/ini_m_j;      // record the actual sim-
ulation output ????
                    purge_index++;
                    if(purge_index >= num_data)
                        purge_index = 0;
                }
            }else{
                /* compute the boundary condition when purge is off;
                note that new_m_j is the current solute mass;
                old_m_j is the solute mass after the last purge being turned off */
```

```
                q[num_r] = (old_m_j-new_m_j)*k_d / v_e;
            }
            /* caculate the coefficiencies d[i], e[i], f[i] */
            for(i=1; i<=num_r; i++)
            {
                /* update the new values of d[i] */
                d[i] = -a[i]*q[i+1] + (2-b[i])*q[i] - c[i]*q[i-1];
                /* forward propagation to get all the values of e[i] and f[i] */
                e[i] = -a[i]/(b[i] + c[i]*e[i-1]);
                f[i] = (d[i] - c[i]*f[i-1])/(b[i] + c[i]*e[i-1]);
            }
            /* backward calculate the values of all q[i] */
            for(i=num_r-1; i>=1; i–)
            {
                q[i] = e[i]*q[i+1] + f[i];
            }
        }
        delete q;
        delete a;
        delete b;
        delete c;
        delete d;
        delete e;
        delete f;
}
/************************************************
*
* Compute m_j - the total solute mass at the current time j
*
************************************************/
double ComputeMj(double *q)
{
        double tmp = 4.0/3.0 * 3.14159 * rho_a;
        double total_m = 0;
        for(int i=1; i<=num_r; i++)
        {
                total_m += (r[i]*r[i]*r[i] - r[i-1]*r[i-1]*r[i-1]) * (q[i] + q[i-1])/2;
        }
        return tmp * total_m;
}
/************************************************
*
* Compute v_e - the volume external to the particle
*
************************************************/
```

```
double ComputeVe()
{
     return 4.0*radius*radius*radius/3.0 * 3.14159 * rho_a*k_d *
   (1 - fractional_uptake)/fractional_uptake;
}
/***********************************************
*
* To test if the purge is on at a given time t_day
*
***********************************************/
bool IsPurgeOn(double t_day, int purge_index)
{
     if( (t_day >= time_purge_on[purge_index]) && (t_day < time_purge_off[purge_index])
)
          return true;
     else
          return false;
}
```

A.5 Biphasic polymer diffusion model for searching Φ_s only

Input file

Same as the one for seaching three parameters

C++ program listing

```
#include <stdio.h>
#include <stdlib.h>
#include <math.h>
#include <imsl.h>
int num_iter;            // the total number of iterations to estimate Ds value
int num_data;            // the total number of data points to be fitted
double simulation_time; // the simulation time (in days)
double delta_t;                  // time step size: delta t (in minutes)
int num_t; // the number of time steps; the number of time index is (num_t+1):
0,1,...,num_t
int num_r;      // the number of radial intervals; the number of spatial index is (num_r+1):
0,1,...,num_r
double delta_r;           // the size of radial interval along the radial direction
double radius;                 // the radius of particle
double rho_a;                 // the apparent density of the particle [Ms/L^3]
double k_d;                     //
double fractional_uptake;      //
double *r;                     // the position of each radial grid; (num_r + 1) elements
double *time_purge_on;      // the time when the purge i is turned on (in days)
double *time_purge_off;     // the time when the purge i is turned off (in days)
```

```
double *actual_data;      // the actual data to be fitted with
double d_s;      // the fixed d_s
double d_r;      // the fixed d_r
FILE *fp_out;
extern void CrankLinearTwoParts(int m, int n, double x[], double f[]);
extern void CrankLinear(double diff_coef, double phi, double *out_q);
extern double ComputeVe();
extern bool IsPurgeOn(double t_day, int purge_index);
extern double ComputeMj(double *q);
extern void Initialize();
extern void CleanUp();
void main()
{
    Initialize();
    int m = num_data; // dimension of function values
    int n = 1;            // dimension of variable
    double *result_x;
    double xguess[1]; //initial phi_s;
    printf("fixed d_s:");
    scanf("%lf", &d_s);
    printf("\nfixed d_r:");
    scanf("%lf", &d_r);
    printf("\ninitial phi_s:");
    scanf("%lf", &xguess[0]);
    fprintf(fp_out, "fixed d_s: %lf\n", d_s);
    fprintf(fp_out, "fixed d_r: %lf\n", d_r);
    fprintf(fp_out, "initial phi_s: %lf\n", xguess[0]);
    double xlb[1] = {0};
    double xub[1] = {1};

    result_x = imsl_d_bounded_least_squares(CrankLinearTwoParts, m, n, 0, xlb, xub,
        IMSL_XGUESS, xguess, IMSL_MAX_ITN, 500, IMSL_MAX_FCN, 2000, 0);
    CleanUp();
}
void Initialize()
{
    FILE *fp;
    int i;
    fp = fopen("input.dat", "r");
    fscanf(fp, "%d\n", &num_data);
    fscanf(fp, "%d\n", &num_iter);
    fscanf(fp, "%lf\n", &simulation_time);
    fscanf(fp, "%lf\n", &delta_t);
    num_t = int(simulation_time*24*60/delta_t);
    fscanf(fp, "%lf\n", &radius);
```

```
        fscanf(fp, "%d\n", &num_r);
        delta_r = radius / num_r;
        fscanf(fp, "%lf\n", &rho_a);
        fscanf(fp, "%lf\n", &k_d);
        fscanf(fp, "%lf\n", &fractional_uptake);
        time_purge_on = new double [num_data];
        time_purge_off = new double [num_data];
        actual_data = new double [num_data];
        for(i=0; i<num_data; i++)
        {
            fscanf(fp, "%lf %lf %lf\n", &(time_purge_on[i]), &(time_purge_off[i]), &(actual_data[i]));
        }
        fclose(fp);
        r = new double [num_r+1];
        for(i=0; i<=num_r; i++)
        {
            r[i] = i * delta_r;
        }
        fp_out = fopen("output.dat", "w");
    }
    void CleanUp()
    {
        fclose(fp_out);
        delete time_purge_on;
        delete time_purge_off;
        delete actual_data;
        delete r;
    }
    void CrankLinearTwoParts(int m, int n, double x[], double f[])
    {
        double phi_s = x[0];
        double phi_r = 1 - phi_s;
        double *out_q_s = new double [num_data];
        double *out_q_r = new double [num_data];
        CrankLinear(d_s, phi_s, out_q_s);
        CrankLinear(d_r, phi_r, out_q_r);
        printf("d_s:%e d_r:%e phi_s:%lf\n", d_s, d_r, phi_s);
        fprintf(fp_out, "d_s:%e d_r:%e phi_s:%lf\n", d_s, d_r, phi_s);
        double mse = 0;
        for(int k=0; k<num_data; k++)
        {
        //      f[k] = (actual_data[k]-out_q_s[k]-out_q_r[k])/actual_data[k];
    //      mse = mse + f[k]*f[k]*actual_data[k]*actual_data[k];
            f[k] = (actual_data[k]-out_q_s[k]-out_q_r[k]);
```

```
        mse = mse + f[k]*f[k];
        printf("%lf\n", out_q_s[k]+out_q_r[k]);
        fprintf(fp_out, "%lf\n", out_q_s[k]+out_q_r[k]);
    }
    //imsl_d_write_matrix("the solution is", 1, n, x, 0);
    //imsl_d_write_matrix("the function value is", 1, m, f, 0);
    printf("mse: %lf\n\n", mse);
    fprintf(fp_out, "mse: %lf\n\n", mse);
    delete out_q_s;
    delete out_q_r;
}
/*************************************************************************
* use Crank-Nicolson method to solve Linear PDE:
*          dq/dT = (1/R^2) * d(R^2*dq/dR)/dR
* the PDE is discretized to:
*          a[i]q[i+1] + b[i]q[i] + c[i]q[i-1] = d[i], i=1,2,...,num_r-1
* the boundary conditions are:
*          (1) (dq/dR|R=0) = 0 => q[0] = q[1]
*          (2) q[num_r] = 0 if purge on; = (m_i - m_t)/v_e if purge off
* the initial condition is:
*          at time t=0, the concentration q=1.0 at everywhere in the sphere
*************************************************************************/

void CrankLinear(double diff_coef, double phi, double *out_q)
{
    int i;      /* i is used for the index of grid */
    int j;      /* j is used for the index of time */
    int purge_index=0;      // the index of purges
    double *a, *b, *c, *d, *e, *f, *q;
    q = new double [num_r+1];
    a = new double [num_r+1];
    b = new double [num_r+1];
    c = new double [num_r+1];
    d = new double [num_r+1];
    e = new double [num_r+1];
    f = new double [num_r+1];
    /* transform from dimensional data (r, t) to non-dimensional data (R, T) */
    double delta_R = delta_r / radius;
    double delta_T = diff_coef * delta_t/(radius * radius);
    //printf("delta_T:%lf", delta_T);
    /* the initial condition: at time t=0, q[i] is phi at every grid point */
    for(i=0; i<=num_r; i++)
        q[i] = phi;
    /* compute the initial solute mass at the beginning of the experiment for part 1*/
    double ini_m_j1 = ComputeMj(q);      // initial m_j
```

```
        /* compute the initial solute mass at the beginning of the experiment for part 2*/
        double *q2;
        q2 = new double [num_r+1];
        for(i=0; i<=num_r; i++)
            q2[i] = 1-phi;
        double ini_m_j2 = ComputeMj(q2);      // initial m_j
        delete q2;
        /* the initial solute mass is the summation of those for part 1 and part 2 */
        double ini_m_j = ini_m_j1 + ini_m_j2;
        /* the boundary condition at the center of the sphere:
            (dq/dR|R=0)=0 => q[0] = q[1].
        since q[0] = e[0]*q[1] + f[0], we have */
        e[0] = 1.0;
        f[0] = 0.0;
        /* compute the coefficiencies for the equation */
        /* a[i]*q[i+1] + b[i]*q[i] + c[i]*q[i-1] = d[i] */
        double alpha = delta_T/(8*delta_R*delta_R);
        for(i=1; i<=num_r; i++)
        {
            a[i] = -alpha*(2+1.0/i)*(2+1.0/i);
            c[i] = -alpha*(2-1.0/i)*(2-1.0/i);
            b[i] = 1 - a[i] - c[i];
        }
        double v_e = ComputeVe();
        for(j=0; j<=num_t; j++)
        {
            double t_day = j*delta_t / (24*60);      // the current time grid (in days)
            double old_m_j, new_m_j;
            /* compute the solute mass at the current time */
            new_m_j = ComputeMj(q);
            /* set the boudary condition at the border of the sphere */
            if(IsPurgeOn(t_day, purge_index) == true)
            {
                if(t_day < 1e-6)
                    q[num_r] = phi;      // at time 0, the boundary concentration should
be phi
                else
                    q[num_r] = 0.0;      // at any other time point, when purger is on,
the boundary concentration should be 0.0
                /* to see if at the next time step, we enter another purge or
                    the current purge is turned off.
                if it is true, then save the current solute mass as
                the solute mass after this purge being turned off */
                double next_t_day = (j+1)*delta_t / (24*60);      // the next time grid (in
days)
```

```
                    if(IsPurgeOn(next_t_day, purge_index) == false)
                    {
                        old_m_j = new_m_j;
                        out_q[purge_index] = new_m_j/ini_m_j;      // record the actual sim-
ulation output ????
                        purge_index++;
                        if(purge_index >= num_data)
                            purge_index = 0;
                    }
                }else{
                    /* compute the boundary condition when purge is off;
                    note that new_m_j is the current solute mass;
                    old_m_j is the solute mass after the last purge being turned off */
                    q[num_r] = (old_m_j-new_m_j)*k_d / v_e;
                }
                /* caculate the coefficiencies d[i], e[i], f[i] */
                for(i=1; i<=num_r; i++)
                {
                    /* update the new values of d[i] */
                    d[i] = -a[i]*q[i+1] + (2-b[i])*q[i] - c[i]*q[i-1];
                    /* forward propagation to get all the values of e[i] and f[i] */
                    e[i] = -a[i]/(b[i] + c[i]*e[i-1]);
                    f[i] = (d[i] - c[i]*f[i-1])/(b[i] + c[i]*e[i-1]);
                }
                /* backward calculate the values of all q[i] */
                for(i=num_r-1; i>=1; i–)
                {
                    q[i] = e[i]*q[i+1] + f[i];
                }
            }
            delete q;
            delete a;
            delete b;
            delete c;
            delete d;
            delete e;
            delete f;
        }
        /***********************************************
        *
        * Compute m_j - the total solute mass at the current time j
        *
        ***********************************************/
        double ComputeMj(double *q)
        {
```

```
        double tmp = 4.0/3.0 * 3.14159 * rho_a;
        double total_m = 0;
        for(int i=1; i<=num_r; i++)
        {
            total_m += (r[i]*r[i]*r[i] - r[i-1]*r[i-1]*r[i-1]) * (q[i] + q[i-1])/2;
        }
        return tmp * total_m;
    }
    /************************************************
    *
    * Compute v_e - the volume external to the particle
    *
    ************************************************/
    double ComputeVe()
    {
        return 4.0*radius*radius*radius/3.0 * 3.14159 * rho_a*k_d
        * (1 - fractional_uptake)/fractional_uptake;
    }
    /************************************************
    *
    * To test if the purge is on at a given time t_day
    *
    ************************************************/
    bool IsPurgeOn(double t_day, int purge_index)
    {
        if( (t_day >= time_purge_on[purge_index]) && (t_day < time_purge_off[purge_index])
)
            return true;
        else
            return false;
    }
```

A.6 C++ program for predicting desorpiton of alkylbenzene in mix of MSW

Input file

```
2.574079e-009  // D_s(cm^2/min)
2.423674e-007  // D_r (cm^2/min)
0.177312       // Φ_r
48             // Number of data points
100            // Number of iteration
1083.333333    // Total simulation time (days)
1.0            // Timestep size (min)
0.4            // Particle radius (cm)
```

```
200                 // Spatial interval per particle
1.5                  // Solid density
26.28               // Kd
0.68                // Fractional uptake
 // Time for purger on (days)   time for purger off (days)
0                    0.020833333
0.020833333      0.041666667
0.041666667      0.125
0.125                0.833333333
0.833333333      1.833333333
1.833333333      2.833333333
2.833333333      3.833333333
3.833333333      5.833333333
5.833333333      7.833333333
7.833333333      9.833333333
9.833333333      11.83333333
11.83333333      13.83333333
13.83333333      15.83333333
15.83333333      17.83333333
17.83333333      20.83333333
20.83333333      23.83333333
23.83333333      28
28                   32.16666667
32.16666667      41.66666667
41.66666667      50
50                   58.33333333
58.33333333      66.66666667
66.66666667      75
75                   83.33333333
83.33333333      125
125                 166.6666667
166.6666667      208.3333333
208.3333333      250
250                 291.6666667
291.6666667      333.3333333
333.3333333      375
375                 416.6666667
416.6666667      458.3333333
458.3333333      500
500                 541.6666667
541.6666667      583.3333333
583.3333333      625
625                 666.6666667
666.6666667      708.3333333
708.3333333      750
```

750 791.6666667
791.6666667 833.3333333
833.3333333 875
875 916.6666667
916.6666667 958.3333333
958.3333333 1000
1000 1041.666667
1041.666667 1083.333333

Program Listing

```
#include <stdio.h>
#include <stdlib.h>
#include <math.h>
int num_iter;            // the total number of iterations to estimate Ds value
int num_data;            // the total number of data points to be fitted
double simulation_time; // the simulation time (in days)
double delta_t;                  // time step size: delta t (in minutes)
int num_t; // the number of time steps; the number of time index is (num_t+1): 0,1,...,num_t
int num_r;      // the number of radial intervals; the number of spatial index is (num_r+1): 0,1,...,num_r
double delta_r;           // the size of radial interval along the radial direction
double radius;                  // the radius of particle
double rho_a;                  // the apparent density of the particle [Ms/L^3]
double k_d;                      //
double fractional_uptake;      //
double *r;                      // the position of each radial grid; (num_r + 1) elements
double *time_purge_on;      // the time when the purge i is turned on (in days)
double *time_purge_off;      // the time when the purge i is turned off (in days)
double d_s;
double d_r;
double phi_s;
double phi_r;
FILE *fp_out;
extern double CrankLinearTwoParts(double d_s, double d_r, double phi_s, double phi_r);

extern void CrankLinear(double diff_coef, double phi, double *out_q);
extern double ComputeVe();
extern bool IsPurgeOn(double t_day, int purge_index);
extern double ComputeMj(double *q);
extern void Initialize();
extern void CleanUp();
void main()
{
    Initialize();
```

```
    phi_r = 1-phi_s;
    CrankLinearTwoParts(d_s, d_r, phi_s, phi_r);
    CleanUp();
}
void Initialize()
{
    FILE *fp;
    int i;
    fp = fopen("input.dat", "r");
    fscanf(fp, "%lf\n", &d_s);
    fscanf(fp, "%lf\n", &d_r);
    fscanf(fp, "%lf\n", &phi_s);
    fscanf(fp, "%d\n", &num_data);
    fscanf(fp, "%d\n", &num_iter);
    fscanf(fp, "%lf\n", &simulation_time);
    fscanf(fp, "%lf\n", &delta_t);
    num_t = int(simulation_time*24*60/delta_t);
    fscanf(fp, "%lf\n", &radius);
    fscanf(fp, "%d\n", &num_r);
    delta_r = radius / num_r;
    fscanf(fp, "%lf\n", &rho_a);
    fscanf(fp, "%lf\n", &k_d);
    fscanf(fp, "%lf\n", &fractional_uptake);
    time_purge_on = new double [num_data];
    time_purge_off = new double [num_data];
    for(i=0; i<num_data; i++)
    {
        fscanf(fp, "%lf %lf\n", &(time_purge_on[i]), &(time_purge_off[i]));
    }
    fclose(fp);
    r = new double [num_r+1];
    for(i=0; i<=num_r; i++)
    {
        r[i] = i * delta_r;
    }
    fp_out = fopen("output.dat", "w");
}
void CleanUp()
{
    fclose(fp_out);
    delete time_purge_on;
    delete time_purge_off;
    delete r;
}
double CrankLinearTwoParts(double d_s, double d_r, double phi_s, double phi_r)
```

```
{
    double *out_q_s = new double [num_data];
    double *out_q_r = new double [num_data];
    CrankLinear(d_s, phi_s, out_q_s);
    CrankLinear(d_r, phi_r, out_q_r);
    for(int i=0; i<num_data; i++)
    {
        printf("%lf\n", out_q_s[i]+out_q_r[i]);
        fprintf(fp_out, "%lf\n", out_q_s[i]+out_q_r[i]);
    }
    delete out_q_s;
    delete out_q_r;
    return 1;
}
/*************************************************************************
* use Crank-Nicolson method to solve Linear PDE:
*          dq/dT = (1/R^2) * d(R^2*dq/dR)/dR
* the PDE is discretized to:
*          a[i]q[i+1] + b[i]q[i] + c[i]q[i-1] = d[i], i=1,2,...,num_r-1
* the boundary conditions are:
*          (1) (dq/dR|R=0) = 0 => q[0] = q[1]
*          (2) q[num_r] = 0 if purge on; = (m_i - m_t)/v_e if purge off
* the initial condition is:
*          at time t=0, the concentration q=1.0 at everywhere in the sphere
*************************************************************************/

void CrankLinear(double diff_coef, double phi, double *out_q)
{
    int i;      /* i is used for the index of grid */
    int j;      /* j is used for the index of time */
    int purge_index=0;      // the index of purges
    double *a, *b, *c, *d, *e, *f, *q;
    q = new double [num_r+1];
    a = new double [num_r+1];
    b = new double [num_r+1];
    c = new double [num_r+1];
    d = new double [num_r+1];
    e = new double [num_r+1];
    f = new double [num_r+1];
    /* transform from dimensional data (r, t) to non-dimensional data (R, T) */
    double delta_R = delta_r / radius;
    double delta_T = diff_coef * delta_t/(radius * radius);
    /* the initial condition: at time t=0, q[i] is phi at every grid point */
    for(i=0; i<=num_r; i++)
        q[i] = phi;
```

```
/* compute the initial solute mass at the beginning of the experiment for part 1*/
double ini_m_j1 = ComputeMj(q);      // initial m_j
/* compute the initial solute mass at the beginning of the experiment for part 2*/
double *q2;
q2 = new double [num_r+1];
for(i=0; i<=num_r; i++)
     q2[i] = 1-phi;
double ini_m_j2 = ComputeMj(q2);      // initial m_j
delete q2;
/* the initial solute mass is the summation of those for part 1 and part 2 */
double ini_m_j = ini_m_j1 + ini_m_j2;

/* the boundary condition at the center of the sphere:
     (dq/dR|R=0)=0 => q[0] = q[1].
since q[0] = e[0]*q[1] + f[0], we have */
e[0] = 1.0;
f[0] = 0.0;
/* compute the coefficiencies for the equation */
/* a[i]*q[i+1] + b[i]*q[i] + c[i]*q[i-1] = d[i] */
double alpha = delta_T/(8*delta_R*delta_R);
for(i=1; i<=num_r; i++)
{
     a[i] = -alpha*(2+1.0/i)*(2+1.0/i);
     c[i] = -alpha*(2-1.0/i)*(2-1.0/i);
     b[i] = 1 - a[i] - c[i];
}
double v_e = ComputeVe();
for(j=0; j<=num_t; j++)
{
     double t_day = j*delta_t / (24*60);      // the current time grid (in days)
     double old_m_j, new_m_j;
     /* compute the solute mass at the current time */
     new_m_j = ComputeMj(q);
     /* set the boudary condition at the border of the sphere */
     if(IsPurgeOn(t_day, purge_index) == true)
     {
          if(t_day < 1e-6)
               q[num_r] = phi;      // at time 0, the boundary concentration should
be phi
          else
               q[num_r] = 0.0;      // at any other time point, when purger is on,
the boundary concentration should be 0.0
          /* to see if at the next time step, we enter another purge or
               the current purge is turned off.
          if it is true, then save the current solute mass as
```

```
                    the solute mass after this purge being turned off */
                    double next_t_day = (j+1)*delta_t / (24*60);       // the next time grid (in
days)
                    if(IsPurgeOn(next_t_day, purge_index) == false)
                    {
                        old_m_j = new_m_j;
                        out_q[purge_index] = new_m_j/ini_m_j;      // record the actual sim-
ulation output ????
                        purge_index++;
                        if(purge_index >= num_data)
                            purge_index = 0;
                    }
                }else{
                    /* compute the boundary condition when purge is off;
                    note that new_m_j is the current solute mass;
                    old_m_j is the solute mass after the last purge being turned off */
                    q[num_r] = (old_m_j-new_m_j)*k_d / v_e;
                }
                /* caculate the coefficiencies d[i], e[i], f[i] */
                for(i=1; i<=num_r; i++)
                {
                    /* update the new values of d[i] */
                    d[i] = -a[i]*q[i+1] + (2-b[i])*q[i] - c[i]*q[i-1];
                    /* forward propagation to get all the values of e[i] and f[i] */
                    e[i] = -a[i]/(b[i] + c[i]*e[i-1]);
                    f[i] = (d[i] - c[i]*f[i-1])/(b[i] + c[i]*e[i-1]);
                }
                /* backward calculate the values of all q[i] */
                for(i=num_r-1; i>=1; i--)
                {
                    q[i] = e[i]*q[i+1] + f[i];
                }
            }
            delete q;
            delete a;
            delete b;
            delete c;
            delete d;
            delete e;
            delete f;
        }
        /***********************************************
        *
        * Compute m_j - the total solute mass at the current time j
        *
```

```
    ************************************************/
    double ComputeMj(double *q)
    {
        double tmp = 4.0/3.0 * 3.14159 * rho_a;
        double total_m = 0;
        for(int i=1; i<=num_r; i++)
        {
            total_m += (r[i]*r[i]*r[i] - r[i-1]*r[i-1]*r[i-1]) * (q[i] + q[i-1])/2;
        }
        return tmp * total_m;
    }
    /************************************************
    *
    * Compute v_e - the volume external to the particle
    *
    ************************************************/
    double ComputeVe()
    {
        return 4.0*radius*radius*radius/3.0 * 3.14159 * rho_a*k_d *
       (1 - fractional_uptake)/fractional_uptake;
    }
    /************************************************
    *
    * To test if the purge is on at a given time t_day
    *
    ************************************************/
    bool IsPurgeOn(double t_day, int purge_index)
    {
        if( (t_day >= time_purge_on[purge_index]) && (t_day < time_purge_off[purge_index])
)
            return true;
        else
            return false;
    }
```

A.7 SAS Program for Analytical Solution of one-compartment model (HDPE as an example)

```
Data HDPE;
    input t;
    cards;
    0.5
    0.75
    1
```

```
24.25
47.25
72.25
98.25
144.25
168.25
192.25
216.25
240.25
288.25
312.25
336.25
360.25
384.25
408.25
432.25
456.25
480.25
504.25
528.25
552.25
576.25
600.25
624.25
648.25
672.25
696.25
;
data HDPE;
    set HDPE;
    sum=0;
        D=0.0000000000472;
        do n=1 to 100;
        r=0.02;
        sumi=exp(-n*n*3.14159*3.14159*D*t*3600/(r*r))/(n*n);
        mass=sum*6/(3.1415926*3.1415926);
        sum=sumi+sum;
    end;
    keep t mass;
run;
proc print data=HDPE;
run;
```

A.8 SAS Program for Analytical Solution of two-compartment model (fresh rabbit food as an example)

```
Data rb;
    input t; * Units: hour
    cards;
    0.5
    1
    3
    10
    20
    44
    68
    92
    116
    140
    164
    188
    212
    236
    260
    284
    308
    332
    356
    380
    404
    428
    452
    476
    500
    524
    548
    572
    596
    620
    644
    668
    692
    716
    740
    764
    788
    812
    836
```

```
;
data rb;
    set rb;
    sum=0;
    Dr=0.00000000404;
    Ds=0.0000000000429;
    fr=0.8227;
    fs=0.1773;
    do n=1 to 100;
        r=0.016;
        sumi=(fr*exp((-n*n*3.14159*3.14159*Dr*t*3600)/(r*r))+
                fs*exp((-n*n*3.14159*3.14159*Ds*t*3600)/(r*r)))/(n*n);
        sum=sum+sumi;
        mass=sum*6/(3.1415926*3.1415926);
    end;
    keep t mass;
run;
proc print data=rb;
run;
```

B. Desorption Experimental Data

Table B.1. Toluene desorption data from fresh rabbit food after 1 month aging

Methanogenic leachate					Acidogenic leachate				
Time (hrs)	q/q_0 (1)	q/q_o (2)	average	SE	Time (hrs)	q/q_0 (1)	q/q_o (2)	average	SE
0.5	71.87	84.10	77.98	8.65	0.5	74.83	72.58	73.71	1.59
0.75	46.85	58.84	52.84	8.48	0.75	49.31	46.66	47.98	1.88
1	31.19	43.46	37.32	8.67	1	32.53	30.49	31.51	1.44
4.25	20.07	30.00	25.04	7.02	8.25	22.72	21.18	21.95	1.10
19.25	12.69	19.69	16.19	4.95	20.25	14.29	13.24	13.76	0.74
43.25	8.51	13.00	10.76	3.18	23.25	9.81	9.14	9.48	0.48
67.25	6.76	10.04	8.40	2.31	47.25	7.44	7.05	7.25	0.28
115.25	5.84	8.17	7.00	1.65	95.25	4.81	5.57	5.19	0.53
139.25	5.19	6.90	6.05	1.21	119.25	3.36	4.43	3.89	0.75
187.25	4.88	6.33	5.61	13.68	167.25	2.74	3.91	3.33	0.83
235.25	4.73	5.76	5.25	15.34	215.25	2.35	3.67	3.01	0.93
307.25	4.60	5.54	5.07	17.53	263.25	1.99	3.37	2.68	0.97

Table B.2. Toluene desorption data from fresh rabbit food after 8 month aging

Methanogenic leachate					Acidogenic leachate				
Time (hrs)	q/q_0 (1)	q/q_o (2)	average	SE	Time (hrs)	q/q_0 (1)	q/q_o (2)	average	SE
0.5	77.85	75.10	76.48	1.95	0.5	64.34	64.42	64.38	0.06
0.75	57.82	54.69	56.25	2.21	0.75	46.21	46.45	46.33	0.17
1	43.07	40.16	41.62	2.06	1	34.59	34.75	34.67	0.11
3.5	23.87	23.43	23.65	0.31	4.25	24.39	23.43	23.91	0.68
23.25	18.04	17.92	17.98	0.09	25.25	17.94	17.29	17.62	0.46
45.25	13.83	13.93	13.88	0.07	47.25	13.85	12.93	13.39	0.65
71.25	10.77	10.96	10.86	0.14	71.25	10.20	8.84	9.52	0.96
96.25	9.18	9.24	9.21	0.04	96.25	7.89	6.54	7.22	0.96
118.25	7.80	7.77	7.79	0.02	120.25	6.24	4.92	5.58	0.93
142.25	6.93	6.86	6.89	0.05	144.25	5.06	3.65	4.36	1.00
166.25	5.83	5.83	5.83	0.00	168.25	4.11	2.64	3.38	1.04
214.25	5.65	5.65	5.65	0.00	216.25	3.70	2.25	2.97	1.02
240.25	5.49	5.49	5.49	0.00	242.25	3.42	2.00	2.71	1.00

Table B.3. Toluene desorption data from degraded rabbit food after 1 month aging

Methanogenic leachate					Acidogenic leachate				
Time (hrs)	q/q_0 (1)	q/q_o (2)	average	SE	Time (hrs)	q/q_0 (1)	q/q_o (2)	average	SE
0.50	71.94	65.51	68.73	4.55	0.5	57.99	60.34	59.17	1.66
0.75	47.56	40.94	44.25	4.68	0.8	39.34	39.85	39.60	0.36
1.00	37.01	31.64	34.33	3.79	1.0	27.32	26.55	26.93	0.55
3.75	28.44	25.29	26.86	2.23	3.3	21.82	18.95	20.38	2.03
22.25	26.81	22.90	24.85	2.77	20.3	18.48	14.77	16.63	2.62
45.25	25.37	21.90	23.64	2.45	44.3	17.27	12.99	15.13	3.02
61.25	24.89	21.55	23.22	2.37	63.3	16.68	12.17	14.43	3.19
112.25	24.54	21.27	22.91	2.31	111.3	16.28	11.67	13.98	3.26
162.25	24.28	21.08	22.68	2.27	161.3	15.97	11.29	13.63	3.31
238.25	24.05	20.88	22.46	2.24	233.3	15.79	11.07	13.43	3.34
310.25	23.85	20.71	22.28	2.22					

Table B.4. Toluene desorption data from degraded rabbit food after 8 month aging

Methanogenic leachate					Acidogenic leachate				
Time (hrs)	q/q_0 (1)	q/q_o (2)	average	SE	Time (hrs)	q/q_0 (1)	q/q_o (2)	average	SE
0.5	52.32	54.84	1.78	0.54	0.5	68.96	64.11	66.54	3.43
0.75	39.14	40.65	1.07	0.40	0.8	43.84	40.47	42.16	2.38
1	32.81	34.25	1.02	0.34	1.0	32.24	29.21	30.72	2.14
3.5	29.63	31.12	1.06	0.30	4.5	26.46	23.63	25.05	2.00
20.25	28.00	29.57	1.11	0.29	22.3	23.23	20.26	21.75	2.10
51.25	27.26	28.97	1.21	0.28	54.3	22.15	19.17	20.66	2.10
73.25	26.86	28.61	1.24	0.28	76.3	21.57	18.58	20.08	2.11
96.25	26.63	28.44	1.28	0.28	98.3	21.26	18.28	19.77	2.11
117.25	26.48	28.29	1.28	0.27	120.3	21.16	18.18	19.67	2.11
141.25	26.31	28.18	1.32	0.27	144.3	21.06	18.07	19.56	2.11
213.25	26.13	28.08	1.38	0.27	216.3	20.98	18.00	19.49	2.11
					288.3	20.86	17.88	19.37	2.11
					432.3	20.77	17.79	19.28	2.11

Table B.5. Toluene desorption data from fresh newsprint after 1 month aging

Methanogenic leachate					Acidogenic leachate				
Time (hrs)	q/q_0 (1)	q/q_o (2)	average	SE	Time (hrs)	q/q_0 (1)	q/q_o (2)	average	SE
0.5	34.85	38.77	36.81	2.77	0.3	53.6	65.3	59.46	8.22
0.75	17.78	17.08	17.43	0.49	0.5	23.4	35.6	29.47	8.61
1	12.55	9.50	11.03	2.15	0.8	13.3	22.2	17.77	6.27
2.75	10.89	6.92	8.91	2.81	4.0	10.6	16.4	13.46	4.10
20.25	10.34	6.07	8.20	3.02	22.0	9.8	13.5	11.67	2.63
46.25	10.06	5.82	7.94	3.00	46.0	8.2	12.0	10.08	2.71
70.25	9.88	5.62	7.75	3.01	70.0	7.9	11.5	9.68	2.55
142.25	9.74	5.43	7.58	3.05	142.0	7.7	11.3	9.52	2.57

Table B.6. Toluene desorption data from fresh newsprint after 8 month aging

Methanogenic leachate					Acidogenic leachate				
Time (hrs)	q/q_0 (1)	q/q_o (2)	average	SE	Time (hrs)	q/q_0 (1)	q/q_o (2)	average	SE
0.5	51.58	45.52	48.55	4.28	0.25	73.17	72.80	72.98	0.27
0.75	34.22	29.19	31.70	3.56	0.5	44.75	43.25	44.00	1.06
1	23.89	20.78	22.33	2.20	0.75	27.24	25.19	26.22	1.45
6.25	19.03	17.34	18.18	1.19	1	19.77	19.38	19.58	0.27
22.25	16.42	15.61	16.02	0.57	5.25	13.51	13.89	13.70	0.26
47.25	15.34	14.75	15.04	0.42	21.25	12.30	13.21	12.75	0.64
70.25	14.84	14.34	14.59	0.36	45.25	11.30	12.18	11.74	0.62
96.25	14.63	14.05	14.34	0.41	69.25	11.15	12.13	11.64	0.69
					97.25	11.00	12.04	11.52	0.74

Table B.7. Toluene desorption data from degraded newsprint after 1 month aging

Methanogenic leachate					Acidogenic leachate				
Time (hrs)	q/q_0 (1)	q/q_o (2)	average	SE	Time (hrs)	q/q_0 (1)	q/q_o (2)	average	SE
0.5	45.65	40.09	42.87	3.94	0.75	55.92	53.09	54.51	2.01
0.75	28.96	22.96	25.96	4.24	1	40.66	35.67	38.17	3.53
1	24.72	18.69	21.71	4.27	8.25	34.97	29.45	32.21	3.90
3.75	22.11	16.28	19.20	4.12	24.25	31.11	25.17	28.14	4.20
19.25	20.12	14.20	17.16	4.19	55.25	29.57	23.57	26.57	4.25
43.25	19.09	13.14	16.12	4.21	72.25	28.92	22.88	25.90	4.27
67.25	18.51	12.72	15.62	4.10	98.25	27.95	22.30	25.13	3.99
115.25	18.15	12.33	15.24	4.12	122.25	27.61	21.66	24.63	4.20
139.25	17.85	12.09	14.97	4.07	142.25	27.34	21.38	24.36	4.21
163.25	17.68	11.65	14.67	4.27					
211.25	17.38	11.34	14.36	4.27					

Table B.8. Toluene desorption data from degraded newsprint after 8 month aging

Methanogenic leachate					Acidogenic leachate				
Time (hrs)	q/q_0 (1)	q/q_o (2)	average	SE	Time (hrs)	q/q_0 (1)	q/q_o (2)	average	SE
0.75	53.72	57.94	55.83	2.98	0.5	69.13	78.76	73.94	6.81
1	45.55	46.75	46.15	0.84	0.75	50.60	59.92	55.26	6.59
5.25	39.93	38.88	39.41	0.75	1	37.62	45.71	41.66	5.72
17.25	36.78	34.62	35.70	1.53	2.75	28.89	34.04	31.46	3.64
43.25	35.26	32.48	33.87	1.97	19.25	24.17	27.62	25.89	2.43
71.25	34.34	31.12	32.73	2.28	41.25	21.49	23.41	22.45	1.36
95.25	33.92	30.59	32.25	2.35	68.25	20.29	21.66	20.97	0.97
143.25	33.38	29.97	31.67	2.41	92.25	19.71	20.94	20.32	0.87
167.25	32.66	29.48	31.07	2.25	142.25	19.25	20.37	19.81	0.79
					166.25	18.96	20.06	19.51	0.78

Table B.9. Toluene desorption data from fresh office paper after 1 month aging

Methanogenic leachate					Acidogenic leachate				
Time (hrs)	q/q_0 (1)	q/q_o (2)	average	SE	Time (hrs)	q/q_0 (1)	q/q_o (2)	average	SE
0.67	97.60	92.94	95.27	3.29	0.5	86.39	90.39	88.39	2.83
1.00	86.71	76.15	81.43	7.46	0.75	67.09	71.38	69.23	3.04
4.25	81.60	69.68	75.64	8.43	1	56.15	46.03	51.09	7.16
22.25	71.12	63.38	67.25	5.47	21.25	38.62	31.73	35.17	4.87
47.25	66.90	59.02	62.96	5.58	45.25	28.28	26.60	27.44	1.19
71.25	63.76	55.63	59.70	5.75	71.25	25.53	24.30	24.92	0.87
95.25	62.06	53.43	57.74	6.10	95.25	24.09	21.98	23.03	1.49
119.25	61.40	52.57	56.98	6.24	143.25	22.79	20.76	21.78	1.43

Table B.10. Toluene desorption data from fresh office paper after 8 month aging

Methanogenic leachate					Acidogenic leachate				
Time (hrs)	q/q_0 (1)	q/q_o (2)	average	SE	Time (hrs)	q/q_0 (1)	q/q_o (2)	average	SE
1	93.12	95.13	94.13	1.42	0.75	84.45	75.69	80.07	6.19
5.25	83.18	85.20	84.19	1.43	1	67.39	59.81	63.60	5.36
18.25	73.24	75.27	74.26	1.43	6.25	51.50	43.83	47.67	5.42
43.25	66.34	67.73	67.04	0.98	20.25	35.62	31.90	33.76	2.62
67.25	62.02	63.67	62.85	1.16	44.25	24.63	25.24	24.94	0.43
91.25	59.63	61.16	60.40	1.08	68.25	17.83	22.11	19.97	3.03
115.25	57.61	59.11	58.36	1.07	93.25	14.59	18.85	16.72	3.01
162.25	55.52	56.87	56.20	0.95	117.25	11.35	16.01	13.68	3.29
186.25	54.71	55.98	55.34	0.90	163.25	8.38	14.97	11.67	4.66
236.25	53.70	55.04	54.37	0.95	186.25	6.95	13.50	10.23	4.63
286.25	52.89	54.18	53.54	0.92	236.25	5.58	12.60	9.09	4.97
					286.25	4.85	11.53	8.19	4.72

Table B.11. Toluene desorption data from degraded office paper after 1 month aging

Methanogenic leachate					Acidogenic leachate				
Time (hrs)	q/q_0 (1)	q/q_o (2)	average	SE	Time (hrs)	q/q_0 (1)	q/q_o (2)	average	SE
0.5	85.01	74.99	80.00	7.08	0.5	83.14	82.98	83.06	0.11
0.75	72.78	60.92	66.85	8.39	0.75	61.33	65.87	63.60	3.21
1	64.26	52.43	58.34	8.37	1	50.36	56.07	53.21	4.04
3.25	54.93	44.58	49.75	7.32	5.25	41.37	46.84	44.10	3.87
22.25	44.76	34.49	39.62	7.27	24.25	33.69	38.40	36.04	3.33
46.25	36.42	26.58	31.50	6.96	48.25	27.61	30.80	29.21	2.26
72.25	32.37	22.06	27.21	7.29	74.25	23.68	26.60	25.14	2.06
96.25	29.02	18.72	23.87	7.28	98.25	21.54	24.41	22.98	2.03
120.25	26.90	16.24	21.57	7.54	122.25	19.46	22.05	20.76	1.83
144.25	24.35	13.96	19.15	7.35	146.25	17.77	20.60	19.19	2.00
168.25	23.05	12.64	17.85	7.37	170.25	17.06	19.57	18.32	1.77
192.25	22.20	11.85	17.03	7.31	194.25	16.68	18.81	17.74	1.51
216.25	21.52	11.03	16.27	7.41	218.25	16.26	18.33	17.30	1.46
288.25	20.56	10.15	15.36	7.36	290.25	15.77	17.67	16.72	1.35

Table B.12. Toluene desorption data from degraded office paper after 8 month aging

Methanogenic leachate					Acidogenic leachate				
Time (hrs)	q/q_0 (1)	q/q_o (2)	average	SE	Time (hrs)	q/q_0 (1)	q/q_o (2)	average	SE
0.5	82.29	81.33	81.81	0.68	0.5	72.53	91.41	81.97	13.35
0.75	73.33	71.52	72.43	1.28	0.75	63.69	77.93	70.81	10.07
1	68.54	66.14	67.34	1.70	1	60.19	68.87	64.53	6.13
3.5	62.22	59.29	60.76	2.08	4.5	54.05	59.41	56.73	3.79
19.25	54.10	51.42	52.76	1.90	21.25	45.45	48.37	46.91	2.06
45.25	46.76	44.16	45.46	1.84	46.25	38.49	39.97	39.23	1.05
69.25	42.21	39.75	40.98	1.74	70.25	33.94	34.11	34.03	0.12
93.25	37.91	35.78	36.85	1.51	95.25	30.69	30.02	30.36	0.48
117.25	34.57	32.61	33.59	1.39	119.25	27.95	27.08	27.52	0.62
141.25	32.29	30.36	31.32	1.37	143.25	26.11	24.68	25.39	1.01
167.25	30.53	28.54	29.53	1.41	167.25	24.32	22.94	23.63	0.98
189.25	28.89	26.96	27.93	1.36	191.25	23.33	21.54	22.44	1.27
215.25	27.41	25.48	26.44	1.36	217.25	22.48	20.55	21.52	1.36
287.25	26.02	23.97	24.99	1.45	289.25	21.11	18.96	20.04	1.52

Table B.13. Toluene desorption data from HDPE after 1 month aging

Methanogenic leachate					Acidogenic leachate				
Time (hrs)	q/q_0 (1)	q/q_o (2)	average	SE	Time (hrs)	q/q_0 (1)	q/q_o (2)	average	SE
0.5	91.75	91.11	91.43	0.45	0.5	89.97	93.42	91.69	2.44
0.75	86.60	85.55	86.07	0.74	0.75	83.20	85.49	84.34	1.62
1	82.22	81.94	82.08	0.20	1	76.47	78.27	77.37	1.27
24.25	71.63	71.69	71.66	0.04	22.25	66.20	69.14	67.67	2.08
48.25	60.76	60.47	60.62	0.21	46.25	56.85	59.99	58.42	2.22
73.25	49.61	49.80	49.71	0.14	70.25	46.12	49.66	47.89	2.50
100.25	42.07	42.16	42.12	0.07	100.25	37.90	42.46	40.18	3.22
148.25	36.37	35.80	36.08	0.40	148.25	33.75	38.64	36.20	3.46
172.25	31.82	31.25	31.54	0.40	172.25	29.36	34.00	31.68	3.28
216.25	27.06	26.41	26.74	0.46	216.25	26.77	31.06	28.91	3.03

Table B.14. Toluene desorption data from PVC after 1 month aging

Methanogenic leachate					Acidogenic leachate				
Time (hrs)	q/q_0 (1)	q/q_o (2)	average	SE	Time (hrs)	q/q_0 (1)	q/q_o (2)	average	SE
0.5	99.90	99.85	99.88	0.04	0.5	99.37	99.32	99.35	0.04
0.833333	99.55	99.48	99.52	0.05	0.75	99.10	99.00	99.05	0.07
3.25	98.84	98.65	98.74	0.13	1	98.68	98.60	98.64	0.05
20.25	97.91	97.60	97.75	0.22	4.75	97.95	97.89	97.92	0.04
45.25	97.11	96.79	96.95	0.22	18.25	97.03	96.91	96.97	0.08
69.25	96.33	95.95	96.14	0.26	43.25	96.00	95.98	95.99	0.01
93.25	95.62	95.23	95.42	0.28	67.25	94.91	94.87	94.89	0.03
117.25	95.12	94.60	94.86	0.37	91.25	93.64	93.73	93.68	0.06
164.25	94.36	93.73	94.04	0.45	115.25	92.50	92.56	92.53	0.04
188.25	93.63	92.90	93.27	0.51	168.25	91.84	91.85	91.85	0.01
					192.25	90.65	90.95	90.80	0.21

Table B.15. Toluene desorption data from PVC after 8 month agin

Methanogenic leachate					Acidogenic leachate	
Time (hrs)	q/q_0 (1)	q/q_o (2)	average	SE	Time (hrs)	q/q_0 (1)
0.5	99.49	99.76	99.63	0.19	0.5	99.74
0.75	99.43	99.69	99.56	0.19	0.75	99.48
1.25	98.81	99.13	98.97	0.22	1.25	98.25
23.25	98.11	98.41	98.26	0.22	25.25	97.29
47.25	97.61	97.88	97.75	0.20	49.25	96.43
74.25	96.87	97.11	96.99	0.17	73.25	95.25
98.25	96.12	96.34	96.23	0.16	97.25	93.80
146.25	95.42	95.65	95.53	0.16	145.25	92.77
170.25	94.84	95.04	94.94	0.14	169.25	91.78
194.25	94.32	94.68	94.50	0.25	194.25	90.80
218.25	93.71	93.88	93.79	0.12	218.25	89.99
241.25	91.90	92.70	92.30	0.56	242.25	88.45
313.25	90.83	91.51	91.17	0.48	313.25	87.36
361.25	89.86	90.54	90.20	0.48	361.25	86.47
409.25	88.88	89.64	89.26	0.54	409.25	84.78

Table B.16. o-xylene desorption data from fresh and degraded rabbit food in acidogenic leachate after 8 month aging

Degraded rabbit food					Fresh rabbit food				
Time (hrs)	q/q_0 (1)	q/q_o (2)	average	SE	Time (hrs)	q/q_0 (1)	q/q_o (2)	average	SE
0.5	81.13	97.82	89.48	11.80	0.5	91.06	90.67	90.87	0.28
0.75	62.61	78.83	70.72	11.47	0.75	80.54	79.77	80.15	0.54
1	46.46	61.28	53.87	10.47	1	69.25	68.05	68.65	0.85
3.5	30.49	42.40	36.44	8.42	3.5	61.59	60.06	60.83	1.08
27.25	24.61	33.79	29.20	6.49	19.25	53.12	51.58	52.35	1.09
49.25	20.57	27.82	24.20	5.13	26.25	47.97	46.52	47.24	1.02
72.25	17.31	22.60	19.96	3.74	45.25	41.25	39.77	40.51	1.05
93.25	15.12	18.71	16.91	2.54	69.25	35.19	34.19	34.69	0.71
118.25	13.50	15.81	14.66	1.63	117.25	31.17	30.15	30.66	0.72
142.25	12.64	14.12	13.38	1.05	143.25	27.70	26.64	27.17	0.75
190.25	12.04	12.91	12.47	0.61	167.25	23.95	23.03	23.49	0.65
217.25	11.60	12.03	11.82	0.30	191.25	20.64	19.64	20.14	0.71
241.25	11.25	11.25	11.25	0.00	212.25	17.99	16.80	17.40	0.84
263.25	10.97	10.71	10.84	0.18	236.25	15.86	14.69	15.28	0.83
284.25	10.70	10.23	10.46	0.33	264.25	14.16	12.98	13.57	0.83
308.25	10.60	10.03	10.32	0.40	288.25	12.80	11.64	12.22	0.82
360.25	10.53	9.86	10.20	0.48	313.25	11.94	11.20	11.57	0.52
408.25	10.44	9.68	10.06	0.54	337.25	10.55	10.10	10.32	0.32
456.25	10.39	9.60	9.99	0.56	361.25	9.44	8.70	9.07	0.52
504.25	10.36	9.53	9.95	0.59	385.25	8.65	7.91	8.28	0.52
888.25	10.31	9.40	9.86	0.65	409.25	8.00	7.27	7.63	0.52
1584.25	10.18	9.32	9.75	0.61	439.25	7.35	6.64	7.00	0.50
1824.25	10.15	9.25	9.70	0.64	469.25	6.88	6.18	6.53	0.49
1992.25	10.06	9.23	9.64	0.59	497.25	6.53	5.69	6.11	0.60
					518.25	6.08	5.16	5.62	0.65
					542.25	5.75	4.78	5.27	0.68
					568.25	5.58	4.64	5.11	0.67
					592.25	5.37	4.41	4.89	0.67
					664.25	5.17	4.18	4.68	0.70
					688.25	4.96	3.93	4.45	0.73
					736.25	4.72	3.74	4.23	0.69
					856.25	4.68	3.68	4.18	0.71
					1024.25	4.61	3.58	4.09	0.73
					1240.25	4.59	3.56	4.07	0.73
					1480.25	4.55	3.52	4.04	0.72
					1648.25	4.52	3.50	4.01	0.72

Table B.17. o-xylene desorption data from fresh and degraded newsprint in acidogenic leachate after 8 month aging

Degraded newsprint					Fresh newsprint				
Time (hrs)	q/q_0 (1)	q/q_o (2)	average	SE	Time (hrs)	q/q_0 (1)	q/q_o (2)	average	SE
0.5	75.67	82.55	79.11	4.86	0.5	63.29	73.19	68.24	6.998081
0.75	54.64	60.69	57.67	4.28	0.75	37.62	48.41	43.02	7.63
1	41.13	46.84	43.99	4.04	1	26.25	32.36	29.31	4.32
2.25	30.57	36.02	33.30	3.86	3.25	18.09	23.07	20.58	3.52
20.25	24.66	29.63	27.15	3.51	24.25	11.96	15.83	13.89	2.73
44.25	20.41	24.61	22.51	2.97	46.25	10.41	13.47	11.94	2.16
98.25	17.90	22.10	20.00	2.97	100.25	9.62	12.42	11.02	1.98
122.25	15.89	20.09	17.99	2.96	122.25	9.15	11.76	10.45	1.85
144.25	14.87	19.02	16.94	2.93	146.25	8.86	11.35	10.11	1.76
167.25	13.95	18.18	16.07	2.99	169.25	8.74	11.30	10.02	1.81
193.25	13.36	17.60	15.48	2.99	195.25	8.65	11.24	9.94	1.83
217.25	13.07	17.32	15.19	3.01	363.25	8.60	11.18	9.89	1.82
289.25	12.67	17.00	14.83	3.06	411.25	8.56	11.14	9.85	1.82
307.25	12.59	16.79	14.69	2.97	579.25	8.56	11.14	9.85	1.83
385.25	12.38	16.57	14.47	2.96					
553.25	12.07	16.28	14.18	2.97					
721.25	11.87	16.09	13.98	2.99					

Table B.18. o-xyolene desorption data from fresh and degraded office paper in acidogenic leachate after 8 month aging

Degraded office paper					Fresh office paper				
Time (hrs)	q/q_0 (1)	q/q_o (2)	average	SE	Time (hrs)	q/q_0 (1)	q/q_o (2)	average	SE
0.5	83.62	84.05	83.83	0.31	0.5	118.98	106.71	106.71	8.68
0.75	74.72	71.00	72.86	2.63	0.75	95.69	84.96	84.96	7.59
1	67.24	63.14	65.19	2.90	1	81.06	73.24	73.24	5.54
6.5	62.12	57.75	59.93	3.09	5.5	71.95	65.39	65.39	4.64
25.25	57.23	52.44	54.84	3.39	24.25	60.74	55.50	55.50	3.70
49.25	53.63	48.67	51.15	3.51	47.25	53.34	48.68	48.68	3.29
79.25	49.68	44.33	47.01	3.78	75.25	48.04	43.68	43.68	3.09
103.25	47.21	42.08	44.65	3.63	99.25	44.35	39.78	39.78	3.23
128.25	45.38	40.34	42.86	3.56	124.25	41.70	37.12	37.12	3.24
152.25	43.21	38.36	40.78	3.43	148.25	39.68	35.24	35.24	3.14
176.25	41.40	36.67	39.03	3.35	172.25	37.33	33.10	33.10	2.99
200.25	39.99	35.38	37.69	3.26	196.25	35.32	31.25	31.25	2.88
224.25	38.39	33.81	36.10	3.24	222.25	34.38	30.35	30.35	2.85
248.25	37.32	32.85	35.09	3.16	246.25	33.42	29.43	29.43	2.83
278.25	36.10	31.81	33.96	3.04	275.25	32.68	28.82	28.82	2.73
325.25	34.84	30.40	32.62	3.14	321.25	31.42	27.77	27.77	2.58
349.25	33.58	29.16	31.37	3.12	345.25	30.32	26.83	26.83	2.46
373.25	32.53	28.17	30.35	3.08	369.25	29.41	26.02	26.02	2.40
397.25	31.55	27.27	29.41	3.03	393.25	28.55	25.20	25.20	2.37
421.25	30.61	26.37	28.49	3.00	417.25	27.91	24.69	24.69	2.28
493.25	30.08	25.34	27.71	3.36	489.25	26.63	23.61	23.61	2.13
517.25	28.89	24.60	26.75	3.03	513.25	25.88	22.89	22.89	2.11
565.25	27.64	23.86	25.75	2.67	561.25	22.86	22.63	22.63	0.16
613.25	26.51	23.26	24.89	2.30	609.25	22.23	22.09	22.09	0.09
685.25	25.17	22.44	23.80	1.93	681.25	21.25	21.21	21.21	0.03
757.25	24.82	21.09	22.96	2.64	753.25	19.22	19.44	19.44	0.16
805.25	24.54	20.25	22.39	3.03	811.25	18.53	18.53	18.53	0.00
878.25	23.46	19.12	21.29	3.07	883.25	17.60	17.78	17.78	0.13
974.25	22.61	18.10	20.35	3.19	979.25	16.91	16.75	16.75	0.12
1118.25	21.85	17.75	19.80	2.90	1123.25	16.21	16.21	16.21	0.00
1310.25	21.15	17.60	19.37	2.51	1315.25	15.48	15.27	15.27	0.15
1478.25	20.29	17.30	18.79	2.11	1483.25	14.94	14.54	15.27	0.29
1646.25	19.42	17.08	18.25	1.65	1651.25	14.51	13.98	15.27	0.38

Table B.19. o-xylene desorption data from PVC and HDPE in acidogenic leachate after 8 month aging

PVC					HDPE				
Time (hrs)	q/q_0 (1)	q/q_o (2)	average	SE	Time (hrs)	q/q_0 (1)	q/q_o (2)	average	SE
1	99.99	99.69	99.84	0.21	0.5	98.09	97.74	97.92	0.25
21.5	99.35	99.18	99.26	0.12	0.75	92.04	95.16	93.60	2.20
45.25	98.85	98.74	98.80	0.08	1	89.59	89.13	89.36	0.32
69.25	98.25	98.22	98.23	0.02	24.5	85.00	84.50	84.75	0.35
100.25	97.55	97.62	97.59	0.05	48.25	80.75	81.13	80.94	0.27
145.25	96.84	96.99	96.92	0.11	120.25	71.88	71.85	71.86	0.02
169.25	96.21	96.43	96.32	0.15	144.25	67.70	67.80	67.75	0.07
193.25	95.56	95.83	95.70	0.19	164.25	63.07	63.29	63.18	0.16
217.25	94.93	95.46	95.20	0.38	190.25	59.27	59.87	59.57	0.43
241.25	94.30	94.84	94.57	0.38	212.25	55.95	56.82	56.39	0.61
313.25	93.68	94.15	93.92	0.33	260.25	52.66	53.98	53.32	0.94
337.25	92.99	93.60	93.29	0.43	284.25	49.41	50.70	50.05	0.91
385.25	92.58	93.23	92.91	0.46	302.25	46.89	48.40	47.65	1.06
433.25	92.15	92.85	92.50	0.49	328.25	40.79	43.01	41.90	1.57
505.25	91.50	92.30	91.90	0.56	352.25	38.77	40.93	39.85	1.52
673.25	90.42	91.77	91.10	0.95	376.25	36.91	38.84	37.87	1.36
721.25	89.66	91.06	90.36	1.00	448.25	33.76	34.55	34.15	0.56
794.25	88.48	90.30	89.39	1.28	472.25	31.77	32.02	31.89	0.18
866.25	86.97	89.50	88.23	1.79	496.25	29.80	29.68	29.74	0.09
1010.25	86.15	88.62	87.39	1.75	520.25	28.11	27.59	27.85	0.37
1202.25	85.16	87.65	86.40	1.76	544.25	26.79	26.01	26.40	0.55
1370.25	84.27	86.53	85.40	1.60	640.25	16.64	18.22	17.43	1.11
1538.25	83.93	85.85	84.89	1.36	664.25	15.97	17.77	16.87	1.27

C. Isotherms

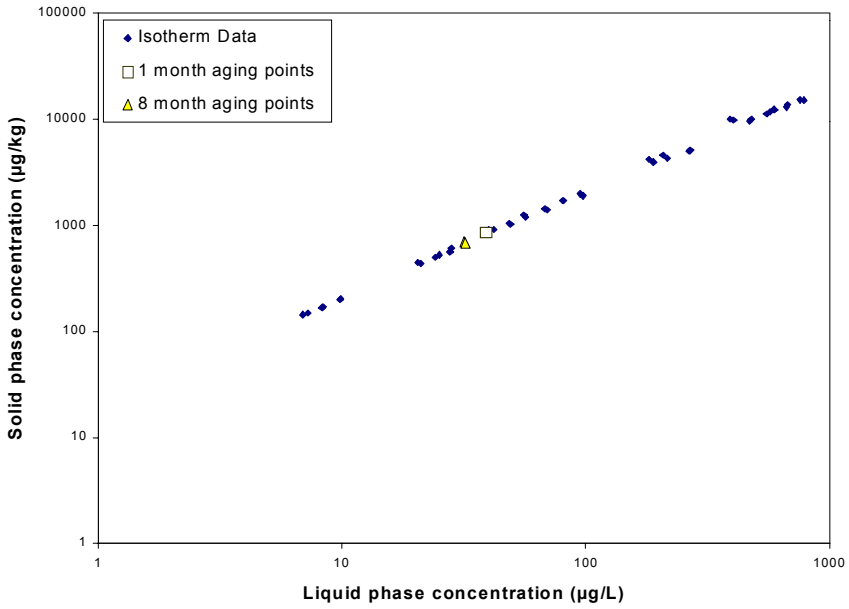

Figure C-1: Toluene isotherm with degraded newsprint in acidogenic leachate

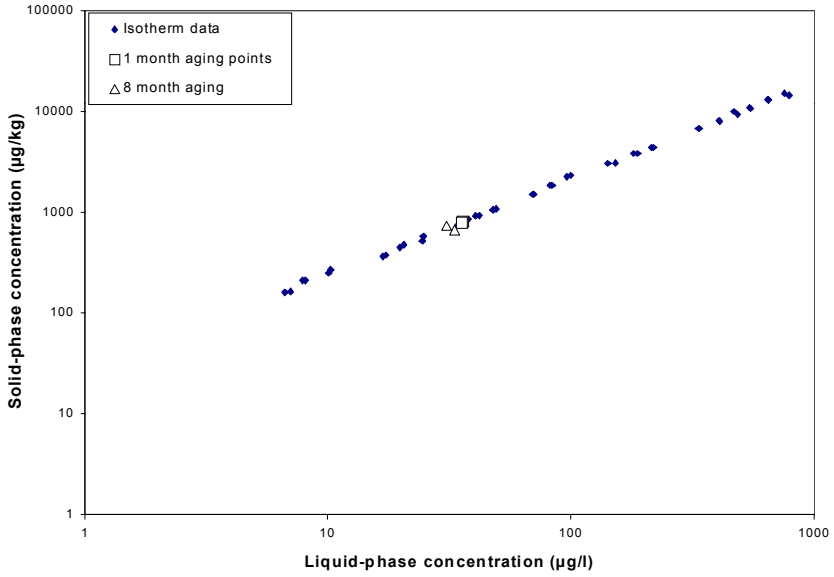

Figure C-2: Toluene isotherm with fresh newsprint in acidogenic leachate

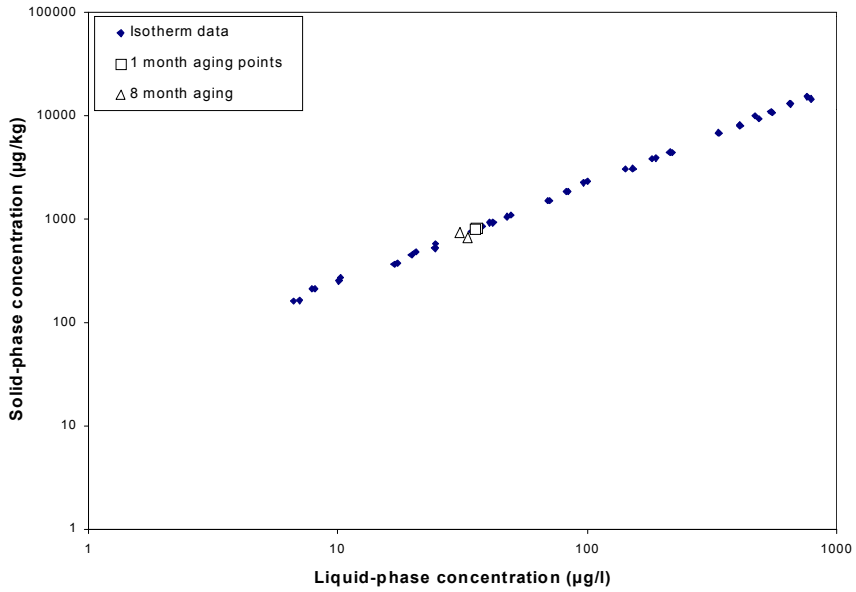

Figure C-3: Toluene isotherm with degraded office paper in acidogenic leachate

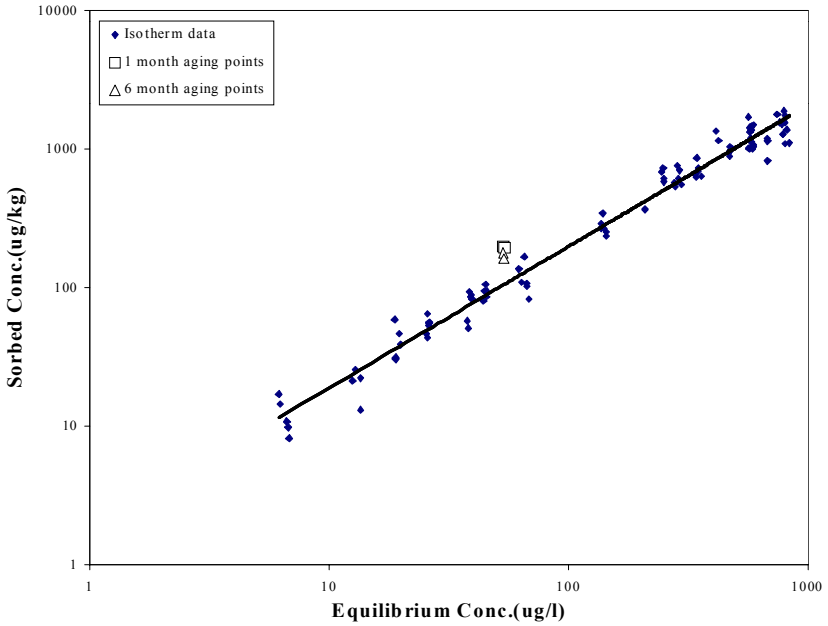

Figure C-4: Toluene isotherm with fresh office paper in acidogenic leachate

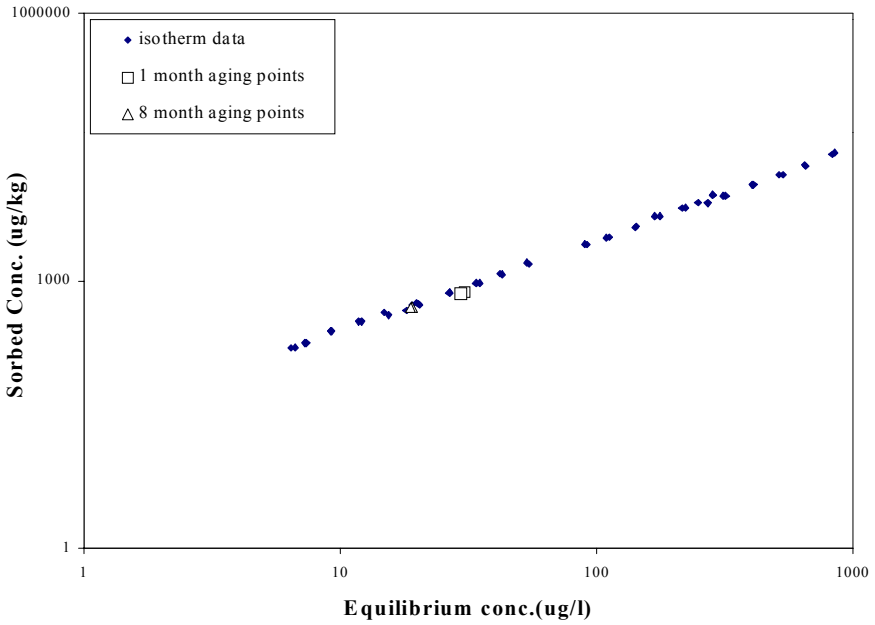

Figure C-5: Toluene isotherm with fresh rabbit food in acidogenic leachate

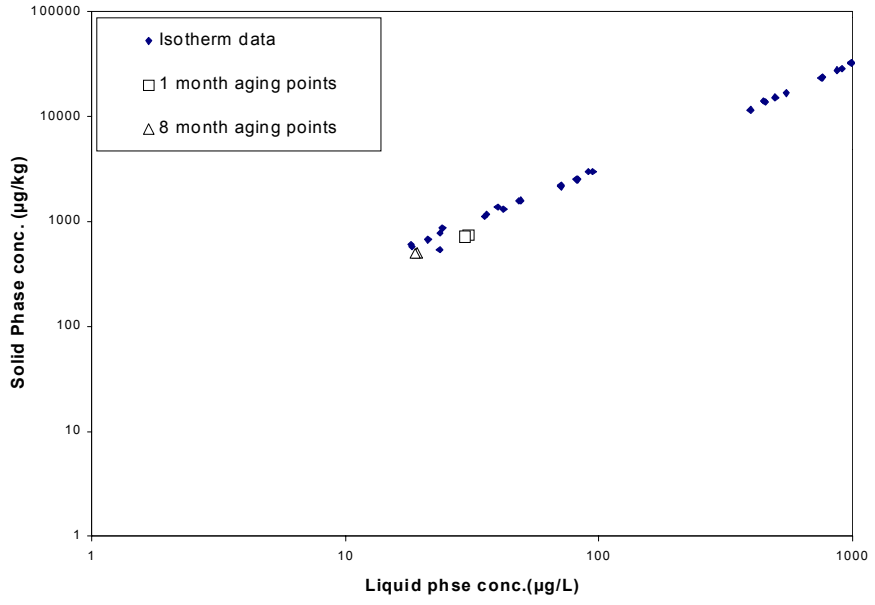

Figure C-6: Toluene isotherm with degraded rabbit food in acidogenic leachate

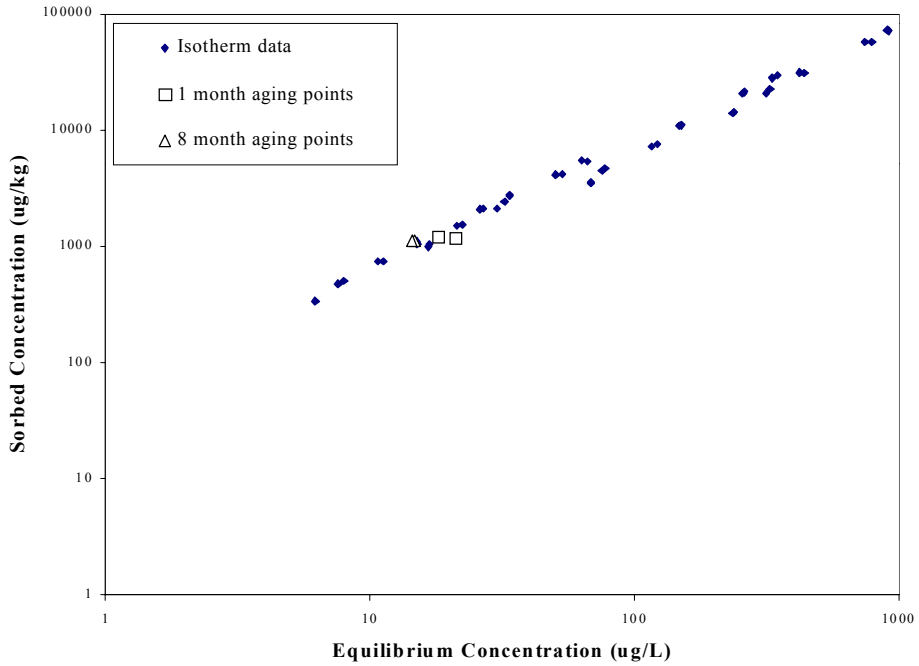

Figure C-7: Toluene isotherm with HDPE in acidogenic leachate

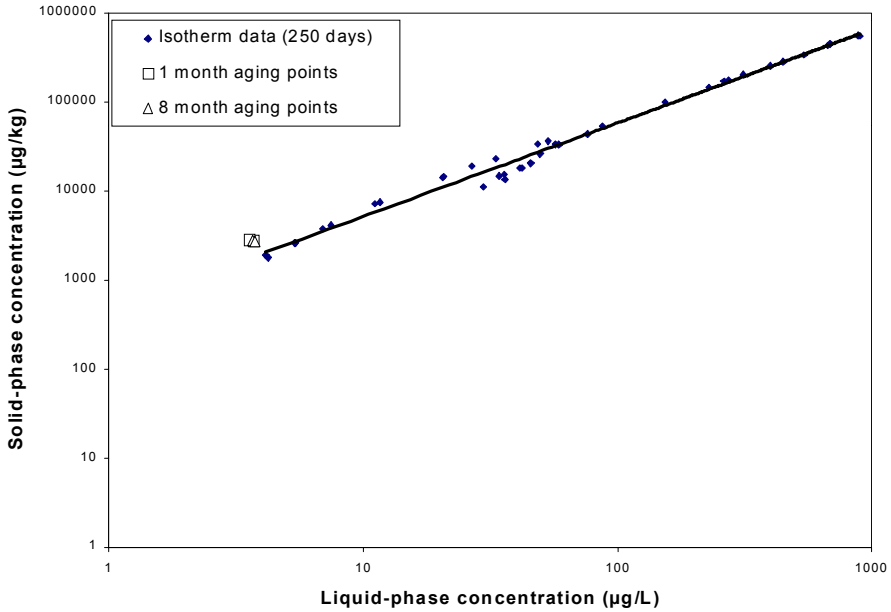

Figure C-8: Toluene isotherm with PVC in acidogenic leachate

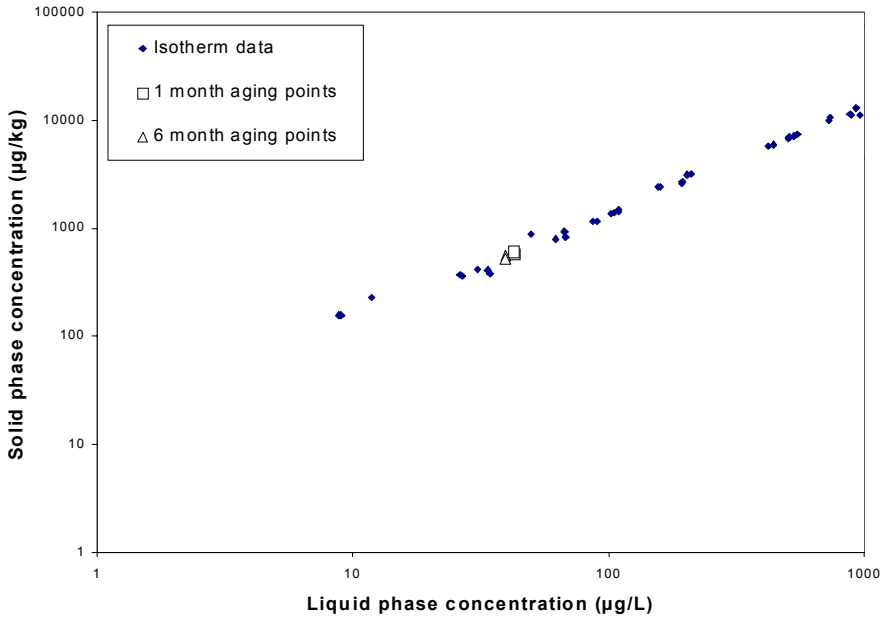

Figure C-9: Toluene isotherm with degraded newprint in methanogenic leachate

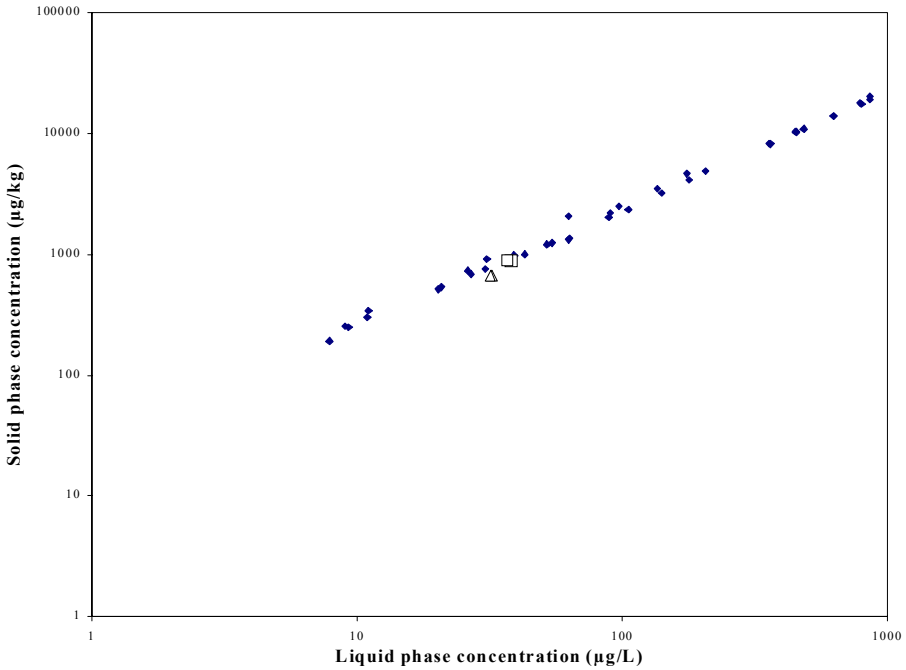

Figure C-10: Toluene isotherm with fresh newprint in methanogenic leachate

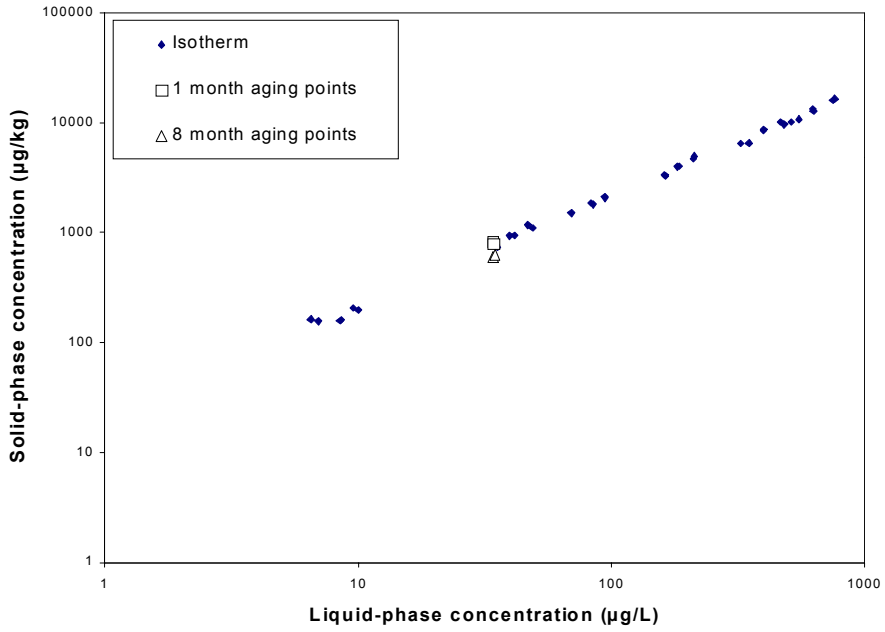

Figure C-11: Toluene isotherm with degraded office paper in methanogenic leachate

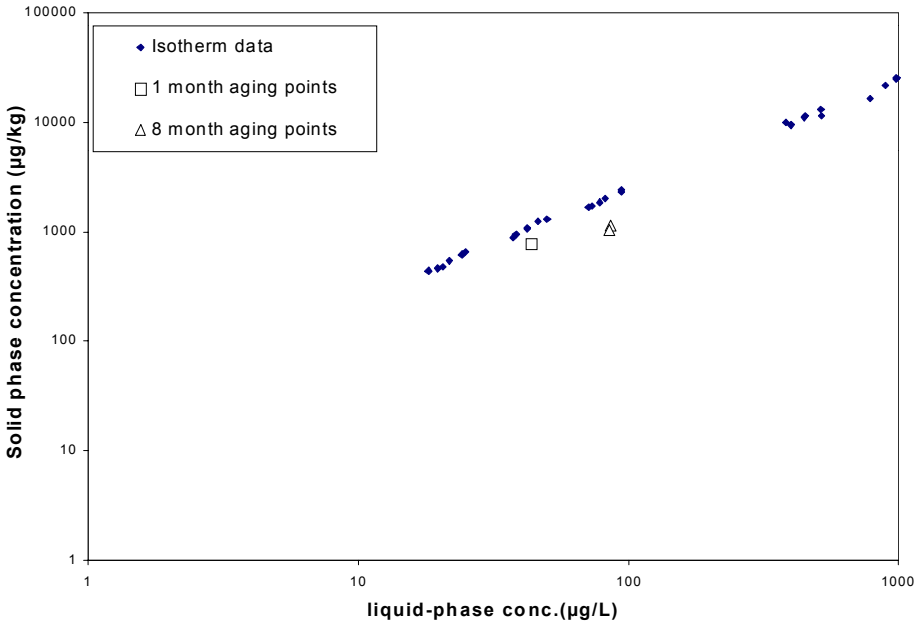

Figure C-12: Toluene isotherm with degraded rabbit food in methanogenic leachate

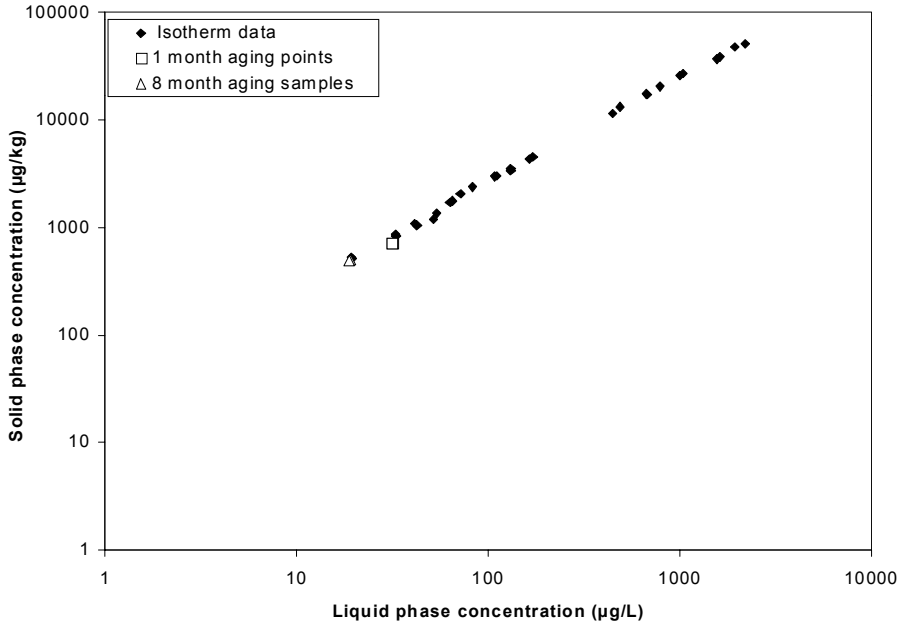

Figure C-13: Toluene isotherm with fresh rabbit food in methanogenic leachate

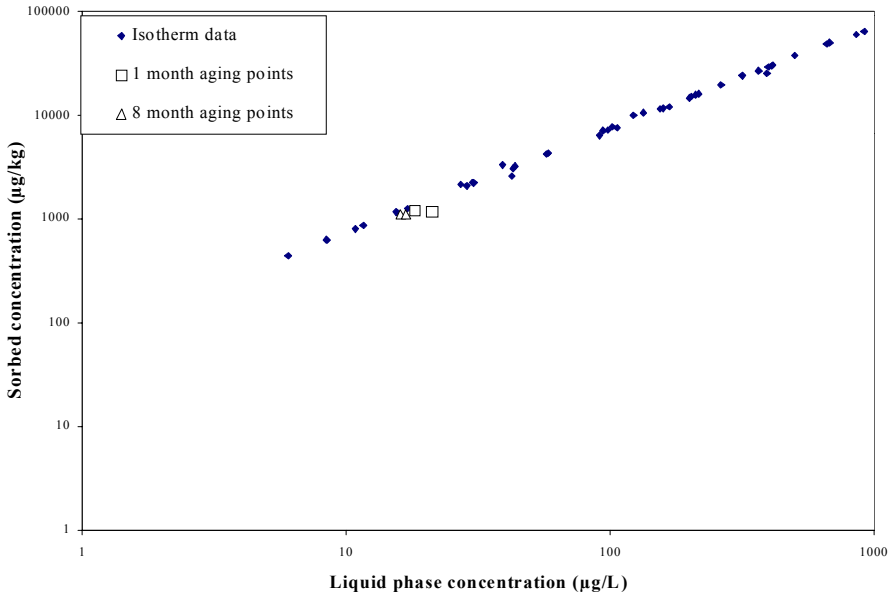

Figure C-14: Toluene isotherm with HDPE in methanogenic leachate

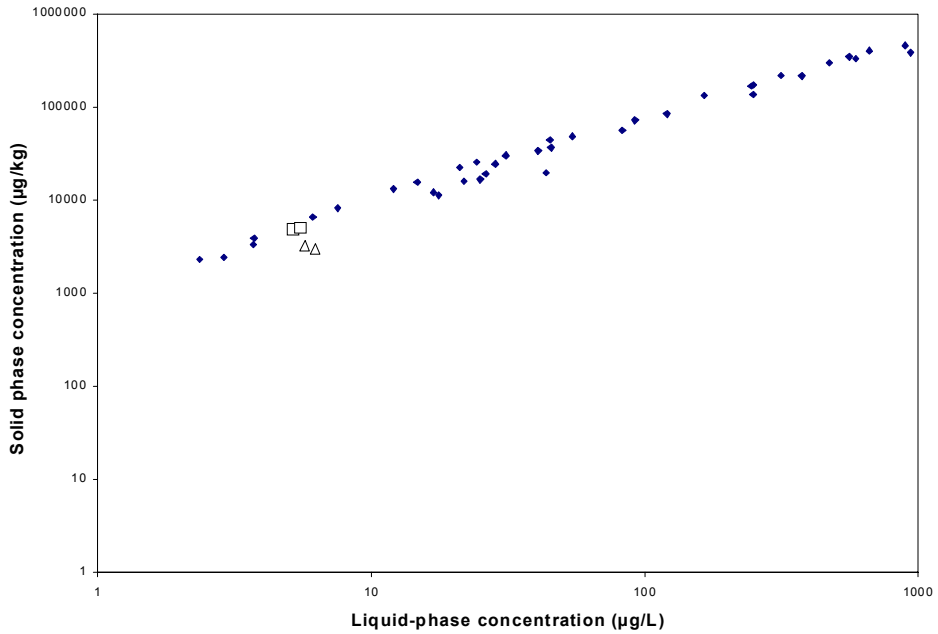

Figure C-15: Toluene isotherm with PVC in methanogenic leachate

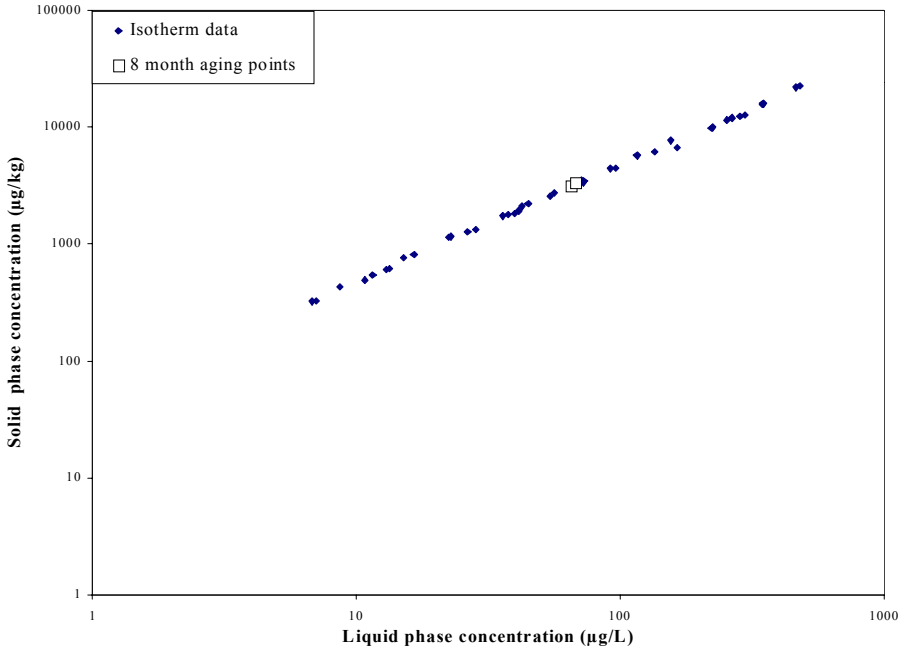

Figure C-16: o-xylene isotherm with degraded newsprint in acidogenic leachate

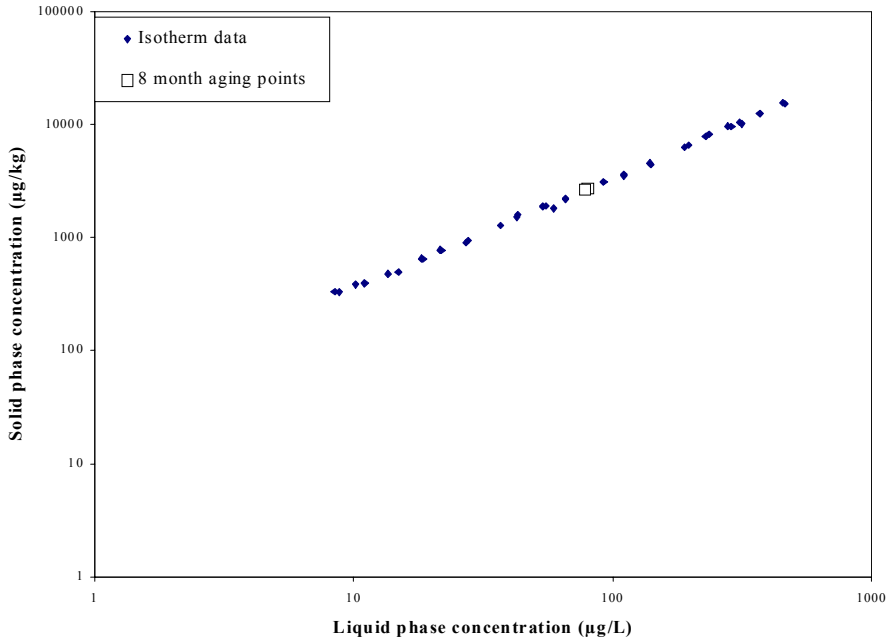

Figure C-17: o-xylene isotherm with fresh newsprint in acidogenic leachate

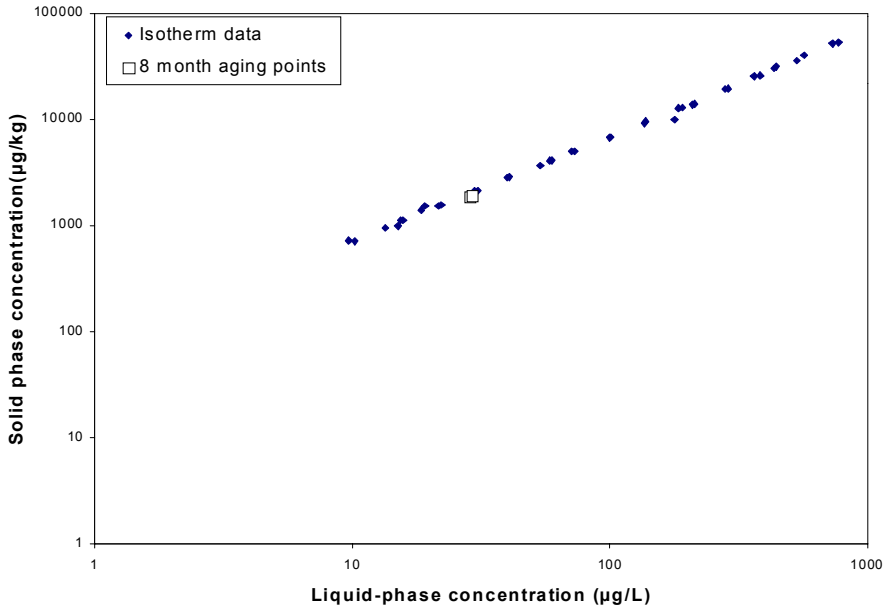

Figure C-18: o-xylene isotherm with fresh rabbit food in acidogenic leachate